STUDIES IN THE SOLID STATE:

OPTICAL SPECTRA OF $IrCl_6^{2-}$ AND $PtCl_6^{2-}$ COMPLEXES

A thesis presented for the degree of
Doctor of Philosophy in Physics
in the University of Canterbury,
Christchurch, New Zealand.

by

I.N. Douglas

1969

To the memory of my father

'Ah, but a man's reach should exceed his grasp,
Or what's a heaven for?'

Robert Browning.

Andrea del Sarto.

PREFACE

This investigation is concerned with the experimental observation and interpretation of the spectra of 4d and 5d transition-metal ion complexes. In particular, a detailed study has been made of the optical absorption spectra of the $IrCl_6^{2-}$ and $PtCl_6^{2-}$ complexes in Cs_2ZrCl_6, Cs_2HfCl_6 and K_2SnCl_6, and of $PdCl_6^{2-}$ in Cs_2ZrCl_6. The luminescence spectra of $PtCl_6^{2-}$ in several compounds was also investigated. As this luminescence had not been reported before, much time was spent trying to understand the nature of it, including a study of the temperature dependence of the band shape.

This is the first time the spectra of $IrCl_6^{2-}$ and $PtCl_6^{2-}$ have been investigated at liquid helium temperature, and the results show an abundance of vibrational structure not seen at higher temperatures.

Calculations have been carried out and these showed that ligand field theory alone does not provide a satisfactory explanation of the spectra. It was found necessary to use a combination of ligand field theory and molecular orbital theory to explain the spectra observed.

In keeping with the best scientific tradition, the work for this thesis was sparked off by a mistake. While the optical absorption spectrum of K_2PtCl_6 was being

investigated photographically, prior to using it as a host crystal in the study of interactions between iridium ions in K_2IrCl_6, a spectral line from the neon room lights appeared above the background which seemed at first to be an emission line. When the crystal was irradiated with ultraviolet light at low temperatures a bright red luminescence was observed. Because this could not be readily explained in terms of the absorption spectrum of $PtCl_6^{2-}$, as then known, the low temperature absorption spectrum of $PtCl_6^{2-}$ was investigated, resulting in the discovery of a very weak band. The original interest in $IrCl_6^{2-}$ led naturally to a detailed study of its optical spectrum at liquid helium temperature.

I would like to thank the staff and research students of both the Physics and Chemistry Departments for many useful discussions. In particular I am very grateful to Professor B.G. Wybourne for his supervision and Dr G.D. Jones for his help and interest.

I would also like to thank Mr D. Greig for assisting with the liquid helium runs; Mr R. Ritchie for growing the crystals; Mr A. Smith of the Geology Department for obtaining the X-ray data; and Mrs M. Sewell for typing this thesis.

Financial assistance has been received from the New Zealand University Grants Committee, and from the United States Air Force Office of Scientific Research under AFOSR Grant No. 1275-67. The Grants Committee also provided a Postgraduate Scholarship.

CONTENTS

LIST OF FIGURES

LIST OF TABLES

ABSTRACT

The optical absorption spectra of the complexes $IrCl_6^{2-}$ and $PtCl_6^{2-}$ in single crystals of Cs_2ZrCl_6, Cs_2HfCl_6 and K_2SnCl_6, and $PdCl_6^{2-}$ in Cs_2ZrCl_6 have been studied at liquid helium temperature. Both molecular orbital theory and ligand field theory are used to interpret the results. The rich vibrational structure observed in many of the bands is analysed in terms of the vibrational modes of the complexes. Several long progressions involving up to twelve quanta of the totally symmetric vibration, ν_{1g}, were observed throughout the spectra, indicating that the transitions are to states in which the bond length has changed.

Luminescent bands due to transitions from the triplet states of the $5d^6$ configuration of Pt^{4+} in crystals of the type K_2PtCl_6 have been found in the red and green regions of the spectrum. A study of the temperature dependence of the band width of the red luminescence in K_2PtCl_6 powder has been made and fitted to a coth function. At liquid helium temperature both bands showed vibrational progressions, involving several quanta of the totally symmetric vibration.

CHAPTER 1

INTRODUCTION

1-1 TRANSITION-METAL ION COMPLEXES

It is well known that many solids containing transition-metal ions are found to absorb light in the visible and near-visible regions of the electromagnetic spectrum. These absorptions which cause the bright colourings evident in such salts, are due mainly to transitions between electronic energy levels arising from the partly filled d shells characteristic of the transition-metal ions. The energies of these d electrons are modified by the surrounding ligands, whose orbitals can mix with the d orbitals. The group of ions consisting of the transition-metal ion and the surrounding ligands is termed a complex. The energy levels in complexes consisting of a central platinum or iridium ion surrounded by an octahedron of six chlorine ions are the subject of investigation in this thesis.

Transitions between energy levels in complexes can be of four basic types:

1. excitation within the metal ion — these are often referred to as d-d or ligand-field transitions

2. excitation within the ligands
3. electron-transfer from the ligands to the metal ion
4. electron-transfer from the metal ion to the ligands.

In the hexachloro complexes considered here only the first and third types of transitions are likely to occur.

Several excellent review articles and books on absorption spectra have been written[1-7]. Ballhausen[4] includes a comprehensive survey and bibliography of work carried out on the transition-metal ions prior to 1962. More recent articles by Ferguson[6] and Jorgensen[7] deal with the spectra of the 3d transition-metal ions and electron-transfer spectra respectively.

1-2 NOTATION

A certain amount of confusion often arises in the discussion of spectra because of the different notations used to label the states. Throughout this thesis an effort has been made to keep the notation consistent with that most commonly used to describe the spectra of ions in strong crystal fields, where the levels are labelled according to the irreducible representations of the appropriate symmetry group.

Both Mulliken's and Bethe's notations are used to describe the irreducible representations of the

octahedral group O_h. The representations A_1, A_2, E, T_1 and T_2 in Mulliken's notation correspond to Γ_1, Γ_2, Γ_3, Γ_4 and Γ_5 in Bethe's notation. Each of these representations can have odd or even parity denoted by a subscript u (ungerade) or g (gerade). If a system has an odd number of electrons the additional irreducible representations Γ_6, Γ_7 and Γ_8 of the double group O_h^* are required to label the spin-orbit states. Mulliken did not use these, but Griffith labels them E', E" and U'.

Where the spin S of a state can be specified this is given by a superscript 2S + 1, the spin multiplicity, before the irreducible representation.

Upper case letters are used to describe the state of a complete system, as well as the irreducible representations of the symmetry group, while the lower case letters are used for the representations of the individual orbitals an electron can fill, whether the orbital is occupied or not. Lower case Greek letters are also used for the representations of the fundamental vibrational modes.

1-3 OUTLINE OF THE PROJECT

No previous work has been published on the details of the vibrational structure of the spectra of the $IrCl_6^{2-}$ and $PtCl_6^{2-}$ spectra at liquid helium temperature.

In this Department Schroeder[8] has measured the solution and reflection spectra of several of the hexachloro complexes of the 4d and 5d transition-metal ions at room temperature and liquid nitrogen temperature. In the present work a detailed study is made of the spectra of the hexachloroiridate ($IrCl_6^{2-}$) and the hexachloroplatinate ($PtCl_6^{2-}$) complexes at liquid helium temperature.

The discussion in Chapter 2 provides a background to the theory used in the interpretation of the spectra. The experimental methods used to observe the spectra and the methods of growing the crystals are described in Chapters 3 and 4. Chapters 5, 6 and 7 contain the experimental results of the absorption and luminescence spectra, and show how a knowledge of the vibrational frequencies can be used to help assign the spectra. From these results it is apparent that the interpretation of these spectra is more complex than originally thought. In the conclusion several ways of extending this study are discussed.

In the course of this project, several efforts were made to compute the energy levels and to compare them with the experimental results, but these calculations were inconclusive and are not considered in great depth.

C H A P T E R 2

THEORY

This chapter provides the background of the theory used to interpret the spectra. A detailed treatment and evaluation of the theory is beyond the scope of this present work, but a fuller treatment and discussion can be found in the literature cited[1-5].

A brief outline of ligand field theory is followed by a survey of the molecular orbital theory required for the interpretation of the spectra of the 5d transition-metal ion complexes. The general problem of selection rules and intensities is discussed, and, finally, the important effect of vibrations is considered.

2-1 LIGAND FIELD THEORY

It is only during the last decade that the term ligand field theory has come into common usage. The interpretation of spectra was first carried out using the original electrostatic crystal field theory based on the work of Bethe[9] and Van Vleck[10-12]. During the 1950's this received considerable refinement and modification from Tanabe and Sugano[13-15] and Orgel[16-18]. The resulting

ligand field theory is to some extent a hybridization of the electrostatic model and the molecular orbital model developed by Mulliken[19-22] to enable electron-transfer spectra and chemical bonding to be discussed.

Much of the confusion which has arisen over the difference between crystal field theory and ligand field theory is due to the fact that a lot of the formal calculations in the two theories are very similar. The important assumption which distinguishes ligand field theory from crystal field theory, is, that although the wavefunctions of the partly filled electronic shells associated with the central ion span the same irreducible representations of the symmetry group (determined by the location of the ligands) as the free ion d orbitals, they are not necessarily the same. This means that the orbitals used can include linear combinations of the ligand orbitals. This is in contrast to the older crystal field theory in which the partly filled shells were assumed to be composed of pure d orbitals. The hyperfine structure observed in the e.s.r. spectrum of $IrCl_6^{2-}$, inexplicable using the crystal field model, can be explained by considering the effect of the nuclear spin of the chlorine on the ligand orbitals which mix with those of the central iridium ion[23,24]. The mixing of the metal

and ligand orbitals also provides the mechanism for exchange interaction between neighbouring complexes[25-28].

The energy levels of a complex ion can be calculated by a method analogous to that used for a free ion. The chief difference between the two cases is that the free ion possesses spherical symmetry, while in a complex ion the electrons move in the potential field of the ligands which has a lower symmetry.

In discussing the effect of the ligand field on the energy levels of an ion it is usual to divide the field into two parts (i) the octahedral or tetrahedral field, which is the larger and can have a major influence on the energy levels, and (ii) any non-cubic field, generally small or zero, which can be treated as a perturbation on the system after other effects such as the electrostatic interaction and the spin-orbit coupling have been considered. Since all the complexes investigated here are essentially octahedral, only ions with octahedral symmetry will be considered.

If the vibrational effects are neglected, the Hamiltonian for a many-electron ion in a complex may be written[29]

$$H = H_o + H_e + H_{so} + V_c \qquad (1)$$

$$= \sum_{i=1}^{n} \frac{1}{2m} \underline{p}_i^2 + \sum_{i<j} \frac{e^2}{r_{ij}} + \sum_{i=1}^{n} \zeta \underline{\ell}_i \cdot \underline{s}_i + V_c \qquad (2)$$

where the summation is over the n electrons outside the closed shell of the central ion, and the ligand field term, V_c, represents an interaction with all the nuclei (including that of the central ion) and all the electrons of the filled shells. Since H_o has the full symmetry of the group, it is combined with V_c to give the ligand field operator $V = H_o + V_c$, so that the Hamiltonian (1) can now be written

$$H = H_e + H_{so} + V \qquad (3)$$

The relative importance of these terms is taken into account when carrying out energy calculations, and for the transition-metal ions this leads to two different ways of labelling the states:

(a) *The weak field scheme* — the ligand field interaction is weaker than the electrostatic interaction and is treated as a perturbation on the free ion eigenstates. The free ion spectroscopic notation is used to label the states. Many of the complexes of the 3d transition series belong to this scheme, which will not be discussed any further.

(b) *The strong field scheme* — the ligand field interaction is stronger than the electrostatic interaction and the orbitals are labelled by the irreducible representations of the symmetry group. H_e and H_{so} are then treated as

perturbations of the strong field terms. All the complexes investigated belong to this group.

The strong field configurations take the form

$$(\alpha_1\Gamma_1)^{n_1}(\alpha_2\Gamma_2)^{n_2}\cdots(\alpha_k\Gamma_k)^{n_k}$$

where Γ is an irreducible representation of the appropriate symmetry group and the α_k, corresponding to the principal quantum numbers of free ion theory, are used to distinguish between orbitals with the same Γ.

As in the free ion theory it is convenient to simplify the calculations by considering only the partly filled shells (although the possibility of configuration interaction should be kept in mind). Hence for the transition-metal ions only the d electrons are considered.

In an octahedral crystal field the d orbitals are separated into two sets which transform as the e_g and t_{2g} representations of the symmetry group O_h with energies $+\frac{3}{5}\Delta$ and $-\frac{2}{5}\Delta$ respectively. The strong field configuration is written $t_{2g}^m e_g^n$. When the electrostatic energy is diagonalised each configuration breaks up into a set of *strong field terms* labelled $^{2S+1}\Gamma$ where S is the total spin and Γ is an irreducible representation of O_h. When spin-orbit coupling is included, each term breaks up into a number of *strong field levels* which are labelled by the representations of the double group O_h^*.

The terms of ${}^{\Lambda}t_{2g}^{m}e_{g}^{n}$ which are allowed by the Pauli exclusion principle have been determined by Bethe[9]. The terms of the configuration $t_{2g}^{m}e_{g}^{n}$, obtained by combining the terms of t_{2g}^{m} and e_{g}^{n}, are given by Griffith[29].

2-2 THE LIGAND FIELD PARAMETERS

The theoretical calculation of the energy levels using the Hamiltonian (2) is an extremely complex mathematical problem requiring a knowledge of the exact wavefunctions. Hence a semi-empirical approach is employed, in which group theory is utilized to determine the symmetry properties of the operators and wavefunctions, but the radial parts must be incorporated in a number of parameters to be determined experimentally. Thirteen parameters are needed to calculate the matrix elements between states of the $t_{2g}^{m}e_{g}^{n}$ configuration[30,31], but since it is not usually possible to interpret spectra unambiguously using so many parameters it is common to reduce this number by making further assumptions.

Crystal field theory assumes that the t_{2g} and e_{g} orbitals are obtained purely from the splitting of the d orbitals by the octahedral field. Then the energy levels depend on the four free ion parameters A, B, C and ζ[32,33] and one new parameter Δ, which measures the strength of

the crystal field. For a given d^n configuration A can be neglected as it shifts all the energy levels equally.

Ligand field theory does not assume that the t_{2g} and e_g orbitals are necessarily derivable from the d orbitals. Instead, it is assumed that the five parameters A, B, C, ζ and Δ have the same relationship to the thirteen parameters as before, but that there is no necessity for them to be simply related to the free-ion values.

The electrostatic and cubic field matrices for the strong field coupling scheme have been calculated for all d^n configurations by Tanabe and Sugano[13], while Schroeder[8,34] has calculated the corresponding spin-orbit coupling matrices using the same wavefunctions. Other authors[29] have also calculated the matrix elements but these are inconsistent with those above because they have chosen a different phase for their wavefunctions.

Values of the parameters were chosen and the energy levels calculated. The parameters were then varied to give the best fit to the experimental data. The calculations were carried out on the University of Canterbury's IBM 360/44 computer using a matrix diagonalization programme which has been developed over a number of years by various postgraduate students. A listing of the version of this programme which was used, is given by Robson[35], who also lists another programme

which sorts the eigenvalues into ascending order and prints them out.

2-3 MOLECULAR ORBITAL THEORY

Molecular orbital theory is widely used to interpret the spectra of molecules and complex ions which have covalent bonding where the electrons cannot be considered to be associated with one particular atom, but rather belong to the complex as a whole. Hence the molecular orbitals have, in general, a wider spatial distribution than atomic orbitals, and they are polycentric.

The theory of molecular orbitals was first developed by Mulliken[19-22] and Van Vleck[10,11,36], who used it to discuss valency and magnetism in complex salts. Since the general theory is adequately reviewed in the literature[37-39] only the theory for octahedral complexes will be considered here.

It is usual to take the molecular orbitals to be linear combinations of atomic orbitals (LCAO-MO) of the constituent atoms. The i^{th} molecular orbital is

$$\Psi_i = \sum_j a_{ij}\phi_j$$

where j runs over all the atomic orbitals.

Before the energy levels of the molecules can be calculated it is necessary to obtain values for the polycentric integrals

(a) the overlap integral

$$S = \int \phi_i \phi_j d\tau$$

(b) the resonance integral

$$\beta = \int \phi_i H \phi_j d\tau$$

which is the off-diagonal matrix element of the Hamiltonian. By using the symmetry properties of the molecule many of the resonance integrals can be shown to be zero when ϕ_i and ϕ_j do not belong to the same irreducible representation.

For simple molecules it has been possible, by making suitable approximations, to carry out calculations of the energy levels which agree reasonably well with the observed spectra, but with complex molecules of the heavier atoms the approximations become less exact, the calculations complicated and tedious, and it is doubtful if much meaning can be placed on the results.

2-4 MOLECULAR ORBITAL ENERGY LEVELS FOR OCTAHEDRAL COMPLEXES

For a complete description of the molecular orbital energy levels in an octahedral complex all the atomic orbitals should be included, but, as in the ligand

field theory, it is found that the lower lying filled shells can often be ignored. In the construction of LCAO-MO's the following points enable further simplifications to be made:

1. The energies of the orbitals to be combined must not differ by too much, otherwise there is little interaction between them.
2. The internuclear separation must have the right relationship to the radial distribution functions to promote effective overlap.
3. The combining atomic orbitals must have the same symmetry with respect to the molecular framework, and the molecular orbital formed will also have this same symmetry. This enables the atomic orbitals to be considered in independent groups, reducing the labour considerably.

The first step in forming a set of molecular orbitals is to choose a suitable set of atomic orbitals. One such set for the hexachloro complexes of the platinum group ions is the 5d, 6s and 6p orbitals from the central ion and the 3p orbitals from each of the six surrounding chlorines. Following Schonland[39] linear combinations of these which form bases for irreducible representations of the octahedral group are found by considering the effect of symmetry operations on them. Since the central ion is

always transformed into itself while the ligands can be interchanged, the orbitals can be considered in two groups.

Of the central ion orbitals the s orbital is totally symmetrical and forms the basis for an A_{1g} representation, the p orbitals transform as T_{1u}, and the d orbitals as $T_{2g} + E_g$.

The p orbitals can be further divided into those directed towards the central ion, the p_σ orbitals, and those at right angles, the p_π orbitals. The p_σ orbitals transform as $A_{1g} + E_g + T_{1u}$, while the p_π orbitals transform as $T_{1g} + T_{2g} + T_{1u} + T_{2u}$.

Combinations of the atomic orbitals which transform according to these representations are given by Schonland. Since orbitals having the same representations can combine, molecular orbitals of the following kinds can be formed:

a_{1g} — Two non-degenerate levels with molecular orbitals formed from combinations of the central ion s and ligand σ atomic orbitals.

t_{1u} — Three triply degenerate levels with molecular orbitals formed from combinations of the central ion p and ligand σ and π atomic orbitals.

e_g — Two doubly degenerate levels with molecular orbitals formed from combinations of the central ion d and and ligand σ atomic orbitals.

t_{2g} — Two triply degenerate levels with molecular orbitals formed from central ion d and ligand π atomic orbitals

t_{1g} and t_{2u} — One triply degenerate level of each type with molecular orbitals that depend on the ligand π atomic orbitals only.

The order of these levels is obtained from the combination of qualitative arguments and empirical investigation of spectra, and an energy level diagram can be obtained (Figure 1). However, not all the authors agree on the order, particularly of the t_{1g}, t_{2u}, $1t_{2g}$ and $2t_{1u}$ levels, which are important in the electron-transfer spectra. The electrons will fill these orbitals from the bottom up, in accordance with the Pauli exclusion principle.

The chief features of the diagram are:

(a) A set of low-lying strongly σ-bonding levels $1a_{1g}$, $1t_{1u}$, $1e_g$ which can hold twelve electrons altogether.

(b) A set of levels whose molecular orbitals consist mainly or entirely of combinations of the ligand π orbitals; the bonding $2t_{1u}$ and $1t_{2g}$ and the non-bonding t_{2u} and t_{1g} levels which can hold twenty-four electrons.

(c) The $2t_{2g}$ and $2e_g$ levels whose molecular orbitals are predominantly the central ion d orbitals with a small

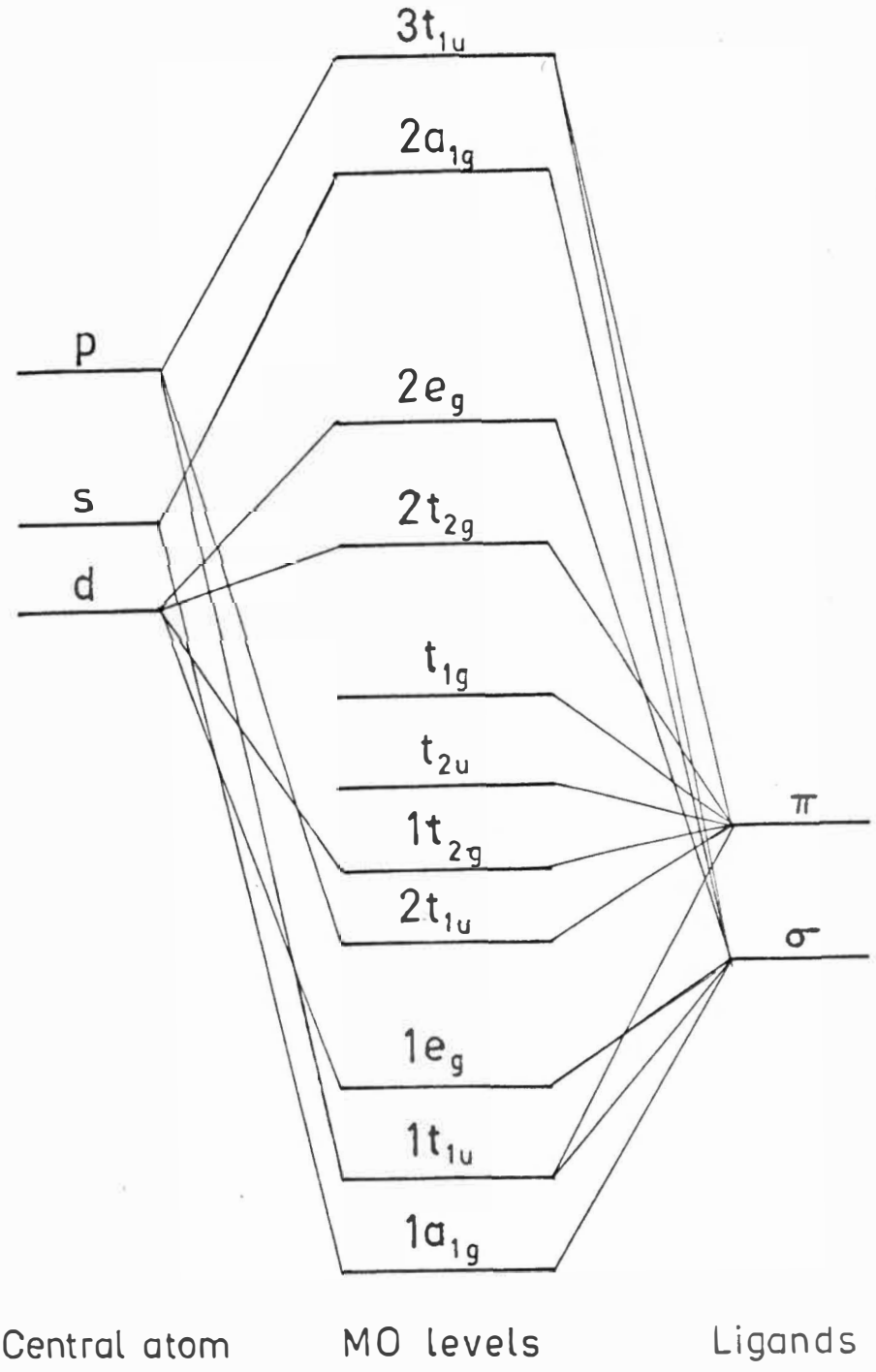

Figure 1. Energy level diagram for an MX_6 complex.

admixture of anti-bonding π and σ ligand orbitals.

(d) The strongly anti-bonding $2a_{1g}$ and $3t_{1u}$ levels.

The actual energy states in a complex are obtained by filling up these molecular orbitals with the appropriate number of electrons. $IrCl_6^{2-}$ and $PtCl_6^{2-}$ have 41 and 42 electrons respectively to fill these orbitals. In the ground state the levels in (a) and (b) will be full, and the remaining 5 or 6 electrons will go into the $2t_{2g}$ level and the picture is the same as that obtained from ligand field theory. However, in the excited states the possibility of an electron moving from one of the predominantly ligand orbitals (b) to a d orbital (c) is present, as well as transitions between the $2t_{2g}$ and $2e_g$ levels.

2-5 COMPARISON OF THE LIGAND FIELD AND MOLECULAR ORBITAL THEORIES

Neither of these theories presents a complete picture of the energy levels of a transition-metal ion in a solid, and so care must be taken with their use. Ligand field theory is the easier to handle mathematically and, since it includes details of the electrostatic interaction, it predicts the splitting of the energy terms. However, it is restricted to electrons which are mainly associated with the central ion and does not

allow for the possibility of electron-transfer transitions.

Molecular orbital theory, on the other hand, emphasises the interaction between the ligand and the central ion orbitals, which depends very strongly on the amount of overlap and the interionic separation. To evaluate the overlap integrals precise wavefunctions are required. Particularly for the 4d and 5d transition ions the calculations are lengthy and tedious, even when approximations are made.

2-6 SELECTION RULES AND INTENSITIES

The intensity of a transition depends on the matrix element $\langle i|K|j\rangle$ where K is an operator which induces the transition between the eigenstates $|i\rangle$ and $|j\rangle$. Group theory enables us to predict that some of these elements will be zero[40]. If $|i\rangle$ and $|j\rangle$ belong to the irreducible representations Γ_i and Γ_j of the symmetry group (O_h for octahedral complexes), and if K transforms as Γ_K, then the matrix element $\langle i|K|j\rangle$ will be zero unless the direct product $\Gamma_i^* \times \Gamma_K \times \Gamma_j$ contains the totally symmetric mode Γ_{1g} (Γ_i^* is the complex conjugate representation). This is equivalent to the condition that $\Gamma_K \times \Gamma_j$ must contain Γ_i. The multiplication table needed to work out these direct products for the O_h group is given in Table I.

	Γ_1	Γ_2	Γ_3	Γ_4	Γ_5	Γ_6	Γ_7	Γ_8
Γ_1	Γ_1	Γ_2	Γ_3	Γ_4	Γ_5	Γ_6	Γ_7	Γ_8
Γ_2	Γ_2	Γ_1	Γ_3	Γ_5	Γ_4	Γ_7	Γ_6	Γ_8
Γ_3	Γ_3	Γ_3	$\Gamma_1+\Gamma_2+\Gamma_3$	$\Gamma_4+\Gamma_5$	$\Gamma_4+\Gamma_5$	Γ_8	Γ_8	$\Gamma_6+\Gamma_7+\Gamma_8$
Γ_4	Γ_4	Γ_5	$\Gamma_4+\Gamma_5$	$\Gamma_1+\Gamma_3+\Gamma_4+\Gamma_5$	$\Gamma_2+\Gamma_3+\Gamma_4+\Gamma_5$	$\Gamma_6+\Gamma_8$	$\Gamma_7+\Gamma_8$	$\Gamma_6+\Gamma_7+2\Gamma_8$
Γ_5	Γ_5	Γ_4	$\Gamma_4+\Gamma_5$	$\Gamma_2+\Gamma_3+\Gamma_4+\Gamma_5$	$\Gamma_1+\Gamma_3+\Gamma_4+\Gamma_5$	$\Gamma_7+\Gamma_8$	$\Gamma_6+\Gamma_8$	$\Gamma_6+\Gamma_7+2\Gamma_8$
Γ_6	Γ_6	Γ_7	Γ_8	$\Gamma_6+\Gamma_8$	$\Gamma_7+\Gamma_8$	$\Gamma_1+\Gamma_4$	$\Gamma_2+\Gamma_5$	$\Gamma_3+\Gamma_4+\Gamma_5$
Γ_7	Γ_7	Γ_6	Γ_8	$\Gamma_7+\Gamma_8$	$\Gamma_6+\Gamma_8$	$\Gamma_2+\Gamma_5$	$\Gamma_1+\Gamma_4$	$\Gamma_3+\Gamma_4+\Gamma_5$
Γ_8	Γ_8	Γ_8	$\Gamma_6+\Gamma_7+\Gamma_8$	$\Gamma_6+\Gamma_7+2\Gamma_8$	$\Gamma_6+\Gamma_7+2\Gamma_8$	$\Gamma_3+\Gamma_4+\Gamma_5$	$\Gamma_3+\Gamma_4+\Gamma_5$	$\Gamma_1+\Gamma_2+\Gamma_3+2\Gamma_4+2\Gamma_5$

$g \times g = g$, $g \times u = u$, $u \times g = u$, $u \times u = g$

Table I. Direct products of the irreducible representations of the double group O_h^*

Electric dipole transitions are the most important for the absorption of light by complex ions. They are about 10^6 times more intense than magnetic dipole transitions. The electric dipole operator transforms as T_{1u} in octahedral symmetry and so, since all the ligand field states have even parity, electric dipole transitions are all forbidden. These transitions, however, are observed experimentally because odd vibrations and odd components of the ligand field enable some odd states to mix with the even ligand field states. Because these perturbations are generally small the observed transitions will be weak.

The spin selection rule, $\Delta S = 0$, is broken down by spin-orbit coupling which is particularly strong in the 5d transition-metal ions.

Approximate selection rules can be obtained by ignoring the parity of the states, and these can be used as a guide to predict the most likely transitions.

The intensities of optical absorption spectra of octahedral complexes have been discussed by a number of authors[41-47]. Jordan et al.[47] have carried out calculations on the intensities in octahedral complexes of the 4d and 5d transition-metal ions within the framework of ligand field theory. They compare their results with the experimental results for the low temperature spectra

of Os^{4+} and Re^{4+} in crystals of Cs_2ZrCl_6. For Ir^{4+} they predict that the strongest transitions will be to the Γ_{8g} and Γ_{6g} states.

2-7 VIBRATIONS

Vibronic interaction between the electronic states and the vibrational modes of the complex is very important in the interpretation of the spectra of complex ions, particularly when the electronic transition is forbidden.

The crystals used all have the face-centred anti-fluorite structure of the K_2PtCl_6 type, $Fm3m$[48]. Pollack[49] has shown that the vibrations of crystals of this type consist of the following fundamental modes:

(1) γ_{4u}, an acoustical lattice mode,

(2) $\gamma_{4u}(\nu_7)$, γ_{5g}, due to the vibrations of the cation relative to the MX_6^{2-} complex,

(3) $\gamma_{1g}(\nu_1)$, $\gamma_{3g}(\nu_2)$, $\gamma_{4u}(\nu_3)$, $\gamma_{4u}(\nu_4)$, $\gamma_{5g}(\nu_5)$, $\gamma_{5u}(\nu_6)$, due to the internal vibrations of the MX_6^{2-} complex.

Satten[50] has shown that if an odd vibrational mode is coupled to an electronic eigenstate the only forbidden transitions are

for a γ_{4u} vibration, Γ_1 to Γ_2,

for a γ_{5u} vibration, Γ_1 to Γ_1 and Γ_2 to Γ_2.

This means that by considering the effect of vibrations we pass from having all the transitions forbidden to having very few forbidden.

The way in which a knowledge of the vibrational energies is used to interpret spectra is best illustrated by referring to a specific example, such as the $IrCl_6^{2-}$ spectra in Chapter 5.

C H A P T E R 3

THE LOW TEMPERATURE OBSERVATION OF SPECTRA

3-1 INTRODUCTION

The measurement of spectra at low temperatures requires some means of keeping the sample at the required temperature for the complete time it takes to record the spectrum. Suitable spectrometers and recording equipment are needed to observe the spectra. This chapter describes the means by which the spectra were obtained.

The Physics Department, in recent years, has been acquiring equipment to enable spectra to be observed over the widest possible spectral range and at various temperatures. It is now possible to measure spectra in the microwave, infrared, visible and ultraviolet regions of the spectrum at any temperature down to liquid helium temperature. There is also an X-ray machine to assist in the determination of crystal structures, and a Raman spectrometer using an argon gas laser is at present being installed. It is hoped that the scope of the work possible will be extended by the addition of a Zeeman magnet and a far infrared Fourier transform interferometer.

Not all of these facilities were available while this project was being undertaken, which meant that some lines of investigation could not be pursued.

Most of the luminescence spectra were recorded photographically on two Hilger prism spectrographs. A simple quartz-tipped glass dewar was used for measurements at liquid nitrogen temperature (77^{o}K), while a glass helium dewar was used at liquid helium temperature (4.2^{o}K) (section 3-6). The temperature dependence of the $PtCl_6^{2-}$ luminescence was investigated on the 3.4m Jarrell-Ash using the Andonian dewar, but, because of the high dispersion and the rapid falling off of the photomultiplier's sensitivity in the red, the signal was weak and noisy.

The absorption spectra were all taken on the Cary 14R spectrophotometer using one of the conduction dewars described in section 3-6.

3-2 THE PHOTOGRAPHIC SPECTROGRAPHS

Because a photographic plate can integrate weak signals over a long period of time it is well suited for recording the weak luminescence spectra. Two Hilger prism spectrographs were used. The Hilger Medium Quartz (type E498, 60 cm focal length) was much faster than the Hilger Large Quartz and Glass (type E478, 170 cm focal

length). At 7000Å the dispersion of the Medium was 160Å/mm, while that of the Large using the glass prism was 25Å/mm. A typical slit width used, 100μ, gives a resolution of 16Å on the Medium and 2.5Å on the Large at 7000Å. This is more than sufficient for observing the broad luminescence bands. The Medium had an internal wavelength calibration scale which made it very convenient to use, while an iron arc was used to calibrate the Large.

The optical arrangement used most with both instruments is shown in Figure 2. Light from the source, S, (one of the mercury lamps described in section 3-7) was passed through a combination of filters which let through only the ultraviolet radiation. This was focussed by a spherical quartz lens onto the sample mounted in an immersion dewar. Light from the sample was then focussed by a cylindrical lens onto the slit of the spectrograph.

No single filter could be found which transmitted only the ultraviolet from the mercury lamp. A Corning 2-54 filter was the best, but it also transmitted in the red above 6000Å. This was most troublesome as it was very close to the red luminescence being observed. However, it was found that a concentrated solution of copper sulphate would absorb this. An ON22 heat filter

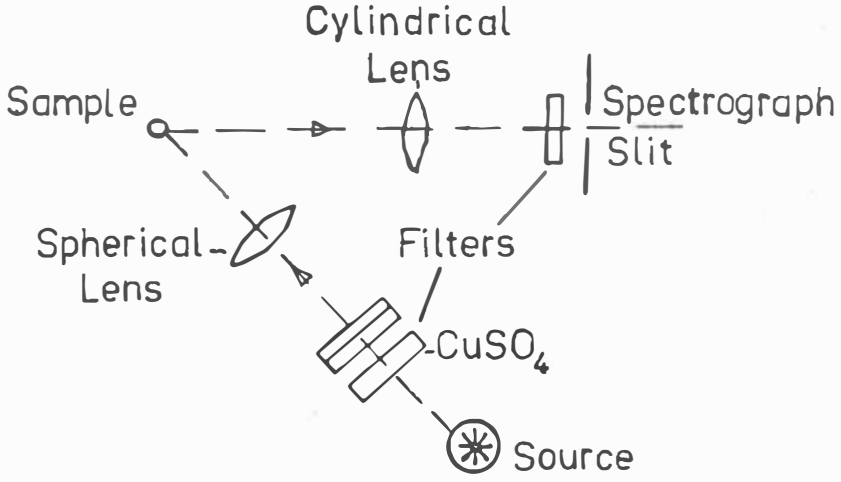

Figure 2. Optical arrangement used for luminescence

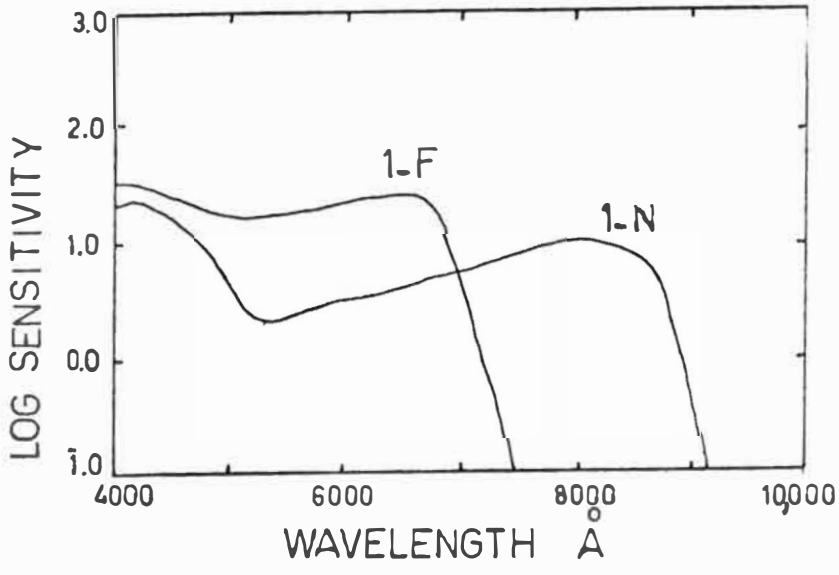

Figure 3. Plate response of the photographic plates

was also placed in front of the lamp to reduce the boil-off of the liquid nitrogen or helium. When using the Medium an OY3 filter was placed in front of the slit to eliminate the ultraviolet radiation reflected from the sample and the mounting. This was not necessary on the Large where the higher dispersion ensured that the ultra-violet did not fall on the photographic plate.

The two photographic plates most commonly used were the Kodak 1-N and the Kodak 1-F plates. These both have very high speed and fairly high contrast. The 1-F has the better sensitivity in the green, but its sensitivity drops rapidly above 6900Å (Figure 3), while the 1-N is sensitive out to almost 9000Å. Consequently the 1-F was used for the green luminescence and the 1-N for the red. The Kodak II-L plate has a smoother response but was not used because it is several times slower than the other two.

The plates were measured on a Joyce recording microdensitometer and examples of the spectra obtained can be seen in Figures 25 and 26.

3-3 THE CARY SPECTROPHOTOMETER

The Cary 14R recording spectrophotometer, which arrived shortly after this project was commenced, was used to record the absorption spectra. This double beam

instrument, designed for the rapid recording of solution spectra, required only slight modification to enable the spectra of crystals at low temperatures to be recorded. The crystals were mounted in one of the conduction dewars described in section 3-6.

The optical system of the Cary is shown in Figure 4. Dispersion is produced by a double monochromator consisting of a 30° fused silica prism (D) in series with a 600 lines/mm echelette grating (E). This combination enables advantage to be taken of the high resolving power of the grating at long wavelengths with the high optical efficiency and lower scattered light characteristic of the prism.

Four different combinations of light source and detector enable the spectrum to be scanned from 2000Å to 2.6 microns. A deuterium lamp (A) and a 1P28 photomultiplier (G) are used in the ultraviolet from 2000Å to 3500Å. A quartz-iodine lamp (B) is used in conjunction with the photomultiplier over the range 3000Å to 6500Å. Above 6000Å either of two infrared detectors can be used. Up to 17,000Å the quartz-iodine lamp is used as the source and a lead sulphide cell (H) is the detector. A special filter, which excludes radiation above 17,000Å, is used to prevent radiation emitted by the chopper (F) reaching the detector. In the range 6000Å to 26,000Å the tungsten

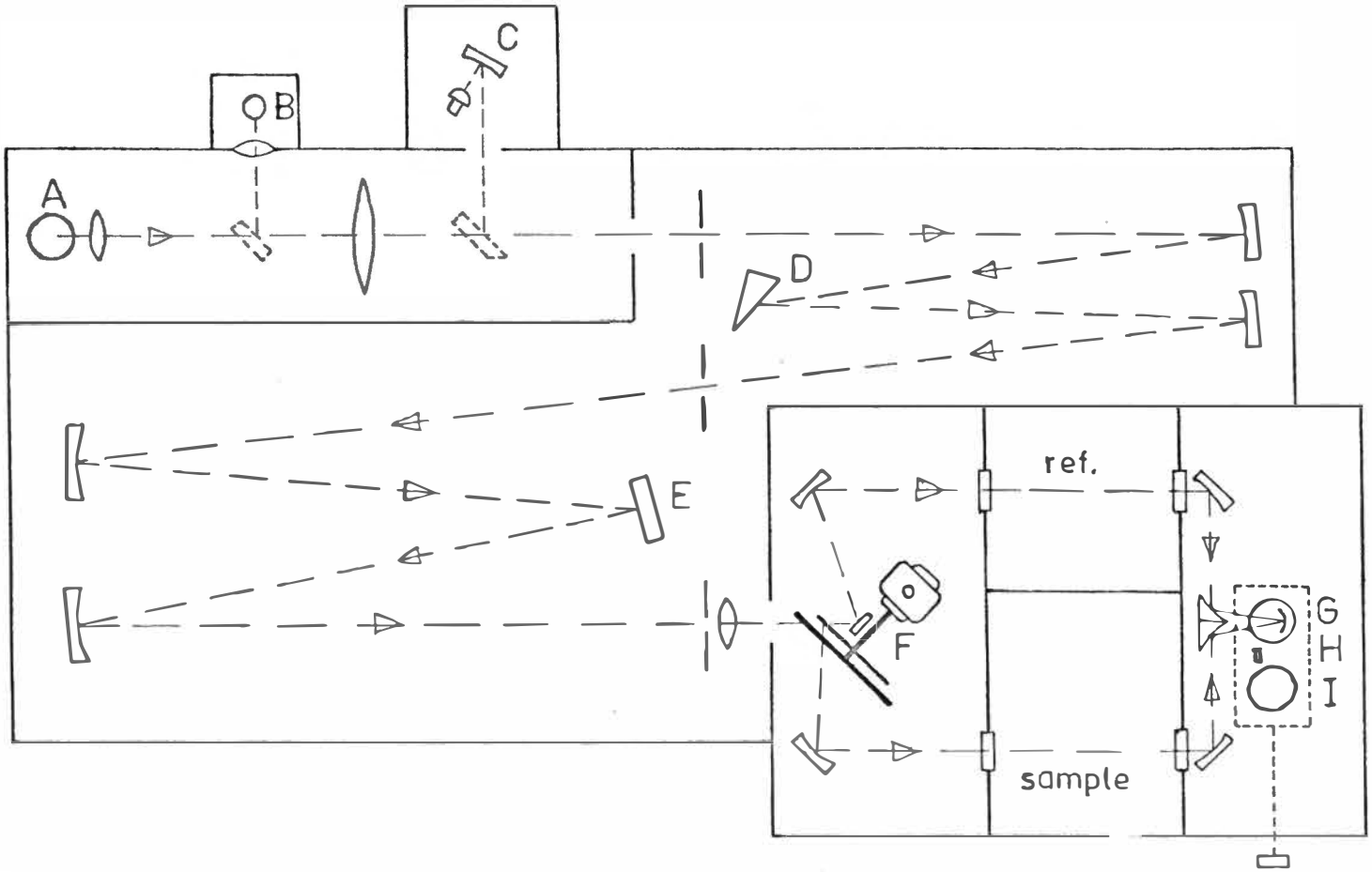

Figure 4. Cary optics

lamp (I) is used with the lead sulphide cell (C). In this second infrared range the optical path is reversed and the light passes through the sample and the chopper before being dispersed. Thus only a very small fraction of the radiation from the chopper is detected. Controls on the front of the instrument enable rapid interchange between the ranges to be made.

The need to calibrate the instrument's response to the various light sources is eliminated by dividing the light emerging from the monochromator into two by a beam splitter(F). The beam passing through the sample is compared with that passing through the empty reference cell and the difference is amplified and recorded on a chart. A marker pen on the chart recorder marks every 100Å.

The speed of the scan could be varied from 0.5Å/sec. to 500Å/sec., but the higher speeds were never used while recording. The spectra recorded were linear in wavelength. The wavelength counter was checked by replacing the quartz-iodine lamp with a small mercury lamp. In the visible region it was found that the counter reading was about 8Å too high. (See Table II below).

Table II. Cary Calibration Using a Mercury Lamp

Counter Reading (to 0.25 Å)	Wavelength of Hg line (Å)	Correction required
5799.0	5791	8
5777.5	5770	7.5
5468.5	5461	7.5
4366.5	4358	8.5
4055.25	4047	8.25
3672.75	3663	9.75

The resolution in Angstroms is given by

$$R = W.D + C + L$$

where W = monochromator slit width (mm)

D = reciprocal dispersion (Å/mm)

C = slit curvature mismatch (Å)

L = Rayleigh diffraction limit (Å)

The slit width is automatically controlled so that the same amount of energy from the reference beam falls on the detector all the time. For the best crystals used (less than 1 mm thick and about 1% concentration of the dopant) a typical slit width used was 0.02 mm which at 5000Å gave a resolution of 1Å (6 cm^{-1}). When

recording the spectra of more heavily absorbing crystals it was necessary to attenuate the energy of the reference beam using a fine gauze screen. This attenuation was kept to a minimum to avoid loss of resolution.

3-4 THE 3.4 METRE JARRELL-ASH EBERT SPECTROGRAPH

This is a high dispersion grating instrument which is most useful for the study of narrow emission lines. The sample and light source are external to the instrument giving a greater versatility in the optical arrangement used to observe the luminescence. However, an intensity calibration of the wavelength response for the system used (spectrograph, detector, and any filters used) must be made. This was done by placing a standard quartz-iodine lamp, whose intensity has been calibrated, in the position of the sample and measuring the response of the system over the spectral range of interest. The observed spectra can then be corrected.

A study of the temperature dependence of the $PtCl_6^{2-}$ luminescence was carried out using the Andonian variable temperature helium dewar. Because the luminescence band is very broad the high resolution of the instrument was not necessary and the slits could be opened up to 100μ to compensate for the weak signal and the low light gathering power (f/35).

A grating with 7500 grooves/inch gave a dispersion of 10Å/mm in the first order. With 100μ slits this gave a spectral slit width of 1Å which is much narrower than any structure observed on the photographic plates.

The wavelength calibration of the spectrograph was checked using a Philips Potassium Spectral Lamp and the spectra corrected.

The signal was detected by a red-sensitive EMI 9558 photomultiplier, amplified by an electrometer amplifier, and recorded on charts.

The optical arrangement used was similar to that used with the Hilgers (Figure 2). The black mercury lamp was used as the exciting source. A Corning 2-54 filter and a heat filter, ON22, were used in front of the sample. An OY3 or OY8 filter was used in front of the slit to prevent any higher order mercury lines being detected. Copper sulphate solution was not used initially, which meant that the red band from the mercury lamp, centred at 7300Å, could pass through the system, but this could be prevented from reaching the slit by positioning the lamp slightly above the rest of the optical system.

3-5 SAMPLE HOLDERS

The crystals all had to be mounted in the dewars so that they were firmly held in position while the spectra were being recorded.

For the nitrogen immersion dewar this was done by mounting the crystal on a computer card with some black plasticine. The pressure of the card on the walls of the dewar held it firmly in place.

The sample holder in the helium immersion dewar consisted of a thin stainless steel rod with a small loop of wire at the bottom to which the crystal was attached with plasticine. The top of the rod passed into black wax in a glass rod which passed out of the dewar through an O-ring seal.

The powders used for luminescence in the immersion dewars were sealed off in fine capillary tubing. For the nitrogen dewar sufficient tubing was left to enable the sample to be held in place by a wad of cotton wool at the top of the dewar, while in the helium dewar the capsule was taped to the steel rod.

The sample holders for the conduction dewars had to be designed to provide good thermal contact between the sample and the dewar. One of the sample holders, made from high purity copper, is shown in Figure 5. Thermal contact between the top of the sample holder and the tip of the dewar was improved by including a small piece of indium foil. The crystal was attached to the holder with a little vacuum grease, to improve thermal contact, and held in place by a copper clamp. The size

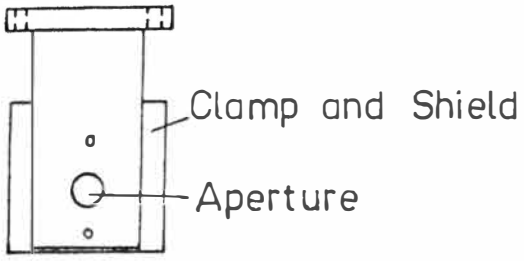

Front View

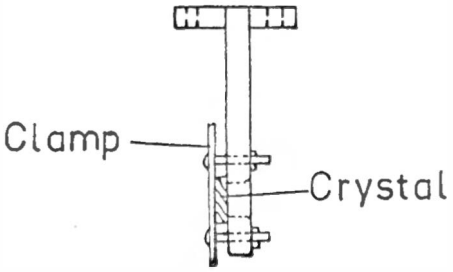

Side View

Figure 5. Sample holder

of the hole depended on the crystal's size but it was usually 5 mm in diameter. Because the crystals were poor conductors they were kept as thin as possible so that the temperature difference between the crystal faces was not too great. The powders used in the temperature dependence study of the luminescence were pressed into a recess in one of the sample holders and held in place by a quartz plate clamped to the holder.

3-6 THE DEWARS

In order to measure the spectra at low temperatures several dewars were used. These are basically of two different types: the direct immersion dewar and the conduction dewar.

In a direct immersion dewar the sample is completely immersed and so is held at the temperature of the coolant. A simple glass dewar with a quartz tip, used at liquid nitrogen temperature, has the vacuum space permanently sealed off and does not required to be pumped down between runs.

The glass helium dewar with quartz windows (Figure 6) could be used with either liquid nitrogen or liquid helium. By pumping on the liquid helium the temperature could be reduced to below 4.2^{o}K. The lowest temperature reached was 2^{o}K but, as it was wasteful of helium and

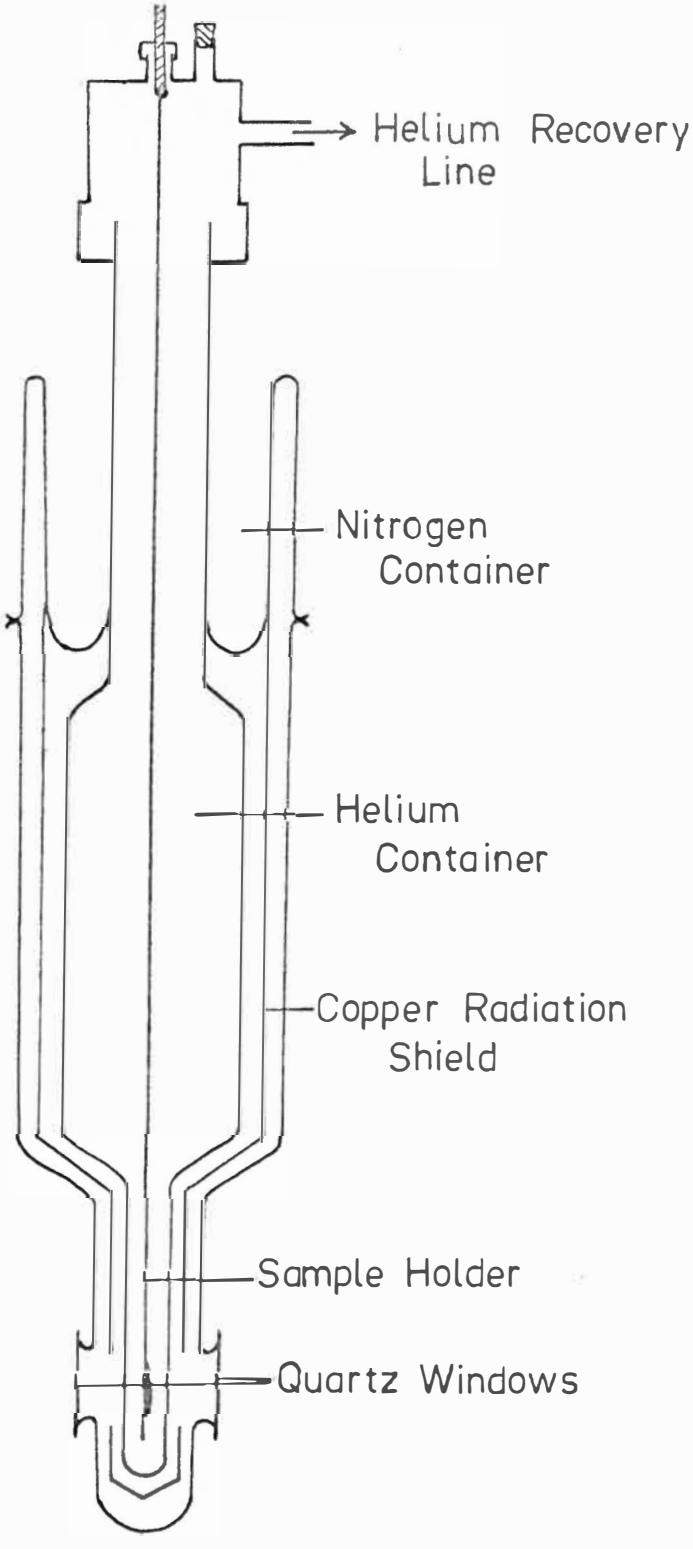

Figure 6. Glass helium dewar

did not make any noticeable difference to the spectra, no extensive studies were made at this temperature. The dewar held one litre of liquid helium which lasted up to four and a half hours.

The immersion dewars were ideally suited for use with photographic plates as they kept the sample at a constant temperature over a long period of time. As the photographic plate integrates the signal over the time of the exposure, the bubbling of the coolant has no effect on the spectrum. However, for direct photoelectric recording, in which the spectrum is scanned, the bubbles produce noise in the signal and so it is necessary to use the conduction dewars.

There are several conduction dewars in the Department. A Hoffman helium dewar and a similar one constructed in the Department's workshop were used to obtain many of the absorption spectra. A variable temperature dewar, made by Andonian Associates, was used for the temperature dependence study of the luminescence and also for absorption spectra when the other fixed temperature dewars were not available.

Figure 7 shows the basic features of the Andonian. After the crystal has been mounted, the vacuum jacket is pumped down to less that 50μ , the outer can filled with liquid nitrogen or air, and the inner can filled with

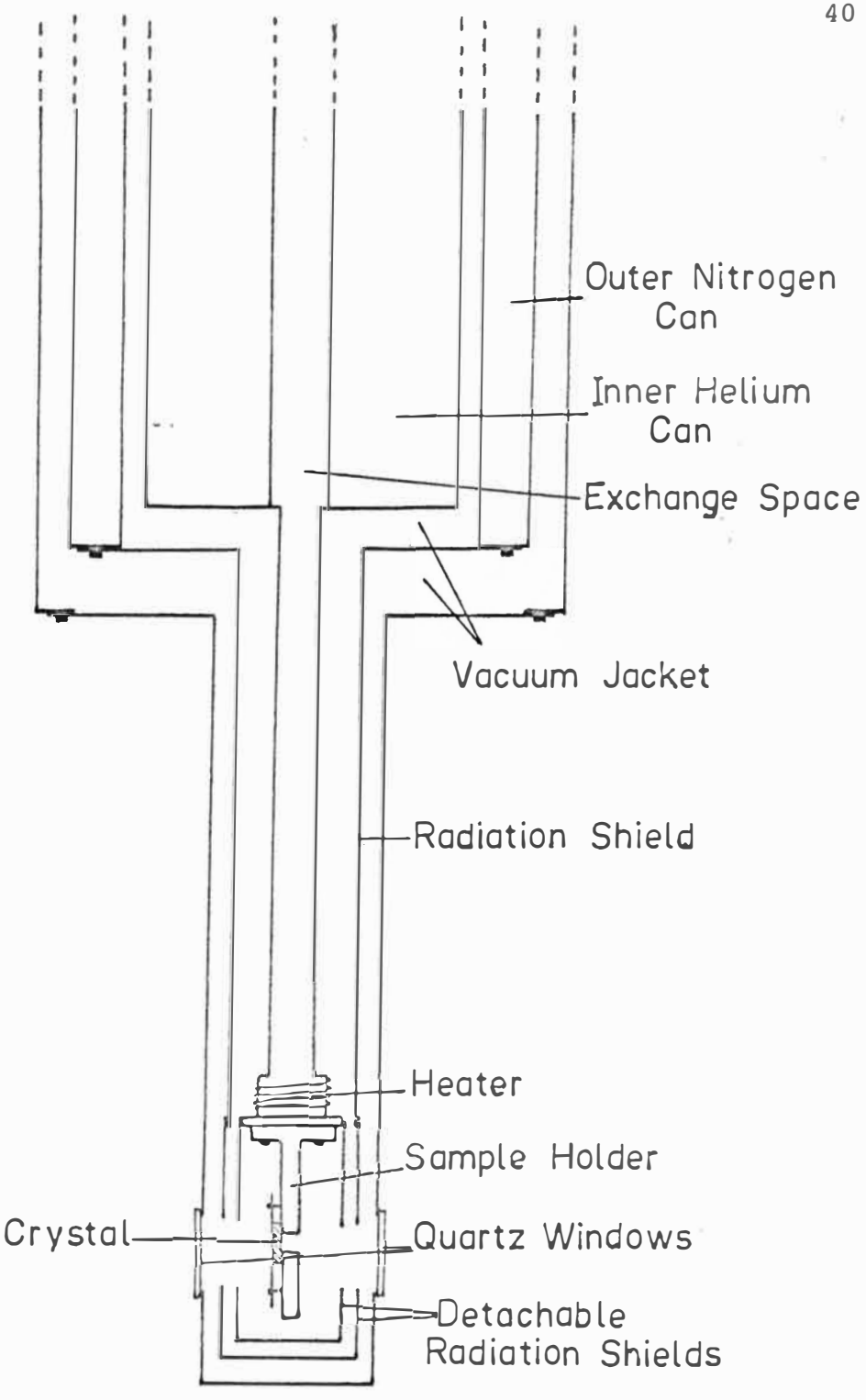

Figure 7. Andonian dewar

liquid helium. The exchange space, previously evacuated is pressurized to just above one atmosphere with helium gas, when some of it will liquify and the crystal will be cooled by conduction through the copper block to 10^{o}K. For operation at higher temperatures the heater and the pressure of the helium in the exchange space are controlled to give the required temperature, which is measured by a copper-constantan thermocouple mounted just above the crystal. For use at nitrogen temperature and above, liquid nitrogen is used in the inner can and nitrogen gas in the exchange space.

The other fixed temperature dewars consist of a nitrogen can and an inner helium can which extends down to the copper block on which the crystal is mounted. These could be used at either liquid nitrogen or liquid helium temperatures.

3-7 LIGHT SOURCES

Two light sources were used to excite the luminescence spectra. A G.E.C. 125 watt high pressure mercury vapour lamp with a black glass bulb (which transmits mainly ultraviolet) was used for the earlier photographic work and the temperature dependence studies on the 3.4 metre Jarrell-Ash. Later a Philips 500 watt, high pressure, water-cooled mercury lamp became

available and was used for further photographic work, where the sample was immersed in the coolant. The higher power enabled the exposure times to be greatly reduced.

CHAPTER 4

THE GROWTH AND STRUCTURE OF CRYSTALS

4-1 THE CHOICE OF CRYSTALS

The interpretation of spectroscopic data on ions, molecules and complexes in the solid state can be greatly facilitated by the choice of an appropriate host crystal. The absorption bands in a pure substance are often too strong for the details to be studied directly, so it is diluted by doping it into another crystal. This dilution also eliminates unwanted exchange effects.

When choosing a suitable host crystal several important factors should be considered.

1. It must be possible to grow relatively large (several millimetres across), single crystals of good optical quality, containing the required concentration of the impurity. The methods used to produce the crystals will be described in the next section.

2. The impurity must be incorporated into the lattice with the minimum of distortion. In ionic compounds this is best achieved when the impurity ion has the same charge as, and a similar mass to, the ion which it is replacing. If it is too large it will distort the lattice or not enter it at all. If it is very small it

will be able to move around creating its own localised vibrational modes. Heavy or light impurities (compared to the ions they replace) will also produce noticeable changes in the crystal's vibrational spectrum. The table below shows the electronic configuration of all the quadruply ionised central ions used, their mass and their ionic radii[51].

	Zr	Hf	Sn	Ir	Pt	Pd
Ionised configuration	$4d^0$	$5d^0$	$4d^{10}$	$5d^5$	$5d^6$	$4d^6$
Mass	91.22	178.49	118.69	195.09	192.2	106.4
Ionic radius (Å)	.79	.78	.71	.65	.68	.65

3. For optical studies the host crystal should have no absorption bands in the range being studied. The colour of transition-metal ions is due to transitions between states arising from a partly filled d shell. If the central metal ion has either an empty or a completely full d shell, then the first absorption, generally occurring at higher energies, will be due to an electron-transfer transition. The absorption spectrum of the $ZrCl_6^{2-}$ complex in acetonitrile has been measured by Brisdon, Lester and Walton[52]. They found the lowest absorption band in the ultraviolet at 42,400 cm^{-1}. Axe[53]

reports that Cs_2ZrCl_6 crystals are transparent down to 3000Å. Dorain et al.[54] report that the first absorption of properly prepared Cs_2HfCl_6 crystals occurs at a wavelength of less than 2400Å. The crystals grown here were far from perfect and the start of the absorption bands generally occurred at lower energies. No data was available for $SnCl_6^{2-}$, but in the K_2SnCl_6 crystals used, the cut-off was at about 30,000 cm^{-1}. The K_2SnBr_6 crystals were yellow, showing that the electron-transfer band had moved into the visible.

4. If the symmetry of the crystal is known, group theory can be used to label the states and to obtain selection rules for possible transitions.

5. Choosing a host crystal which has already been used for other studies enables the results obtained to be correlated to earlier results. Knowledge of the vibrational modes, their symmetries and frequencies, is most helpful in interpreting the vibronic sidebands which are frequently observed in transition-metal ion spectra.

It is not usually possible to find a host crystal satisfying all these requirements, and so some compromise is necessary.

4-2 GROWTH OF CRYSTALS

All the crystals used were grown in the Physics Department, either from aqueous solution (the tin salts) or from the melt (the zirconium and hafnium salts). The platinum group compounds used as starting materials were supplied by New Metals and Chemicals Ltd, London, and were 99.9% pure. All other materials used were high grade Analar reagents.

The K_2SnCl_6 crystals were grown from acid solutions containing 0.1% to 5% of the dopant. The K_2SnCl_6 was prepared by evaporation from an acid solution containing stoichometric quantities of KCl and $SnCl_4$. While K_2SnCl_6 is readily soluble in water, the platinum group complexes are almost insoluble in cold water (.48 gm/cc at 2^oC for K_2PtCl_6) and only slightly soluble at higher temperatures (5.22 gm/cc at 100^oC for K_2PtCl_6). Because of this large difference in solubility it was extremely difficult to produce large, single, doped crystals. The K_2PtCl_6, or K_2IrCl_6, would usually precipitate out first, forming nuclei for a mass of polycrystals. Only in one attempt were the crystals containing K_2IrCl_6 of usable size. The concentration of iridium in these crystals varied; those which grew first being the most heavily doped. None of the platinum doped crystals were large enough to use as single

crystals, but some absorption spectra were taken on an aggregrate of polycrystals.

Yellow K_2SnBr_6 crystals were grown by the same method, but attempts to dope them with K_2PtBr_6 and K_2IrBr_6 were unsuccessful.

Pure crystals of K_2PtCl_6 and K_2PtBr_6 were grown by cooling hot acid solutions which were nearly saturated with K_2PtCl_6 or K_2PtBr_6[55]. These were optically too dense to obtain spectra from. Crystals containing various concentrations (up to 10%) of iridium were also grown. These would be suitable for e.s.r. measurements, but the platinum absorption makes it impossible to observe the optical spectrum of the iridium.

The Cs_2ZrCl_6 and Cs_2HfCl_6 crystals were grown from the melt by Mr R. Ritchie, using the Bridgeman method described by Axe, Stapleton and Jefferies[56]. The Cs_2ZrCl_6 (Cs_2HfCl_6) was prepared by dissolving $ZrCl_4$ ($HfCl_4$) in HCl saturated methanol, adding the appropriate amount of CsCl, and refluxing for several hours. The white precipitate was washed with HCl saturated methanol and dried in a vacuum. It was then sublimed under vacuum and sealed off in a quartz tube under half an atmosphere of nitrogen. By lowering the capsule through a gradient furnace, with a maximum temperature of 850^{o}C, the impurities were concentrated at the bottom and were readily removed.

When the pure Cs_2ZrCl_6 (Cs_2HfCl_6) had been obtained it was ground to a fine powder, mixed with the appropriate amount of Cs_2PtCl_6 or Cs_2IrCl_6 (1-5%), sealed off and recrystallised. There was considerable variation in the quality of the crystals obtained; the best were large single crystals of reasonably good optical quality which cleaved easily, but most were strained, and shattered when cut. No satisfactory method of polishing the crystals was found. Those which cleaved easily had good surfaces already which did not require polishing, while those with poor surfaces shattered while being polished. It was noticeable that the dopant, particularly in the Cs_2ZrCl_6/Ir crystals, tended to concentrate near the bottom and sides of the crystals so that several samples of different concentration could be obtained from one crystal*.

---

*Since the experimental work has been completed the method used to purify the Cs_2ZrCl_6 and Cs_2HfCl_6 has been improved, resulting in better quality crystals. Instead of purification by sublimation, the powder, together with the dopant, is placed on a sintered quartz filter in a quartz tube. Just below the filter a side arm enables HCl gas to be blown up through the filter and powder. After all the air has been flushed out of the system, the tube is placed in a vertical furnace, heated to about 50^{o} above the

The hexabromo complexes of zirconium and hafnium were unstable and decomposed on heating.

In order to lower the symmetry of the octahedral MX_6^{2-} complex some Cs_2IrBr_6 was doped into a crystal of Cs_2ZrCl_6 in the hope that some of the chlorine and bromine atoms would be interchanged, producing a mixed halide complex of lower symmetry. It appeared from the spectra that most of the $IrBr_6^{2-}$ had been converted to $IrCl_6^{2-}$, although there was some evidence that the crystal was distorted.

4-3 CRYSTAL STRUCTURE

All of the crystals used had the face-centred cubic structure of the K_2PtCl_6 type, $Fm3m$[48]. It has an anti-fluorite structure with the octahedral $PtCl_6^{2-}$ complex

---

*(contd)

powder's melting point, and held at this temperature for one or two hours while HCl is blown through. The HCl is then passed through in the opposite direction forcing the molten salt through the filter into the quartz tubing below, where it is sealed off before being passed through the gradient furnace. Using this method it should be possible to control the concentration of the dopant and to produce single crystals of good optical quality.

replacing the Ca^{2+}, and the K^{+} replacing the F^{-}. The portion of the unit cell shown in Figure 8 shows the symmetry of the Pt^{4+} site. The cube formed by the potassium ions is repeated throughout the crystal, but the $PtCl_6^{2-}$ complexes are alternately placed in these cubes so that the six cubes which share faces with the one shown are empty. Thus each platinum ion has a regular octahedron of chlorine ions around it. Each of these octahedra is surrounded by eight potassium ions, each of which is itself surrounded by four $PtCl_6^{2-}$ complexes.

Table III lists a number of compounds, which have the K_2PtCl_6 structure, and their cell dimensions[48]. The cell sizes of all the substances used, except Cs_2HfCl_6, are either given in the table or can be estimated from the data given for closely related compounds. Because no data was available for Cs_2HfCl_6 it was decided to measure its cell size, along with those of the other host lattices, Cs_2ZrCl_6 and K_2SnCl_6.

Since the cell dimensions of the dopant materials differ by less than two per cent from those of the host lattices, the amount of distortion in the doped crystals will be small.

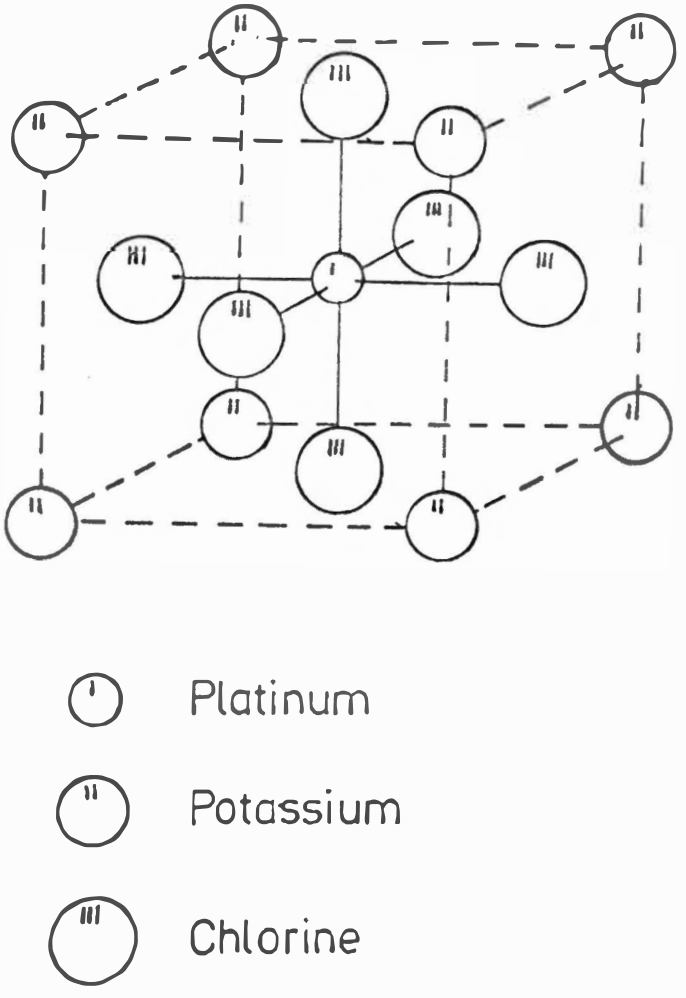

Figure 8. Structure of K_2PtCl_6

Table III. Crystal cell dimensions

Compound	Unit cell dimension a_o (Å)
Cs_2ZrCl_6	10.407
K_2SnCl_6	10.002
K_2PtCl_6	9.755
Cs_2PtCl_6	10.215
$(NH_4)_2PtCl_6$	9.858
$(NH_4)_2IrCl_6$	9.87

4-4 X-RAY DETERMINATION OF CELL DIMENSIONS

Because hafnium is just below zirconium in the periodic table, and their tetrapositive ions have almost the same radius, it is most likely that the structure of Cs_2HfCl_6 will be the same as Cs_2ZrCl_6. Since X-ray data on Cs_2ZrCl_6 is available[48,53], a comparison of the diffraction patterns of the two compounds should make it possible to determine the cell dimensions of Cs_2HfCl_6.

The Physics Department has a Philips PW 1009/30 X-ray generator. A small Debye-Scherrer powder camera was used to record the diffraction patterns of Cs_2ZrCl_6 and Cs_2HfCl_6. The powder was mounted in a fine capillary tube at the centre of the camera. The two diffraction patterns were almost exactly the same, confirming that

Cs_2ZrCl_6 and Cs_2HfCl_6 have the same structure and similar lattice constants.

The cell sizes were determined from measurements made on a Philips 1050/25 wide range goniometer diffractometer in the Geology Department. (I am indebted to Mr A. Smith for making these measurements.) The powdered samples were mounted on a flat plate and irradiated with CuK_α radiation. The diffraction pattern was scanned from $2\theta = 14^o$, just below the first diffraction, to $2\theta = 70^o$, where the lines became very weak and broad. The indices were determined using $a_o = 10.4\text{Å}$ for Cs_2ZrCl_6.

By comparing the recordings of the X-ray spectra of Cs_2HfCl_6 and K_2SnCl_6 with that of Cs_2ZrCl_6 the observed lines were indexed. A small computer programme was written to calculate the cell dimensions. The results were

Cs_2ZrCl_6, $a_o = 10.41 \pm 0.02\text{Å}$

K_2SnCl_6, $a_o = 10.01 \pm 0.02\text{Å}$

Cs_2HfCl_6, $a_o = 10.38 \pm 0.02\text{Å}$

The values obtained agree with the previously published results (Table III).

An independent attempt was made to determine the crystal structure using a Buerger precession camera. This

method requires very small, perfect, single crystals. It was found that even the crystals which appeared to be perfect under the microscope were not single crystals. It was not possible to determine whether they were grown like that or whether they fractured while being cut. After many attempts this approach was abandoned.

C H A P T E R 5

THE SPECTRUM OF THE HEXACHLOROIRIDATE COMPLEX

5-1 INTRODUCTION

Until recently the only work done on the optical spectrum of the hexachloroiridate complex ion, $IrCl_6^{2-}$, had been carried out in solutions at room temperature, when only very broad absorption bands with no structure were observed. Babaeva[57] was the first to measure the spectrum, and he found three bands at 4900Å, 4240Å and 2860Å. The second band at 4240Å was resolved into a doublet by Inamura and Kondu[58]. In 1956 Jorgensen[59] reported another weaker band at 5750Å. The reflection absorption spectra of several compounds containing the $IrCl_6^{2-}$ complex have been shown to have the same features as the solution spectra[60]. These bands were all assigned as electron-transfer transitions from the ligand orbitals to the central ion orbitals[61].

During the past two years the $IrCl_6^{2-}$ spectra have been investigated in more detail. Day and Jorgensen[62] have doped methylammonium hexachlorostannate crystals, $(CH_3NH_3)_2SnCl_6$, with $IrCl_6^{2-}$ and measured the spectra of these hexagonal crystals at 20°K. The spectrum is interpreted solely in terms of electron-transfer, the weaker

bands being assigned to forbidden electron-transfer transitions. They do not discuss the possibility of d-d transitions occuring. Sleight and Hare[63] use a combination of ligand field theory and molecular orbital theory to interpret their observed spectrum of $IrCl_6^{2-}$ in K_2SnCl_6 at 80^oK. McCaffery et al.[64,65] have used magnetic circular dichroism measurements on $IrCl_6^{2-}$ to assist in the assignment of the $IrCl_6^{2-}$ spectra.

5-2 ENERGY LEVELS IN OCTAHEDRAL $IrCl_6^{2-}$

Ir^{4+} has a $5d^5$ configuration which, when placed in a strong octahedral electrostatic crystal field, splits into the following terms[29]:

t_{2g}^5 : $^2T_{2g}$ the ground state;

$t_{2g}^4e_g$: $^2A_{1g}$, $^2A_{2g}$, $^2E_g(2)$, $^2T_{1g}(2)$, $^4T_{1g}(2)$, $^4T_{2g}$;

$t_{2g}^3e_g^2$: $^2A_{1g}(2)$, $^4A_{1g}$, $^6A_{1g}$, $^2A_{2g}$, $^4A_{2g}$, $^2E_g(3)$, $^4E_g(2)$, $^2T_{1g}(4)$, $^4T_{1g}$, $^2T_{2g}(4)$, $^4T_{2g}$;

$t_{2g}^2e_g^3$: $^2A_{1g}$, $^2A_{2g}$, $^2E_g(2)$, $^2T_{1g}(2)$, $^4T_{1g}$, $^2T_{2g}(2)$, $^4T_{2g}$;

$t_{2g}e_g^4$: $^2T_{2g}$.

These terms are further split by spin-orbit coupling, which, in the 5d transition-metal ions, is very strong and cannot be neglected. The resulting levels are labelled by the representations Γ_6, Γ_7 and Γ_8 of the octahedral double group.

Because the energy difference between the t_{2g} and the e_g orbitals, Δ, is expected to be large (about 30,000 cm^{-1}) the optical spectrum of Ir^{4+} will involve only transitions between the t_{2g}^5 and the $t_{2g}^4 e_g$ configurations.

The electrostatic and crystal field matrices of Tanabe and Sugano[13] and Schroeder's spin-orbit matrices[8] were diagonalized using the parameters $\Delta = 30{,}600$ cm^{-1}, $B = 340$ cm^{-1}, $C = 3060$ cm^{-1} and $\zeta = 0$ or 2400 cm^{-1}. These calculated energy levels are shown at the left in Figure 9.

If the $IrCl_6^{2-}$ complex is considered, instead of only the Ir^{4+}, and electrons from the ligands are included in the energy calculation, the energy of possible electron-transfer states can be obtained. This involves making several approximations, and, until accurate wavefunctions for all the ions involved are known, only approximate energies can be calculated. Sleight and Hare[63] have carried out some calculations for $IrCl_6^{2-}$ which show that the low energy electron-transfer states lie

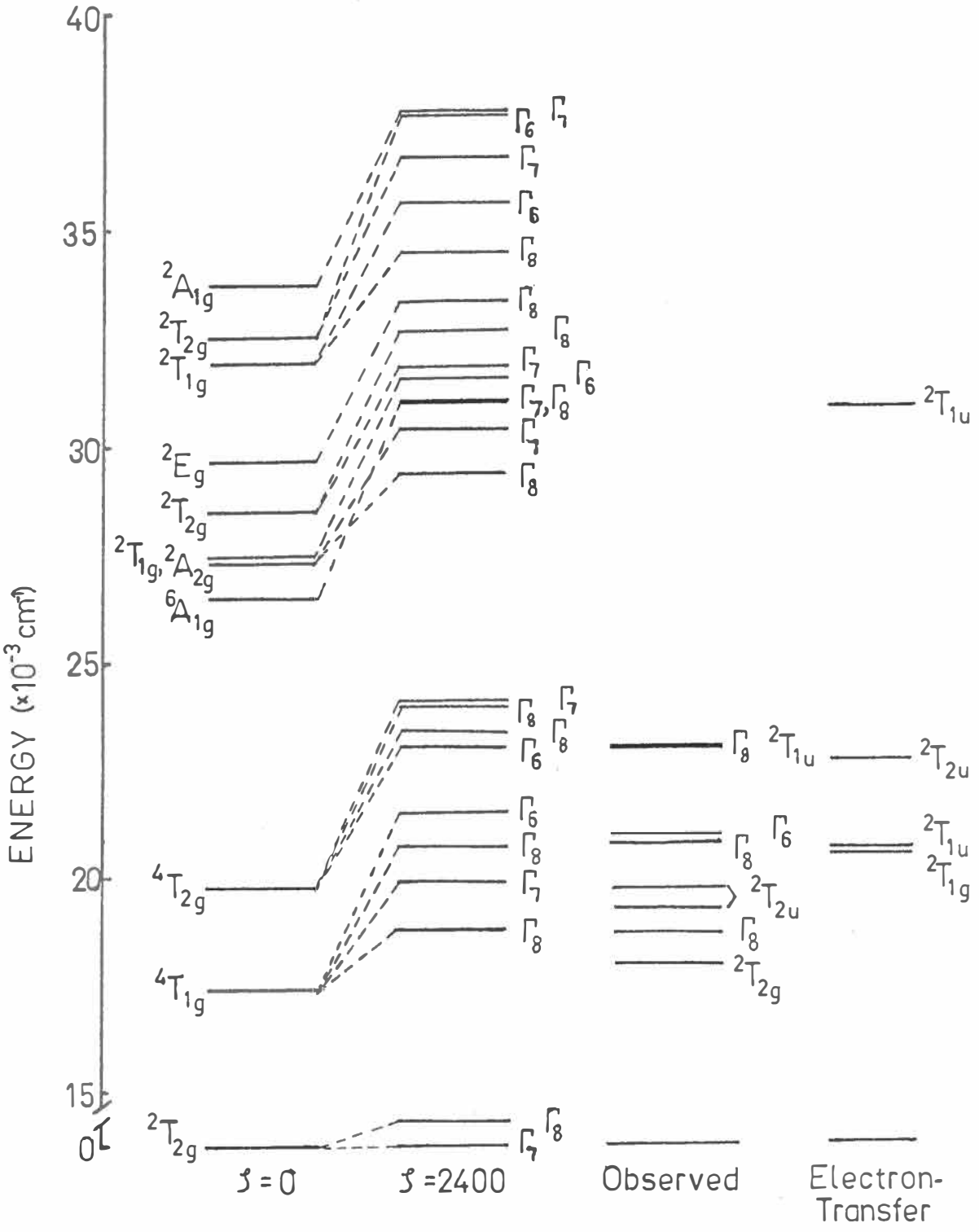

Figure 9. Energy levels in $IrCl_6^{2-}$

in the optical region of the spectrum and overlap the ligand field levels. Their results are shown at the right in Figure 9. Thus the usual assumption that the electron-transfer states are at a much higher energy and can be ignored, is no longer valid, and considerable mixing of states will occur, making interpretation of the spectra difficult.

5-3 VIBRATIONAL MODES

No measurements of the infrared or Raman spectra of Cs_2IrCl_6 have yet been published, but Hendra and Park[66] have measured the infrared and Raman spectra of K_2IrCl_6. By assuming that changing the cation will cause the frequencies to change in a similar manner to that observed for $PtCl_6^{2-}$ [67], the vibrational frequencies for the ground state of Cs_2IrCl_6 can be estimated to be (in cm^{-1}):

ν_1	ν_2	ν_3	ν_4	ν_5	ν_6	ν_7
340	220	330	170	190	80	70

ν_6 and ν_7 are not given by Hendra and Park but were estimated from the $PtCl_6^{2-}$ values. Comparison with measurements for $ReCl_6^{2-}$ and $OsCl_6^{2-}$ [68] and for $PtCl_6^{2-}$ [67] would suggest that ν_2 should be 270 cm^{-1}, ν_5 170 cm^{-1}, and ν_4 180 cm^{-1}.

It should be noted that these frequencies apply to the ground state and are not necessarily those of the excited states. Because of the difference between the t_{2g} and e_g orbitals, it is expected that the Ir-Cl bond length will increase, reducing the force constant and so, particularly for the stretching modes, the frequency will be reduced. This effect has already been observed in the spectra of $OsCl_6^{2-}$ and $ReCl_6^{2-}$ at helium temperature[54,55] and $IrCl_6^{2-}$ at nitrogen temperature[63].

5-4 EXPERIMENTAL RESULTS I: Cs_2ZrCl_6/Ir

The optical spectrum of Cs_2ZrCl_6/Ir (Figure 10) consists of two very strong bands centred at 23,800 cm^{-1} (A), and 19,600 cm^{-1} (C). Each of these bands has a considerable amount of vibrational structure at liquid helium temperature. Between these two bands are a number of weaker lines (B) which appear to be vibronic in origin. There are also some weak broad bands (D) on the low energy side of the strong bands. Figure 10 has been reconstructed from separate spectra of the four regions. It was necessary to reduce the intensities of bands A and C relative to the others to obtain the complete absorption spectrum on one diagram.

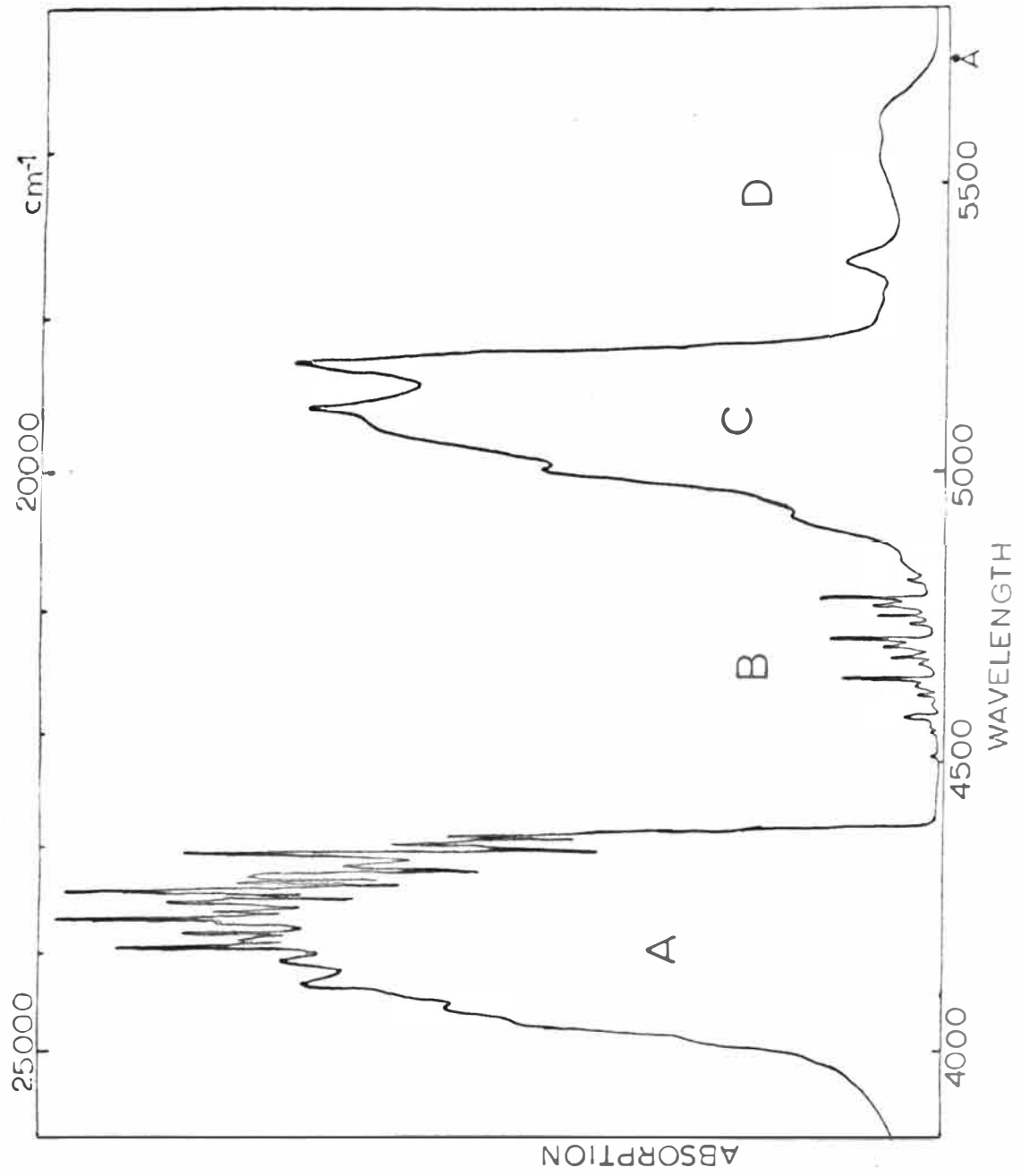

Figure 10. Optical spectrum of Cs_2ZrCl_6/Ir at helium temperature

A. 22,890 cm^{-1} to 24,900 cm^{-1}

The detailed spectrum of this band at helium temperature is shown in Figure 11 and the energies observed are listed in Table IV. The large number of lines observed makes assignment difficult.

Several overlapping progressions can be distinguished in this spectrum. The longest progressions which occur are in the lines 2, 7, 12, 16, 19, and 3, 8, 13, 17, 21, and 5, 10, 15, 18, 22 (Figure 11). Shorter progressions involving only three lines can be seen in lines 1, 6, 11, and 4, 9, 14, and 20, 23, 25. The spacing in all these progressions is 308 cm^{-1}, which can be assigned to the totally symmetrical vibrational mode ν_1. The change in the frequency from 340 cm^{-1} expected in the ground state, to 308 cm^{-1} observed in the excited state, is characteristic of the spectra of the 5d transition-metal hexahalides, and indicates an increase in the bond length.

It is not possible to assign all the lines to one electronic transition and its associated vibrational structure. If line 3 is taken to be a ν_4 vibration coupled to a d-d transition and we assume a value of about 170 cm^{-1}, then the corresponding no-phonon line would be at 22,897 cm^{-1}. A weak shoulder, 0, appears at 22,898 cm^{-1} and is taken to be the no-phonon line. With this assignment ν_4 has a value of 169 cm^{-1}, and line 2 can be

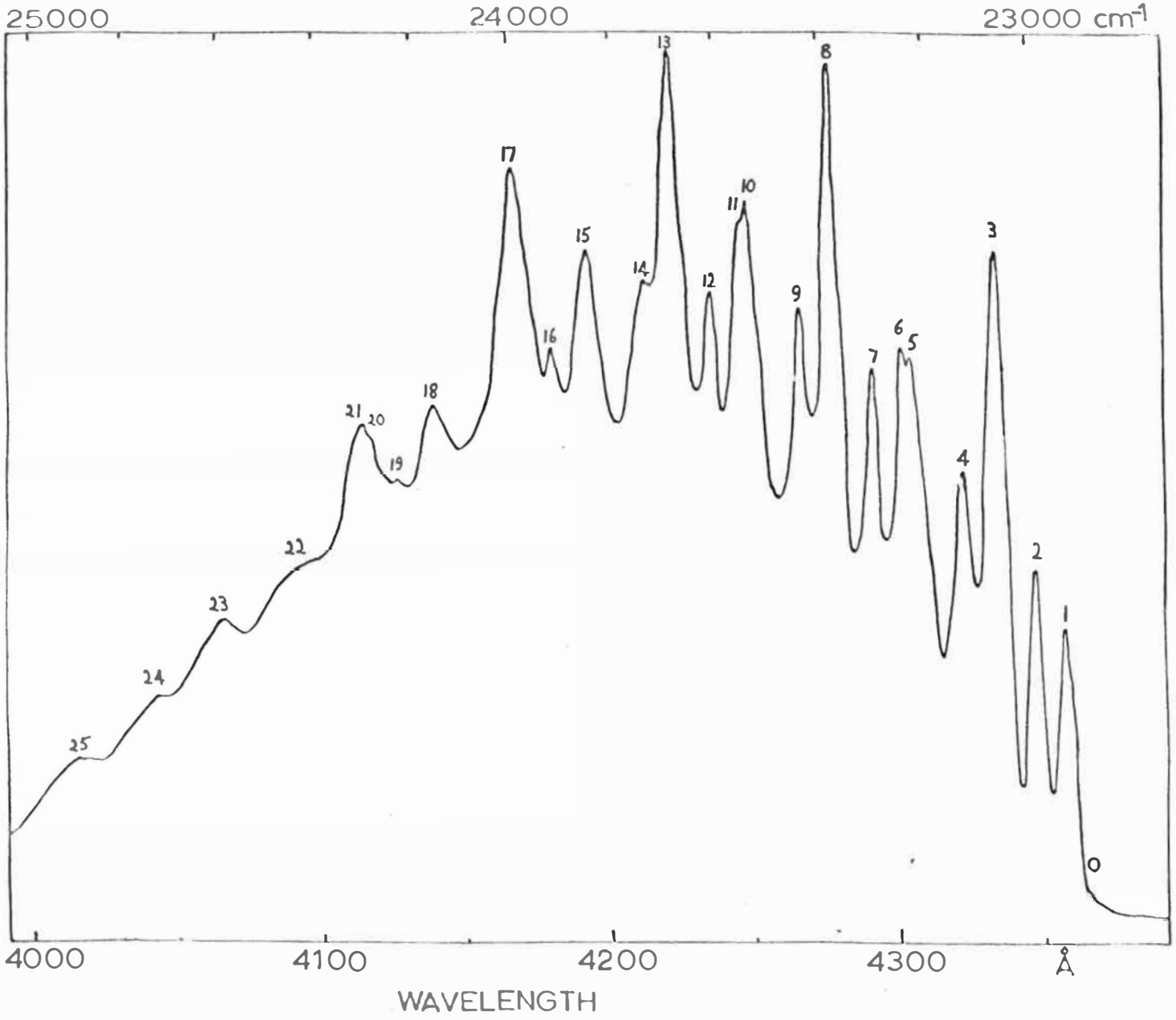

Figure 11. The detailed spectrum of Cs_2ZrCl_6/Ir in region A

Table IV. The observed optical transitions of Cs_2ZrCl_6/Ir and Cs_2HfCl_6/Ir in the energy range 22,890 to 24,900 cm^{-1} at helium temperature.

Fig.-Peak	Observed energy in Cs_2ZrCl_6 (cm^{-1})	Observed energy in Cs_2HfCl_6 (cm^{-1})	Assignment
11 - 0	22 898	22 908	$\Gamma_8(^4T_{2g})$
1	22 940	22 956	$^2T_{1u}$
2	22 992	23 003	$\Gamma_8 + \nu_6$
3	23 067	23 076	$+ \nu_4$
4	23 126	23 142	$^2T_{1u} + \nu_5$
5	23 225	23 238	$\Gamma_8 + \nu_3$
6	23 244	23 255	$^2T_{1u} + \nu_1$
7	23 298	23 314	$\Gamma_8+\nu_1+\nu_6$
8	23 377	23 385	$+\nu_1+\nu_4$
9	23 435	23 451	$^2T_{1u}+\nu_1+\nu_5$
10	23 534	23 550	$\Gamma_8+\nu_1+\nu_3$
11	23 550		$^2T_{1u} + 2\nu_1$
12	23 606	23 620	$\Gamma_8+2\nu_1+\nu_6$
13	23 687	23 690	$+2\nu_1+\nu_4$
14	23 735	23 756	$^2T_{1u}+2\nu_1+\nu_5$
15	23 848	23 854	$\Gamma_8+2\nu_1+\nu_3$
		23 877	$^2T_{1u} + 3\nu_1$
16	23 916	23 928	$\Gamma_8+3\nu_1+\nu_6$
17	23 994	24 003	$+3\nu_1+\nu_4$
18	24 154	24 171	$+ 3\nu_1+\nu_3$
		24 189	$^2T_{1u} + 4\nu_1$

Fig.-Peak	Observed energy in Cs_2ZrCl_6 (cm^{-1})	Observed energy in Cs_2HfCl_6 (cm^{-1})	Assignment
19	24 224	24 241	$\Gamma_8+4\nu_1+\nu_6$
20	24 283	24 291	
21	24 303	24 314	$\Gamma_8+4\nu_1+\nu_4$
22	24 455	24 467	$+4\nu_1+\nu_3$
		24 545	$+5\nu_1+\nu_6$
23	24 587	24 605	
		24 630	$\Gamma_8+5\nu_1+\nu_4$
24	24 715	24 733	
25	24 887	24 903	

assigned as ν_6, giving ν_6 a frequency of 94 cm^{-1}. Line 5 is 327 cm^{-1} above 0 and is assigned as ν_3.

If 308 cm^{-1} (ν_1) is added to the no-phonon line, the vibrational frequencies can be calculated from the second members of the progressions and are found to be ν_6 (92 cm^{-1}), ν_4 (171 cm^{-1}), and ν_3 (328 cm^{-1}), in close agreement with the previous values. Similar values are obtained from the remaining members of the series. Because all the vibronics associated with the line 0 involve one odd vibrational mode, the electronic transition must be to an even parity state, $^4T_{2g}$. This conflicts with the general principle that d-d transitions will be weak compared with the electron-transfer transitions.

The two shorter progressions starting at lines 1 and 4 arise from another transition. There are two reasons for this assumption, (apart from not being able to fit the energies numerically); (i) the ratio of the intensities of these two series with adjacent lines from the previous series do not remain constant, and (ii) in the spectrum taken at 80°K the line at 22,940 cm^{-1} was greatly reduced in intensity and the others belonging to this transition either were not seen at all or appeared only as very weak shoulders. The separation between lines 1 and 4 is 186 cm^{-1} which is very close to the expected value of ν_5. Since ν_5 is a vibration with even parity,

δ_{5g}, this transition must be to an odd state.

A molecular orbital calculation predicts an electron-transfer state in this region, while ligand field calculations also predict a d-d transition. Line 0 is therefore assigned as $^4T_{2g}$ and line 1 as $^2T_{1u}$.

Because the two energies differ by only 42 cm^{-1}, there will be considerable overlap of the wavefunctions, which would explain the unusually high intensity of the 'forbidden' d-d transition.

The progression observed in lines 20, 23 and 25 does not appear to be related to the two transitions above, but there is too little information to make any assignment. Similarly the weak shoulder at 24,715 cm^{-1} cannot be assigned.

B. 20,800 cm^{-1} to 22,200 cm^{-1}

The absorptions observed in this part of the spectrum are much less intense than those of the previous band and can be assigned to vibronics associated with d-d transitions. The spectrum is given in Figure 12 and the observed energies are listed in Table V.

Again several overlapping progressions are observed in lines 1, 7, 12, 17, and 3, 8, 13, 18, 21, and 4, 9, 14, 19, and 5, 10, 15, 20, and 6, 11, 16. Line 2 is very weak and there could be another line between 7 and

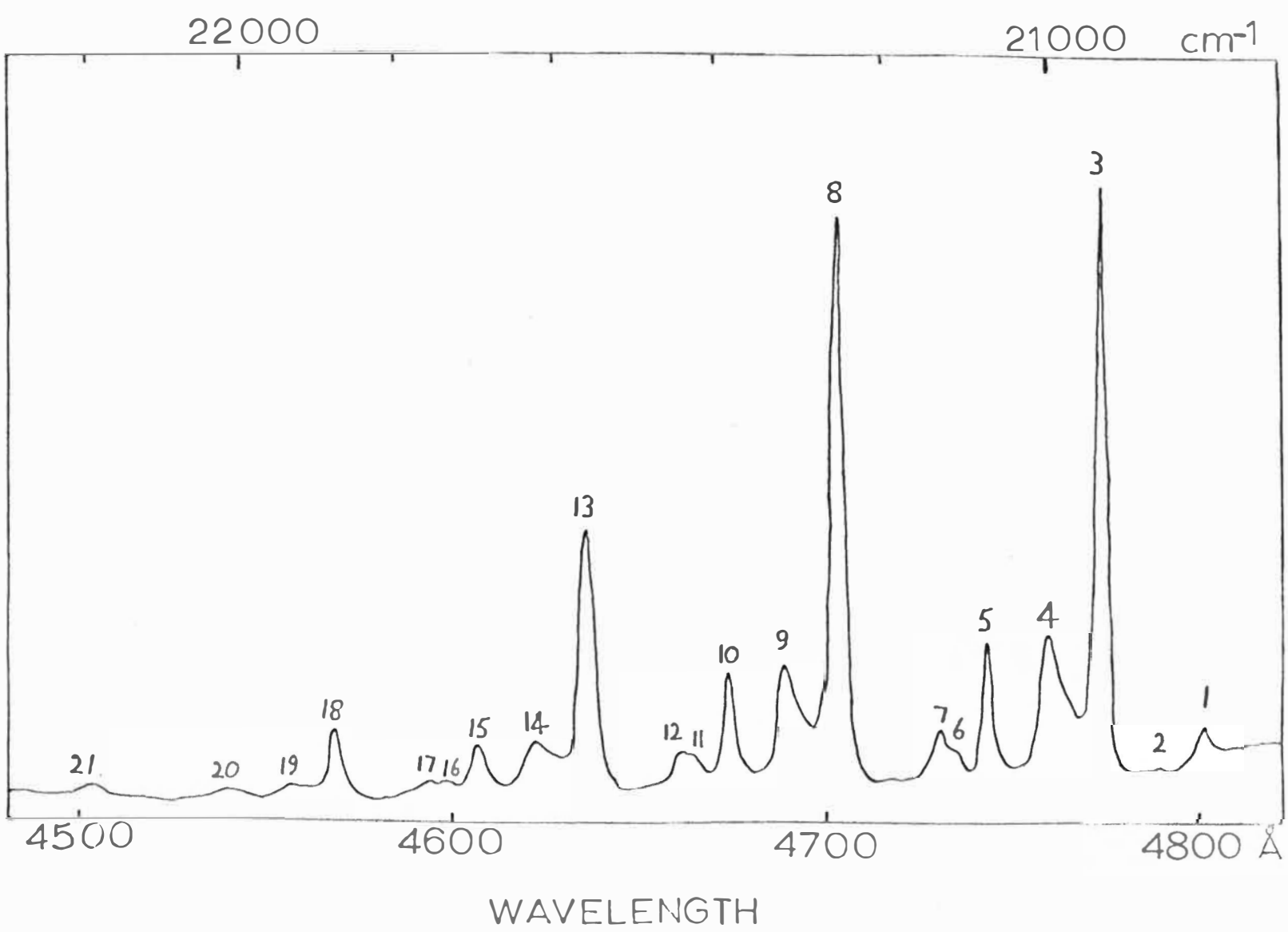

Figure 12. The detailed spectrum of Cs_2ZrCl_6/Ir in region B

Table V. The observed optical transitions of Cs_2ZrCl_6/Ir and Cs_2HfCl_6/Ir in the energy range 20,800 to 22,900 cm^{-1} at helium temperature.

Fig.-Peak	Observed energy in Cs_2ZrCl_6 (cm^{-1})	Observed energy in Cs_2HfCl_6 (cm^{-1})	Assignment
12 - 1	20 819	20 828	$\Gamma_8(^4T_{1g})+\nu_7$
2	20 870	20 880	$+\nu_6$
		20 915	$\Gamma_6(^4T_{1g})$
3	29 940	20 945	$\Gamma_8+\nu_4$
		20 989	
4	21 000	21 014	$\Gamma_6+\nu_6$
5	21 076	21 080	$+\nu_4$
6	21 113	21 118	$\Gamma_8+\nu_3$
7	21 131	21 140	$+\nu_1+\nu_7$
8	21 253	21 262	$+\nu_1+\nu_4$
		21 302	
9	21 314	21 327	$\Gamma_6+\nu_1+\nu_6$
10	21 387	21 394	$+\nu_1+\nu_4$
11	21 426	21 435	$\Gamma_8+\nu_1+\nu_3$
12	21 444	21 449	$+2\nu_1+\nu_7$
13	21 564	21 574	$+2\nu_1+\nu_4$
		21 616	
14	21 625	21 638	$\Gamma_6+2\nu_1+\nu_6$
15	21 698	21 707	$+2\nu_1+\nu_4$

Fig.-Peak	Observed energy in Cs_2ZrCl_6 (cm^{-1})	Observed energy in Cs_2HfCl_6 (cm^{-1})	Assignment
16	21 733	21 742	$\Gamma_8+2\nu_1+\nu_3$
17	21 752	21 761	$+3\nu_1+\nu_7$
18	21 876	21 885	$3\nu_1+\nu_4$
19	21 938	21 948	$\Gamma_6+3\nu_1+\nu_6$
20	22 006	22 020	$+3\nu_1+\nu_4$
		22 088	X
21	22 191	22 201	$\Gamma_8+4\nu_1+\nu_4$
		22 246	$X + \nu_4$
		22 257	$+ \nu_5$
		22 310	$+ \nu_2$
		22 400	$+ \nu_1$
		22 466	$+ \nu_1 + \nu_7$
		22 557	$+ \nu_1 + \nu_4$
		22 587	$+ \nu_1 + \nu_5$
		22 618	$+ \nu_1 + \nu_2$
		22 716	$+ 2\nu_1$
		22 777	$+ 2\nu_1 + \nu_7$
		22 861	$+ 2\nu_1 + \nu_4$

8 which would be the second member of another progression. The small increase of the interval in the progression to 312 cm^{-1} is indicative of a transition to a different state.

No zero-phonon line was observed to help in the analysis. If we assume the strong line 3 to be due to a d-d transition coupled to a ν_4 vibration of frequency 170 cm^{-1}, we get a value of 343 cm^{-1} for ν_3 which is considerably higher than the value found in A. If ν_4 is taken to be 166 cm^{-1} then the no-phonon transition energy would be 20,774 cm^{-1}. Line 1 is assigned to ν_7, a lattice mode, which has a value of 45 cm^{-1}. This is close to the 48 cm^{-1} found in $OsCl_6^{2-}$ by Dorain[54] which, it is noted, is very much smaller than the measured value in pure K_2OsCl_6. As no lattice modes of Cs_2ZrCl_6 have yet been measured, no further comment can be made. Line 6 is assigned to ν_3 which has a value 339 cm^{-1}. The very weak line 2 is 96 cm^{-1} away from the no-phonon energy and is probably a ν_6 mode.

The two remaining progressions, starting at lines 4 and 5, are separated by 76 cm^{-1}, which is close to the difference between ν_4 and ν_6. Hence they are assigned to a second d-d transition coupled to the ν_6 and ν_4 modes, respectively. The energy of the corresponding no-phonon transition would then be 20,910 cm^{-1}. The ν_3 vibronic which

would be expected to appear at 21,250 cm^{-1} is not seen, because it overlaps with the ν_4 vibronic from the first transition.

These two transitions are separated by 156 cm^{-1} and are assigned to transitions to $\Gamma_8(^4T_{1g})$ and $\Gamma_6(^4T_{1g})$.

C. 19,200 cm^{-1} to 20,400 cm^{-1}

The details of the spectrum of this intense absorption band are shown in Figure 13 and the energies are listed in Table VI. The only structure observed consists of two progressions 1, 2, and 3, 4, 5. The interval is 314 cm^{-1}, the ν_1 frequency. The band can be assigned as an electron-transfer transition to the $^2T_{2u}(t_{2u}^5)$ state. Under spin-orbit coupling this splits into a Γ_8 and a Γ_7 state, separated by 3/4 ζ_{Cl}, where ζ_{Cl} = 587 cm^{-1} is the spin-orbit coupling constant for Cl^{61}. This splitting of 440 cm^{-1} is equal to the separation between lines 1 and 3. The $^2T_{1u}$ state also splits under spin-orbit coupling into Γ_8 and Γ_6 states with the same separation. However, this splitting should not be observed because transitions to the Γ_6 state are forbidden.

The order of the levels T_{1u} and T_{2u} has recently been questioned. Jorgensen[3] and Schonland[39] place T_{2u} below T_{1u}, while McCaffery[64,65] has used magnetic

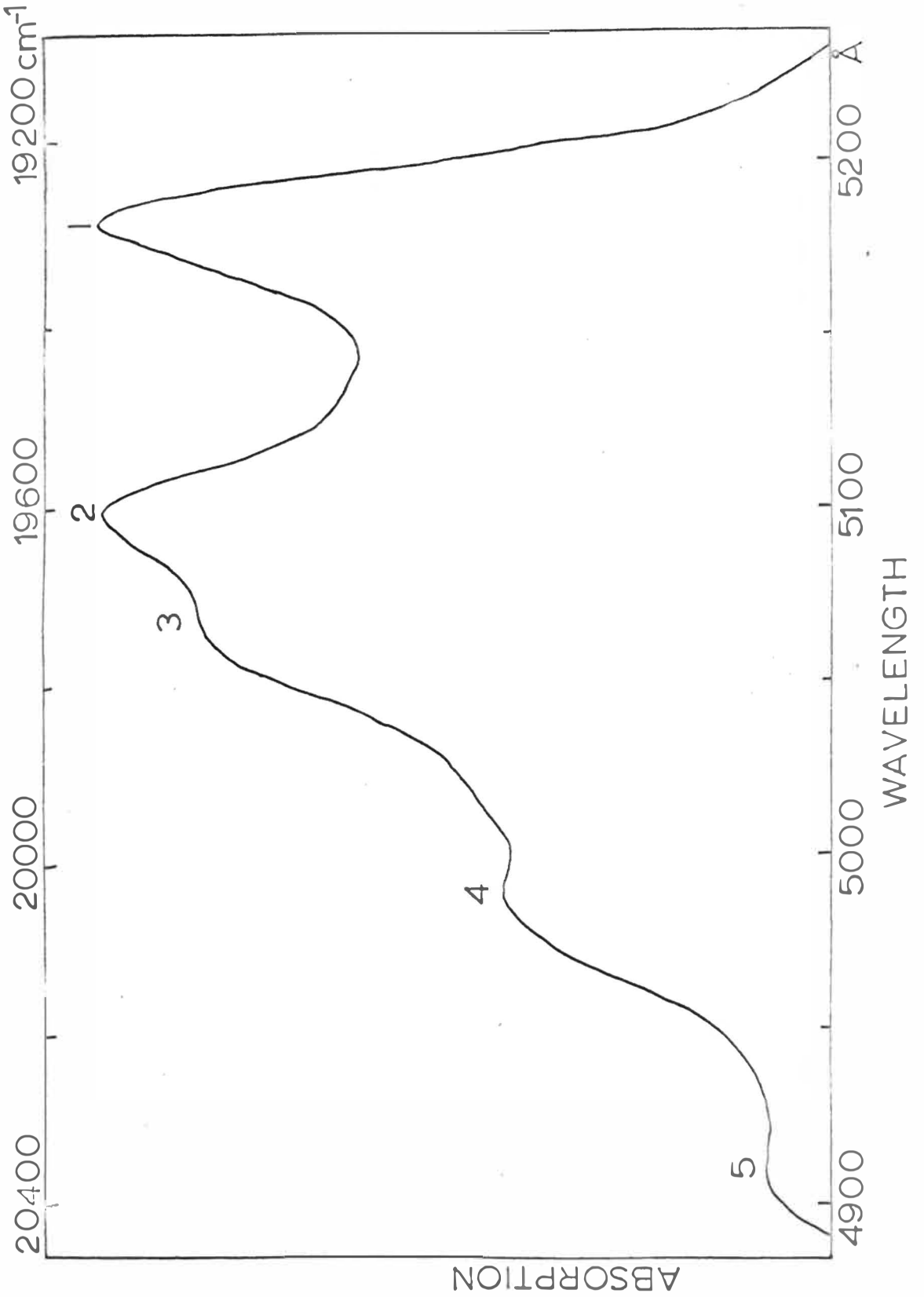

Figure 13. The detailed spectrum of Cs_2ZrCl_6/Ir in region C

Table VI. The observed optical transitions of Cs_2ZrCl_6/Ir and Cs_2HfCl_6/Ir in the energy range 19,200 to 20,400 cm^{-1} at helium temperature.

Fig.-Peak	Observed energy in Cs_2ZrCl_6 (cm^{-1})	Observed energy in Cs_2HfCl_6 (cm^{-1})	Assignment
13 - 1	19 292	19 303	$\Gamma_7(^2T_{2u})$
2	19 606	19 625	$+ \nu_1$
3	19 730	19 730	$\Gamma_8(^2T_{2u})$
4	20 043	20 051	$+ \nu_1$
5	20 357	20 373	$+ 2\nu_1$

Table VII. The observed optical transitions of Cs_2ZrCl_6/Ir and Cs_2HfCl_6/Ir in the energy range 17,790 to 18,980 cm^{-1} at helium temperature.

Observed energy in Cs_2ZrCl_6 (cm^{-1})	Observed energy in Cs_2HfCl_6 (cm^{-1})	Assignment
	17 798	$^2T_{2g}$
17 894	17 942	
18 127	18 137	
18 672	18 677	$\Gamma_8(^4T_{1g})$
18 845	18 857	$+ \nu_5$
18 948	18 980	$+ \nu_2$

circular dichroism measurements to show that the order is reversed. The splitting we have observed supports the earlier assignment.

D. 17,790 cm^{-1} to 18,980 cm^{-1}

This part of the spectrum lacks any detailed structure which might help in the assignment. It consists of a very broad double band, a sharper band, and two very weak bands (Figure 10). The observed energies are listed in Table VII. From previous work[62,63] transitions in this region can be assigned as d-d transitions to $^4T_{1g}$ states and electron-transfer transitions to $^2T_{1g}$ states. The first broad band is assigned as $^2T_{1g}$ while the band at 18,672 cm^{-1} is taken to be a transition to $\Gamma_8(^4T_{1g})$. The weak lines at 18,845 cm^{-1} and 18,948 cm^{-1} are 173 cm^{-1} and 275 cm^{-1} above this, and can be attributed to the ν_5 and ν_2 vibrations.

5-5 EXPERIMENTAL RESULTS II: Cs_2HfCl_6/Ir

The optical spectrum of Cs_2HfCl_6/Ir was so similar to that of Cs_2ZrCl_6/Ir that most of the lines of the two spectra could be placed in a one-to-one correspondence. This is done in Tables IV, V, VI and VII.

In band A the additional lines observed in the Cs_2HfCl_6/Ir spectrum are weak and can readily be assigned as further members of progressions already observed.

Several additional lines appeared in the region B (Table V). The very weak line at 20,915 cm^{-1} can be assigned as a zero-phonon transition to Γ_6. The stronger lines at 20,989, 21,302 and 21,616 cm^{-1} form a progression, which was not seen in the Cs_2ZrCl_6/Ir spectrum, and this could be due to a lattice mode. The most significant difference between the two spectra was a number of weak broad lines stretching from 22,088 to 22,861 cm^{-1} which appeared in the Cs_2HfCl_6/Ir spectrum. (These are listed at the end of Table V). They are assigned as the vibronics associated with an unidentified transition at 22,088 cm^{-1}, which may be due to a non-cubic component of the crystal field.

The strong band C showed identical structure in both crystals.

At the lower energies (Table VII) the broad double band was better defined and three lines could be distinguished.

Changing the host from Cs_2ZrCl_6 to Cs_2HfCl_6 produces an increase of about 12 cm^{-1} in all the energy levels. This change is the same as that observed in the spectrum of $OsCl_6^{2-}$ by Dorain et al.[54]

5-6 EXPERIMENTAL RESULTS III: K_2SnCl_6/Ir

The general features of the optical spectrum of K_2SnCl_6/Ir, which are the same as those of the Cs_2ZrCl_6/Ir spectrum (Figure 10), show two intense bands with weak structure between them, and some broad bands at a lower energy. The spectra do not show as much detailed structure, the lines being much broader, resulting in a decrease in the accuracy of the measurements. The spectrum was separated into the same four regions as before, and the energies of the absorptions observed in each of these are listed in Table VIII. The assignments have been made, where possible, using the previous assignments as a guide.

In band A fewer progressions were observed. Two of these could be assigned to the ν_3 and ν_4 modes coupled to a transition whose no-phonon energy would be at 22,600 cm^{-1}. No line was observed here. Other vibrational structure could well be hidden in these bands which were quite broad. The interval in these progressions was 312 cm^{-1}, the increase being consistent with changing the cation from Cs to K.

The interval in the progressions in the interband structure, B, was 316 cm^{-1}. This interband structure appears to be different from the corresponding region of the Cs_2ZrCl_6/Ir spectrum. The relative intensities and

Table VIII. The observed optical transitions of K_2SnCl_6/Ir at helium temperature.

Region - Number	Observed energy (cm^{-1})	Assignment
D - 1	17 910	$^2T_{1g}$
2	18 203	
3	18 764	$\Gamma_8(^4T_{1g})$
C - 1	19 549	$\Gamma_7(^2T_{2u})$
2	19 867	$+ \nu_1$
3	20 006	$\Gamma_8(^2T_{2u})$
4	20 324	$+ \nu_1$
5	20 634	$+ 2\nu_1$
B - 1	21 056	$\Gamma_8(^4T_{1g}) + \nu_4$
2	21 091	$\Gamma_6(^4T_{1g})$
3	21 225	$\Gamma_8 + \nu_3$
4	21 239	
5	21 266	$\Gamma_6 + \nu_4$
6	21 371	$\Gamma_8 + \nu_1 + \nu_4$
7	21 407	$\Gamma_6 + \nu_1$
8	21 541	$\Gamma_8 + \nu_1 + \nu_3$
9	21 555	
10	21 583	$\Gamma_6 + \nu_1 + \nu_4$
11	21 691	$\Gamma_8 + 2\nu_1 + \nu_4$
12	21 728	$\Gamma_6 + 2\nu_1$

Region - Number	Observed energy (cm^{-1})	Assignment
13	21 857	$\Gamma_8 + 2\nu_1 + \nu_3$
14	21 871	
15	21 900	$\Gamma_6 + 2\nu_1 + \nu_4$
16	22 006	$\Gamma_8 + 3\nu_1 + \nu_4$
17	22 186	$\Gamma_8 + 3\nu_1 + \nu_3$
A - 1	22 773	$\Gamma_8(^4T_{2g}) + \nu_4$
2	22 804	
3	22 929	$+ \nu_3$
4	23 088	$+ \nu_1 + \nu_4$
5	23 120	
6	23 238	$+ \nu_1 + \nu_3$
7	23 402	$+ 2\nu_1 + \nu_4$
8	23 429	
9	23 550	$+ 2\nu_1 + \nu_3$
10	23 712	$+ 3\nu_1 + \nu_4$
11	23 865	$+ 3\nu_1 + \nu_3$
12	24 032	$+ 4\nu_1 + \nu_4$
13	24 171	$+ 4\nu_1 + \nu_3$

separations of the lines have changed (Figure 14). If line 1 is assigned as $\Gamma_8 + \nu_4$, the no-phonon line would be at 20,888 cm^{-1} and lines 5 and 6 could be due to the ν_3 mode split by a non-cubic component of the ligand field. Line 2 is assumed to be the Γ_6 no-phonon line, and 7 is the associated ν_4 vibronic. This gives a separation of 203 cm^{-1} between the two transitions.

The rest of the spectrum differs little from that of Cs_2ZrCl_6/Ir. The intense absorption band, C, shows two progressions, with an interval of 318 cm^{-1}, separated by 457 cm^{-1}. At lower energies both the very broad double band and the single band can be seen, but the two weaker lines were not observed.

The no-phonon energies are higher in the K_2SnCl_6/Ir than in the Cs_2ZrCl_6/Ir except for band A where the energy is 200 cm^{-1} lower.

5-7 EXPERIMENTAL RESULTS IV: Cs_2ZrCl_6/Cs_2IrBr_6

If some of the chlorine atoms in the $IrCl_6^{2-}$ complex were replaced with bromine atoms, the symmetry of the complex would be lowered and some differences in the optical spectra should be observed. Since Cs_2ZrBr_6 was not stable enough to grow crystals from, it was decided to attempt to produce $IrCl_xBr_{6-x}^{2-}$ complexes by doping pure Cs_2ZrCl_6 crystals with Cs_2IrBr_6 in the hope that

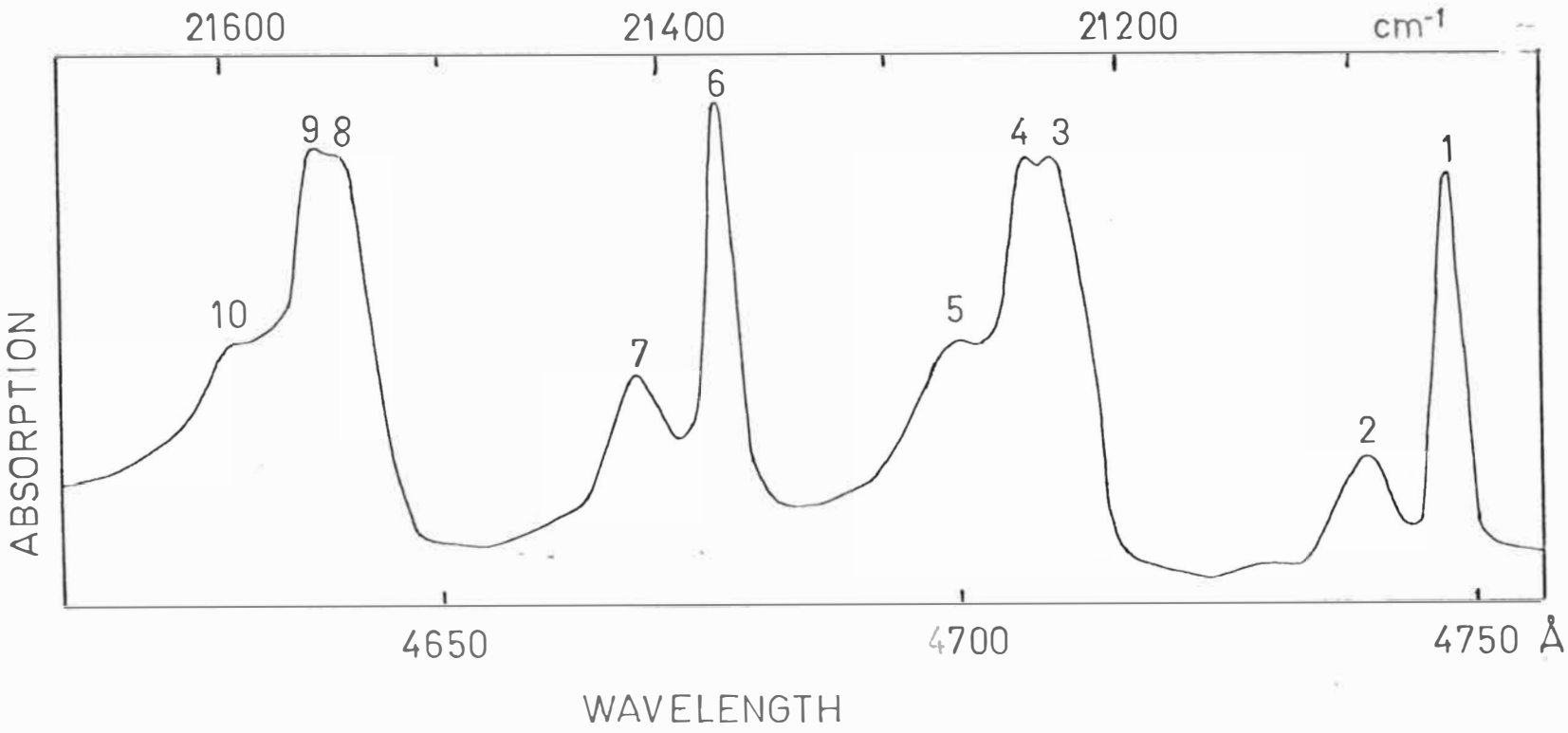

Figure 14. The detailed spectrum of K_2SnCl_6/Ir in region B.

some of the chlorine and bromine atoms would be interchanged.

The crystals produced were not of very good optical quality; most of the iridium was rejected and the remainder was not uniformly distributed throughout the crystal. The composition of the product could not be determined, but it probably contained varying amounts of the different mixed hexahalides. Two of the better pieces of the crystal were used to obtain the spectra, which, because of the low iridium concentration, were quite weak.

The general features of the optical spectrum of Cs_2ZrCl_6/Cs_2IrBr_6 (Figure 15) are the same as those of the Cs_2ZrCl_6/Ir spectrum (Figure 10), with two strong bands, A and C, separated by the weak structure, B, with some weak bands, D, at lower energies. The most notable difference between the two spectra was the appearance of a moderately strong band with considerable structure on the low energy side of band A. Band A itself has several additional lines.

The line and shoulder at 29,851 cm^{-1} and 28,927 cm^{-1} with some weak vibrational structure, which could only be seen indistinctly, can be assigned to either the electron-transfer or d-d transitions which the calculations (Figure 9) predict will occur in this region.

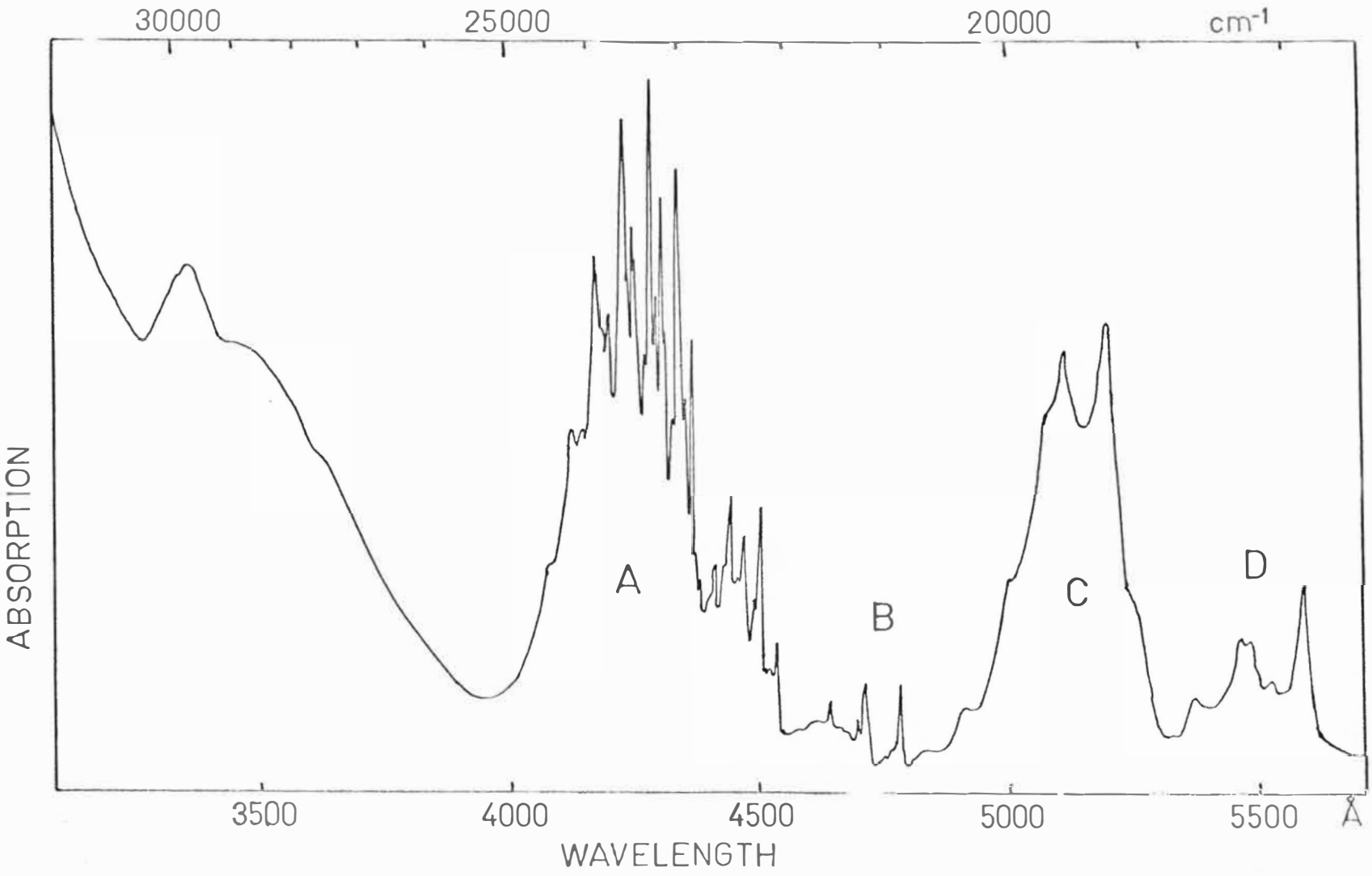

Figure 15. Optical spectrum of Cs_2ZrCl_6/Cs_2IrBr_6 at helium temperature

The detailed spectrum of band A and the band adjacent to it is shown in Figure 16 and the energies of the numbered lines are listed in Table IX. The assignments of most of the structure in band A can be made by comparison with the Cs_2ZrCl_6/Ir spectrum (Table IV). The additional lines observed can be assigned to the vibronics of another transition, which could be due to the non-cubic field splitting of the Γ_8 state. The occurrence of the ν_3, ν_4 and ν_7 vibrational modes, which have odd parity, indicate that it is to an even state.

The appearance of the moderately intense structure on the side of band A is interesting. No positive assignment can be made, but several groups consisting of two or three lines separated by about 312 cm^{-1}, the symmetric ν_1 frequency, can be seen. This band is probably due to transitions made "allowed" by the lowering of the symmetry. This would support the assignment of the weak broad lines in the same region of the Cs_2HfCl_6/Ir spectrum as being due to a non-cubic component of the crystal field.

The energies of the lines in the rest of the optical spectrum of Cs_2ZrCl_6/Cs_2IrBr_6 are listed in Table X together with the assignments, which are based on those made for the Cs_2ZrCl_6/Ir spectrum.

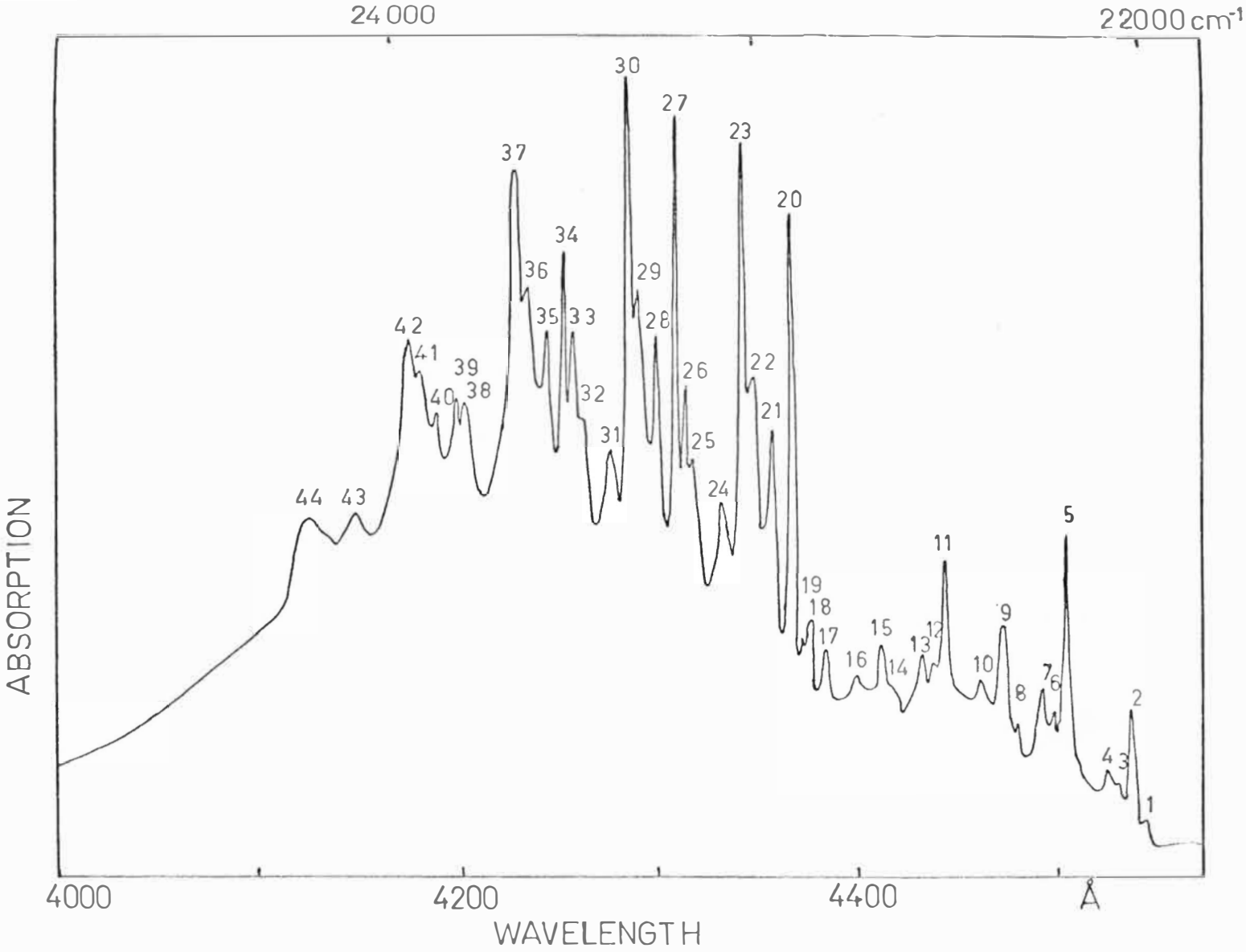

Figure 16. The detailed spectrum of Cs_2ZrCl_6/Cs_2IrBr_6 in region A

Table IX. The observed optical transitions of Cs_2ZrCl_6/Cs_2IrBr_6 in the energy range 22,000 to 24,300 cm^{-1} at helium temperature.

Figure - Peak	Observed energy (cm^{-1})	Assignment
15 - 1	22 040	1
2	22 069	2
3	22 098	3
4	22 127	4
5	22 226	6
6	22 256	7
7	22 290	8
8	22 350	$1 + \nu_1$
9	22 385	$2 + \nu_1$
10	22 448	$4 + \nu_1$
11	22 531	$6 + \nu_1$
12	22 557	$7 + \nu_1$
13	22 598	$8 + \nu_1$
14	22 695	$2 + 2\nu_1$
15	22 757	$4 + 2\nu_1$
16	22 840	$6 + 2\nu_1$

Figure - Peak	Observed energy (cm^{-1})	Assignment
17	22 882	$\Gamma_8(^4T_{2g})$
18	22 903	$A + \nu_7$
19	22 929	$^2T_{1u}$
20	22 982	$\Gamma_8 + \nu_6$
21	23 035	$A + \nu_4$
22	23 062	$\Gamma_8 + \nu_4$
23	23 120	$^2T_{1u} + \nu_5$
24	23 195	$A + \nu_3$
25	23 217	$\Gamma_8 + \nu_3$
26	23 244	$^2T_{1u} + \nu_1$
27	23 293	$\Gamma_8 + \nu_1 + \nu_6$
28	23 347	$A + \nu_1 + \nu_4$
29	23 374	$\Gamma_8 + \nu_1 + \nu_4$
30	23 429	$^2T_{1u} + \nu_1 + \nu_5$
31	23 501	$A + \nu_1 + \nu_3$
32	23 528	$\Gamma_8 + \nu_1 + \nu_3$
33	23 550	$^2T_{1u} + 2\nu_1$
34	23 601	$\Gamma_8 + 2\nu_1 + \nu_6$
35	23 656	$A + 2\nu_1 + \nu_4$
36	23 679	$\Gamma_8 + 2\nu_1 + \nu_4$
37	23 837	$\Gamma_8 + 2\nu_1 + \nu_3$
38	23 860	$^2T_{1u} + 3\nu_1$
39	23 911	$\Gamma_8 + 3\nu_1 + \nu_6$

Figure - Peak	Observed energy (cm^{-1})	Assignment
40	23 963	$A + 3\nu_1 + \nu_4$
41	23 991	$\Gamma_8 + 3\nu_1 + \nu_4$
42	24 142	$\Gamma_8 + 3\nu_1 + \nu_3$
43	24 271	$A + 4\nu_1 + \nu_4$

Table X. The observed optical transitions of Cs_2ZrCl_6/Cs_2IrBr_6 below 22,000 cm^{-1} at helium temperature.

Region - Number	Observed energy (cm^{-1})	Assignment
B - 1	20 902	$\Gamma_6(^4T_{1g})$
2	20 937	$\Gamma_8(^4T_{1g}) + \nu_4$
3	20 994	$\Gamma_6 + \nu_6$
4	21 069	$+ \nu_4$
5	21 216	$+ \nu_1$
6	21 248	$\Gamma_8 + \nu_1 + \nu_4$
7	21 305	$\Gamma_6 + \nu_1 + \nu_6$
8	21 380	$+ \nu_1 + \nu_4$
9	21 462	
10	21 495	
11	21 527	$\Gamma_6 + 2\nu_1$
12	21 560	$\Gamma_8 + 2\nu_1 + \nu_4$
13	21 616	$\Gamma_6 + 2\nu_1 + \nu_6$
14	21 871	$\Gamma_8 + 3\nu_1 + \nu_4$
C - 1	19 292	$\Gamma_7(^2T_{2u})$
2	19 602	$+ \nu_1$
3	19 734	$\Gamma_8(^2T_{2u})$
4	20 043	$+ \nu_1$
5	20 394	$+ 2\nu_1$

Region - Number	Observed energy (cm^{-1})	Assignment
D - 1	17 926	$^2T_{2g}$
2	18 121	
3	18 286	
4	18 337	$\Gamma_8(^4T_{1g}) + \nu_1$
5	18 645	

The structure in region B was much weaker and only the stronger lines were observed. Band C showed the same structure as before. In region D the spectrum was better defined than in the other spectra, showing that it is affected by the lowering of the symmetry. This effect of a non-cubic field component was also noticed in the Cs_2HfCl_6/Ir spectrum.

5-8 CONCLUSION

Arguments based mainly on the energies and vibrational structure have been used to assign the spectra of $IrCl_6^{2-}$ in Cs_2ZrCl_6, Cs_2HfCl_6 and K_2SnCl_6, and Cs_2ZrCl_6/Cs_2IrBr_6. Calculations show that molecular orbital theory, as well as ligand field theory, is necessary to interpret the observed spectra. Considerable mixing of the ligand and central ion orbitals occurs in the excited states. Griffiths et al.[23-25] have shown that, even in the ground state, the hole in the t_{2g} subshell of the iridium ion can be regarded as being about 5% in the p orbitals on each of the chlorine ions.

The similarities of the Cs_2ZrCl_6/Cs_2IrBr_6 and the Cs_2ZrCl_6/Ir spectra indicate that most of the Cs_2IrBr_6 in the former has been converted to Cs_2IrCl_6, but the appearance of the additional lines shows that, at least in some of the complexes, the symmetry has been lowered.

The occurrence of additional lines in the Cs_2HfCl_6/Ir spectrum suggests the presence of a non-cubic field component.

The criterion commonly used to distinguish between d-d and electron-transfer transitions — the d-d transitions are very weak compared to the electron-transfer transitions — has been shown to be unsatisfactory[54,55]. This is the case in band A where too much vibrational structure is present to enable the band to be assigned to electron-transfer only. The odd parity vibrational modes which are observed indicate that the transition is to an even state.

C H A P T E R 6

THE ABSORPTION SPECTRA OF THE HEXACHLORO COMPLEXES OF PLATINUM AND PALLADIUM

6-1 INTRODUCTION

Crystals of potassium hexachloroplatinate, K_2PtCl_6, have been used by Dorain and his co-workers[54,55] as hosts when investigating the low temperature optical spectra of Re^{4+} and Os^{4+}. Griffiths et al.[25] used crystals of it doped with various concentrations of $IrCl_6^{2-}$ to investigate the Ir-Ir exchange interactions in K_2IrCl_6 using e.s.r. methods. The usefulness of K_2PtCl_6 as a host depends on the fact that the Pt^{4+} ion has six d electrons which, in a strong octahedral crystal field, completely fill the t_{2g} orbitals. This means that there is an energy gap of more than 20,000 cm^{-1} from the ground state to the first excited state, which is useful for the observation of the low energy absorption spectra of other platinum group ions. The absence of any ground state splittings make it an ideal host lattice for e.s.r. work.

Despite its being used as a host lattice no work has been published on the optical spectrum of the crystal itself. Jorgensen[59,61] has reported the spectrum of the $PtCl_6^{2-}$ ion in solution. He identifies the lowest band

at 22,100 cm^{-1} as a transition to either the $^3T_{1g}$ or the $^3T_{2g}$ level, and the stronger band at 28,300 cm^{-1} as a transition to the $^1T_{1g}$ level. The intense band at 38,200 cm^{-1} is assigned to an electron-transfer transition.

It was while a preliminary study of the suitability of K_2PtCl_6 as a host lattice was being carried out that the red luminescence (Chapter 7) was found. This led to a detailed investigation of the absorption spectrum.

This chapter deals with the energy levels in the $PtCl_6^{2-}$ complex and the vibrational spectra. The absorption spectra recorded when the luminescence was initially being investigated are described briefly before making a detailed examination of the spectra of $PtCl_6^{2-}$ in crystals of Cs_2ZrCl_6 and Cs_2HfCl_6 at helium temperature. The spectrum of $PdCl_6^{2-}$ in Cs_2ZrCl_6 is discussed in the last section.

6-2 ENERGY LEVELS IN OCTAHEDRAL $PtCl_6^{2-}$

Pt^{4+} has a $5d^6$ configuration which, when placed in a strong octahedral electrostatic crystal field, splits into the following terms[29]:

t_{2g}^6 : $^1A_{1g}$ the ground state;

$t_{2g}^5 e_g$: $^1T_{1g}$, $^3T_{1g}$, $^1T_{2g}$, $^3T_{2g}$;

$t_{2g}^4 e_g^2$: $^1A_{1g}(2)$, $^1A_{2g}$, $^3A_{2g}$, $^1E_g(3)$, ^3E_g, $^1T_{1g}$, $^3T_{1g}(3)$, $^1T_{2g}(3)$, $^3T_{2g}(2)$, $^5T_{2g}$;

$t_{2g}^3 e_g^3$: $^1A_{1g}$, $^3A_{1g}$, $^1A_{2g}$, $^3A_{2g}$, ^1E_g, $^3E_g(2)$, ^5E_g, $^1T_{1g}(2)$, $^3T_{1g}(2)$, $^1T_{2g}(2)$, $^3T_{2g}(2)$;

$t_{2g}^2 e_g^4$: $^1A_{1g}$, ^1E_g, $^3T_{1g}$, $^1T_{2g}$.

These terms are further split by spin-orbit coupling which is strong in the 5d complexes. The resulting levels are labelled by the Γ_1, Γ_2, Γ_3, Γ_4 and Γ_5 representations of the octahedral group. The variation of the energy levels with the spin-orbit coupling constant ζ is shown in Figure 17 where the reduced parameters $\Delta/B = 70$, $C/B = 4.5$ and ζ/B have been used to calculate the energy levels E/B[8].

The electrostatic matrices for the d^6 configuration are the same as those given for the d^4 configuration by Tanabe and Sugano[13], but the crystal field matrix elements have their sign reversed. A change of sign also converts the spin-orbit matrix elements for d^4 given by Schroeder[8,34] into those appropriate for the d^6 configuration. No meaningful calculation of the energy levels could be made since it was not possible to identify the no-phonon energies, and there were too few d-d transitions to fit the parameters satisfactorily.

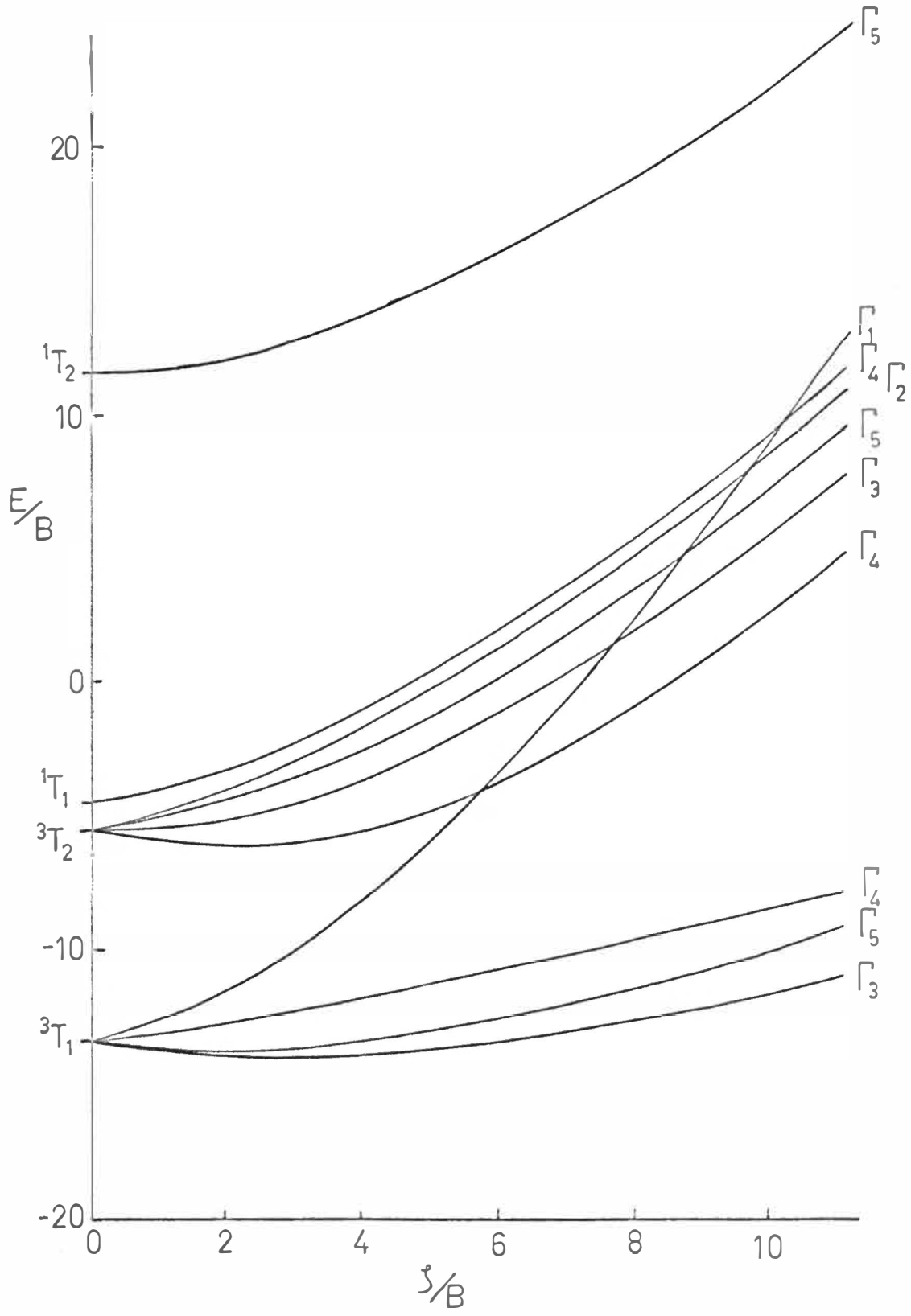

Figure 17. The energy level diagram for the $t_{2g}^5 e_g$ configuration

The electron-transfer transitions are expected to occur at higher energies than in $IrCl_6^{2-}$ since the t_{2g} orbitals are full and so the electron-transfer must be to an e_g orbital. This is in agreement with Jorgensen's assignments of the lower absorption bands in the $PtCl_6^{2-}$ spectra.

6-3 VIBRATIONAL MODES

The infrared and Raman spectra of materials containing the $PtCl_6^{2-}$ complex have been reported by a number of authors. Woodward and Creighton[69] have measured the Raman spectrum of $PtCl_6^{2-}$ in aqueous solution. Hiraishi and Shimanouchi[70] measured the infrared spectrum and used these measurements, together with those of Woodward and Creighton, to calculate the force constants. Hendra and Park[66] have measured both the infrared and Raman spectra and calculated the force constants. Debeau and Krauzman[71] have measured the infrared and Raman spectra of a large number of hexahalide complexes.

The most complete set of measurements of the vibrational spectra of solid hexachloroplatinates is given by Adams and Morris[67] who, besides measuring the vibrational levels of $PtCl_6^{2-}$ with various cations, have calculated the inactive ν_6 frequency and calculated the force constants. Their values for Cs_2PtCl_6 are (in cm^{-1}):

ν_1	ν_2	ν_3	ν_4	ν_5	ν_6	ν_7
337	312	332	186	172	83	73

6-4 EXPERIMENTAL RESULTS I.

The first attempts to measure the absorption spectra of $PtCl_6^{2-}$ met with very limited success because of the difficulty of obtaining a suitable crystal. The principal reason for making these measurements was to find an absorption band corresponding to the luminescence.

The low temperature spectra of pure K_2PtCl_6 crystals showed the major bands reported by Jorgensen[59], but the crystals were too small and too heavily absorbing to show the detailed structure of the bands. Some vibrational structure could be seen on the sides of the bands which could be assigned to the ν_1 vibrational mode.

No large single crystal of K_2SnCl_6 doped with platinum was grown, so an agglomeration of small crystals was used. This increased the scattering considerably, but the bands could still be identified. In addition to the previous bands a very weak shoulder appeared at 18,500 cm^{-1}. Further efforts to identify this band in the pure crystals and concentrated solutions of K_2PtCl_6 were unsuccessful. This is probably because a small crystal field perturbation in K_2SnCl_6/Pt enables the otherwise strongly forbidden band to be observed.

The spectrum of a concentrated K_2PtCl_6 solution (Figure 18) shows an additional band at 26,600 cm^{-1} not previously reported, while the band at 22,100 cm^{-1} shows some structure suggesting that it consists of two bands at 22,300 cm^{-1} and 20,400 cm^{-1}.

Later when it became possible to grow Cs_2ZrCl_6 and Cs_2HfCl_6 crystals doped with Cs_2PtCl_6 a detailed examination of their spectra was made.

6-5 EXPERIMENTAL RESULTS II. Cs_2ZrCl_6/Pt

The optical spectrum of Cs_2ZrCl_6/Pt (Figure 19) consists of a strong band (A) centred at 27,000 cm^{-1}, and a less intense band (B) at 22,300 cm^{-1}. A series of vibrational lines (C) which can only be observed at liquid helium temperature is centred at 18,700 cm^{-1}. There are also some vibrational bands on the side of the lattice absorption at higher energies. Each of these regions will be discussed in more detail.

A. 22,900 cm^{-1} to 28,200 cm^{-1}

The detailed spectrum of this band at liquid helium temperature is shown in Figure 20, and the energies observed are listed in Table XI.

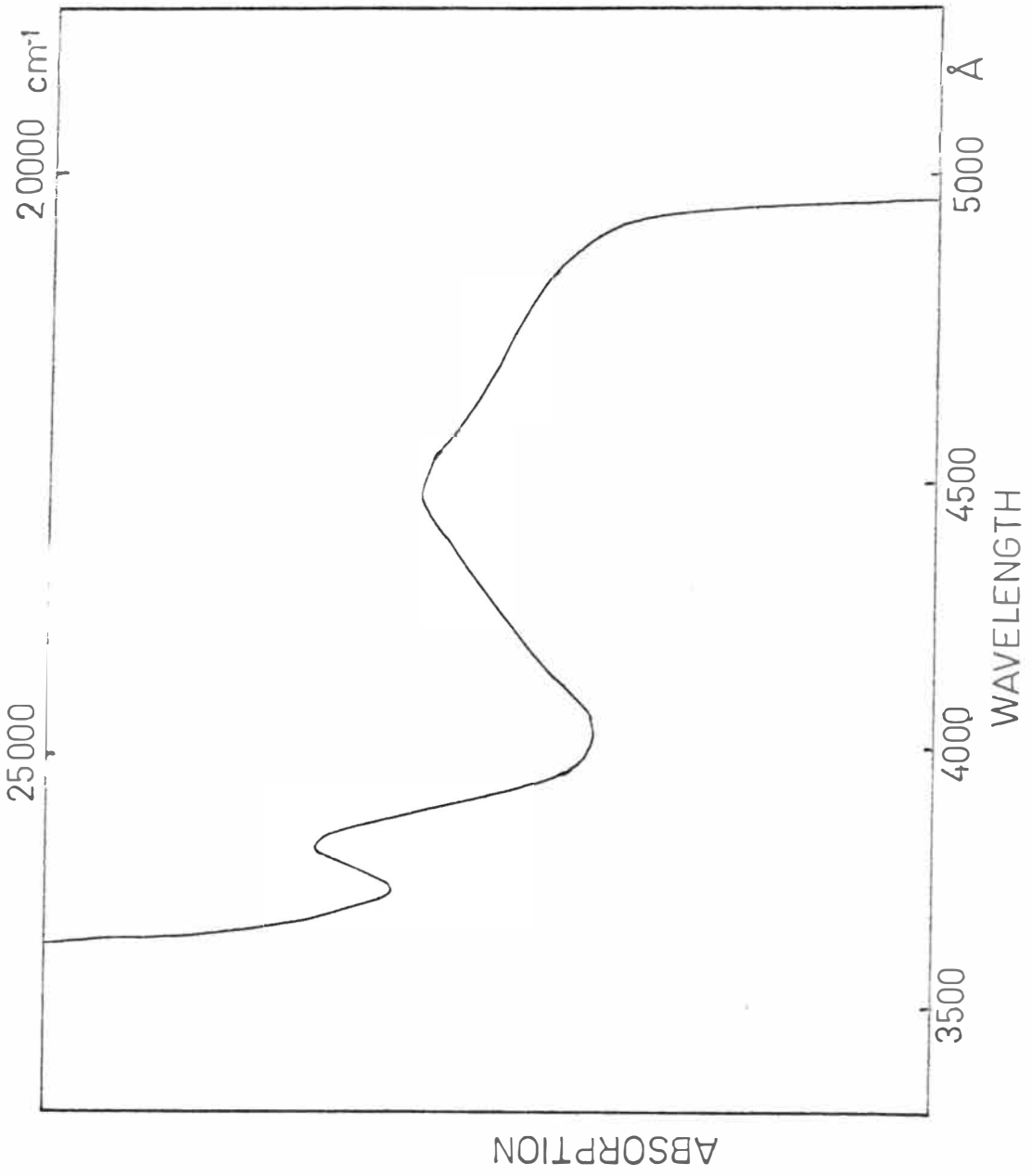

Figure 18. Absorption spectrum of a saturated solution of K_2PtCl_6 in water

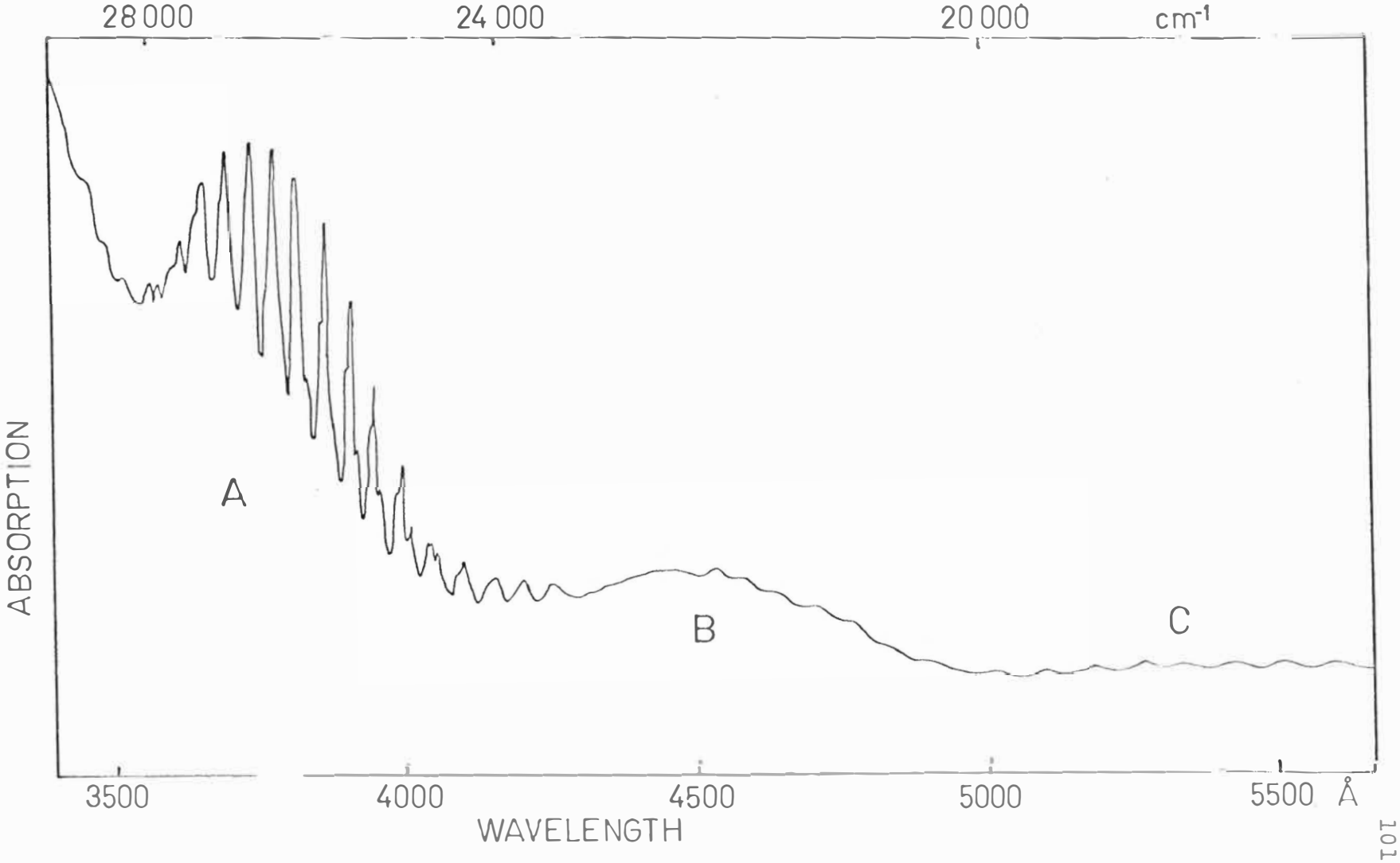

Figure 19. Absorption spectrum of Cs_2ZrCl_6/Pt at helium temperature

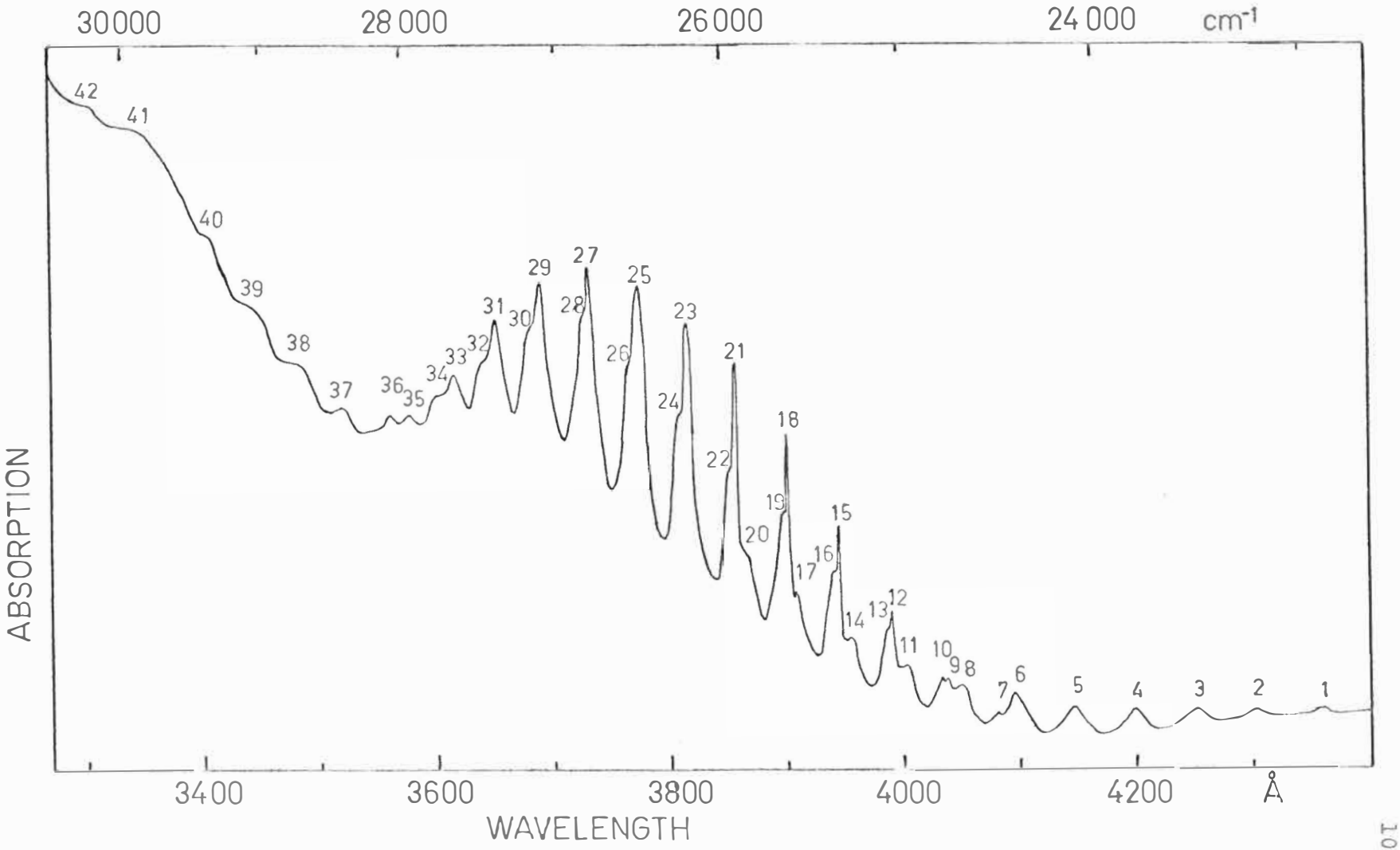

Figure 20. The detailed spectrum of Cs_2ZrCl_6/Pt in region A.

Table XI. The observed optical transitions of Cs_2ZrCl_6/Pt and Cs_2HfCl_6/Pt in the energy range 22,900 to 30,000 cm^{-1} at helium temperature.

Figure-Peak	Observed energy in Cs_2ZrCl_6 (cm^{-1})	Observed energy in Cs_2HfCl_6 (cm^{-1})	Assignment
20-1	22 972		$\Gamma_5(^3T_{2g})$
2	23 260		$+ \nu_1$
3	23 559		$+ 2\nu_1$
4	23 854		$+ 3\nu_1$
5	24 148	24 154	$+ 4\nu_1$
6	24 443	24 449	$+ 5\nu_1$
7	24 539	24 545	$\Gamma_4(^1T_{1g}) + \nu_6$
8	24 727	24 733	$\Gamma_5 + 6\nu_1$
9	24 813	24 819	$\Gamma_4 + \nu_4$
10	24 838	24 838	$+ \nu_1 + \nu_6$
11	25 030	25 037	$\Gamma_5 + 7\nu_1$
12	25 100	25 106	$\Gamma_4 + \nu_1 + \nu_4$
13	25 131	25 125	$+ 2\nu_1 + \nu_6$
14	25 329	25 329	$\Gamma_5 + 8\nu_1$
15	25 399	25 399	$\Gamma_4 + 2\nu_1 + \nu_4$
16	25 425	25 419	$+ 3\nu_1 + \nu_6$
17	25 634	25 640	$\Gamma_5 + 9\nu_1$
18	25 686	25 693	$\Gamma_4 + 3\nu_1 + \nu_4$
19	25 713	25 713	$+ 4\nu_1 + \nu_6$

Figure-Peak	Observed energy in Cs_2ZrCl_6 (cm^{-1})	Observed energy in Cs_2HfCl_6 (cm^{-1})	Assignment
20	25 926	25 926	$\Gamma_5 + 10\nu_1$
21	25 980	25 980	$\Gamma_4+4\nu_1+\nu_4$
22	26 014	26 014	$+5\nu_1+\nu_6$
23	26 277	26 281	$+5\nu_1+\nu_4$
24	26 308	26 301	$+6\nu_1+\nu_6$
25	26 567	26 574	$\Gamma_4+6\nu_1+\nu_4$
26	26 609	26 602	$+7\nu_1+\nu_6$
27	26 859	26 867	$+7\nu_1+\nu_4$
28	26 896	26 896	$+8\nu_1+\nu_6$
29	27 148	27 159	$+8\nu_1+\nu_4$
30	27 203	27 196	$+9\nu_1+\nu_6$
31	27 435	27 450	$+9\nu_1+\nu_4$
32	27 518	27 502	$+10\nu_1+\nu_6$
33	27 724	27 739	$+10\nu_1+\nu_4$
34	27 824	27 832	$+11\nu_1+\nu_6$
35	28 011	28 019	$+11\nu_1+\nu_4$
36	28 137	28 145	$+12\nu_1+\nu_6$
37	28 474	28 466	
38	28 794	28 785	
39	29 095	29 078	
40	29 421	29 421	
41	29 727	29 718	
42	30 003	30 012	

As with the iridium spectra several progressions can be seen. However there is not sufficient information in the platinum spectra to assist in the assignments. The two longest progressions, in the lines 7, 10, 13, 16, 19, 22, 24, 26, 28, 30, 32, 34, and 36, and the lines 9, 12, 15, 18, 21, 23, 25, 27, 29, 31, 33, and 35, appear to be associated. The spacings in these progressions is 295 cm^{-1} which can be assigned to the totally symmetric vibrational mode ν_1. If we use Jorgensen's original assignments as a guide, these two progressions can be assigned to the ν_6 and ν_4 vibronics associated with the $\Gamma_4(^1T_{1g})$ electronic state. Alternatively the first series could originate from the Γ_2 component of the $^3T_{2g}$ state which has a slightly lower energy than $\Gamma_4(^1T_{1g})$ (Figure 17).

The third series, lines 1, 2, 3, 4, 5, 6, 8, 11, 14, 17, and 20, starts at a lower energy, 22,972 cm^{-1}, and is clearly another transition. The repetition frequency, 295 cm^{-1}, is that of the ν_1 vibrational mode.

Unfortunately, there is no way of confirming these assignments, but it can be noted that they do follow the same pattern as the spectral assignments made by Schroeder[8,34] for the spectrum of K_3IrCl_6, which also has the d^6 configuration.

B. 20,500 cm^{-1} to 23,000 cm^{-1}

The vibrational structure observed in band B at helium temperature is shown in Figure 21, and the energies are listed in Table XII. All the vibrational lines observed belong to a progression in the totally symmetric mode, ν_1, which in this band has a frequency of 280 cm^{-1}. The progression is not likely to originate on a no-phonon line as this is a forbidden transition, but rather on one of the odd vibronics such as ν_4 which is generally the most intense. If it is assumed that line 11 is the ν_4 vibronic, then the no-phonon transition would occur at 20,590 cm^{-1}, and it is assigned to a transition to the $\Gamma_4(^3T_{2g})$ state.

Table XII. The observed optical transitions of Cs_2ZrCl_6/Pt and Cs_2HfCl_6/Pt in the energy range 20,500 to 22,900 cm^{-1} at helium temperature.

Figure-Peak	Observed energy in Cs_2ZrCl_6 (cm^{-1})	Observed energy in Cs_2HfCl_6 (cm^{-1})	Assignment
21-11	20 776	20 750	$\Gamma_4(^3T_{2g})+\nu_4$
12	21 047	21 060	$+\nu_1+\nu_4$
13	21 330	21 330	$+2\nu_1+\nu_4$
14	21 606	21 611	$+3\nu_1+\nu_4$
15	21 890	21 890	$+4\nu_1+\nu_4$
16	22 157	22 157	$+5\nu_1+\nu_4$
17	22 456	22 481	$+6\nu_1+\nu_4$
18	22 736	22 814	$+7\nu_1+\nu_4$

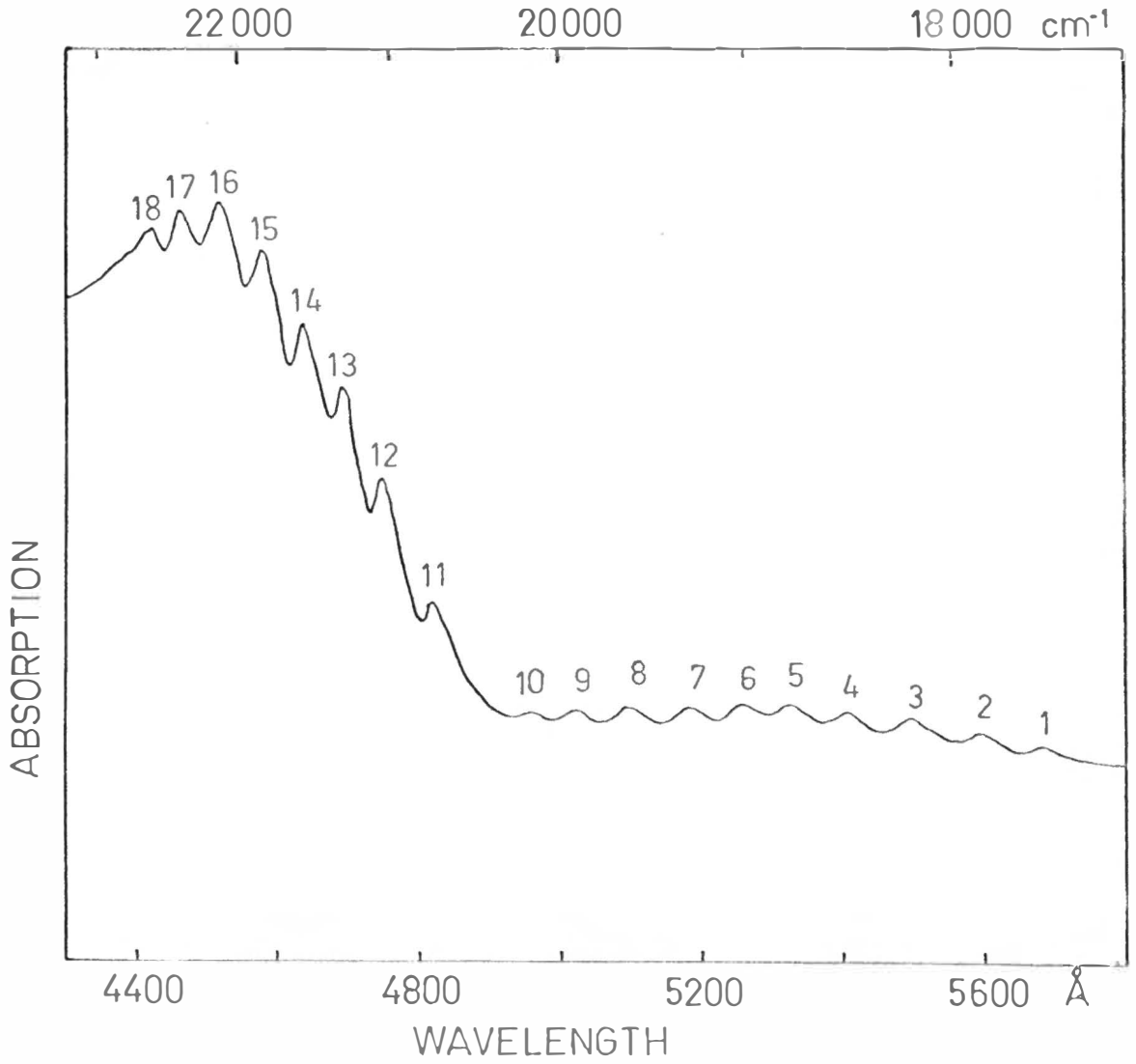

Figure 21. The detailed spectrum of Cs_2ZrCl_6/Pt in regions B and C

C. 17,500 cm^{-1} to 20,400 cm^{-1}

The vibrational structure seen at helium temperature in this region (Figure 21) is very weak. At higher temperatures the structure disappears and the absorption is too weak and broad to be observed. The energies are listed in Table XIII. The frequency of the ν_1 vibration observed in this progression is 288 cm^{-1}. The transition is assigned to the $\Gamma_4(^3T_{1g})$ state.

Table XIII. The observed optical transitions of Cs_2ZrCl_6/Pt and Cs_2HfCl_6/Pt in the energy range 17,500 to 20,400 cm^{-1} at helium temperature.

Figure-Peak	Observed energy in Cs_2ZrCl_6 (cm^{-1})	Observed energy in Cs_2HfCl_6 (cm^{-1})	Assignment
21-1	17 595		$\Gamma_4(^3T_{1g})$
2	17 878	17 878	+ ν_1
3	18 170	18 170	+ $2\nu_1$
4	18 472	18 472	+ $3\nu_1$
5	18 767	18 767	+ $4\nu_1$
6	19 053	19 035	+ $5\nu_1$
7	19 330	19 330	+ $6\nu_1$
8	19 614	19 595	+ $7\nu_1$
9	19 907	19 867	+ $8\nu_1$
10	20 188	20 168	+ $9\nu_1$

6-6 EXPERIMENTAL RESULTS III. Cs_2HfCl_6/Pt

The optical spectrum of Cs_2HfCl_6/Pt is almost identical to that of Cs_2ZrCl_6/Pt. The energies of the lines observed in the two spectra are compared in Tables XI, XII, XIII.

The vibrational structure on the side of the lattice absorption was more pronounced in the Cs_2HfCl_6/Pt spectrum. Band A and the vibrational structure C were the same in both crystals. The structure in band B was much weaker in the Cs_2HfCl_6/Pt spectrum, making it difficult to measure.

6-7 EXCITATION ABSORPTION SPECTRUM

Information about the energy levels in a substance which luminesces can be obtained from the excitation absorption spectrum, where the luminescent output is monitored while the energy of the exciting radiation is varied. The relative importance of the absorption bands in the excitation process can be ascertained by comparing the excitation absorption spectrum with the direct absorption spectrum.

The excitation absorption spectrum of Cs_2ZrCl_6/Pt was measured using the output of the Cary double monochromator as the exciting source. The sample was mounted

on the tip of a conduction dewar in the Cary's sample compartment. One of the quartz windows of the dewar was replaced by a Corning 2-63 filter, which transmits in the red, and a 1P28 photomultiplier was mounted over this to detect the luminescence. The photomultiplier output was passed to a Keithly electrometer and then to a chart-recorder via a voltage dividing circuit. Because the electrometer and recorder were available for only a limited time, measurements were made on just one sample.

Two bands corresponding to A and B in the direct absorption spectrum were seen, but their relative intensities were reversed, showing that, as would be expected, the band at the lower energy is the more important in the luminescence process. The vibrational structure in both bands was weak, particularly in A, but the totally symmetric mode ν_1 could be seen with a frequency of 290 cm^{-1}. The peaks of these two bands were at 25,900 cm^{-1} and 21,400 cm^{-1} respectively, which are about 1000 cm^{-1} below the corresponding peaks observed in the direct absorption spectrum. It is not certain whether this shift is real or due to the response of the system.

At 18,700 cm^{-1} sufficient light from the monochromator passed through the filter to prevent this absorption being observed.

The ultraviolet excitation absorption spectrum showed a broad band, with four peaks, which was hidden by the lattice absorption in the direct absorption spectrum. These peaks at 29,380, 32,360, 34,250 and 37,040 cm^{-1} could be due to either electron-transfer or d-d transitions.

6-8 THE SPECTRUM OF $PdCl_6^{2-}$

One way of identifying the transitions observed in a spectrum is by comparison with other spectra of ions with a similar configuration. Since Pd^{4+} has a $4d^6$ configuration and Pt^{4+} a $5d^6$ configuration, their spectra should bear a strong resemblance. In view of this, crystals of Cs_2ZrCl_6/Pd were grown and their spectra investigated at liquid helium temperature.

The only previous work on the $PdCl_6^{2-}$ spectrum has been carried out on solutions at room temperature. Cohen and Davidson[72] reported bands at 240 mμ (41,700 cm^{-1}) and 340 mμ (29,400 cm^{-1}), and a shoulder at 480 mμ (20,800 cm^{-1}), but did not assign the transitions. Jorgensen assigns the shoulder to a d-d transition to the $^1T_{1g}$ state[3], and the two bands to electron-transfer transitions[61].

The Raman and infrared spectra of K_2PdCl_6 have been measured by Hendra and Park[66]. Their results are (in cm^{-1}):

ν_1	ν_2	ν_3	ν_4	ν_5
317	292	358	175	164

The spectrum of Cs_2ZrCl_6/Pd consisted of some weak bands (Figure 22) showing considerable vibrational structure, and, at higher energies, a few strong absorption bands (Figure 23). (These two figures have different absorption scales and zeros). The observed energies are listed in Table XIV together with possible assignments. Instead of being able to use this spectrum to help interpret the $PtCl_6^{2-}$ spectrum, it was necessary to use the $PtCl_6^{2-}$ spectrum to interpret the $PdCl_6^{2-}$ spectrum. It is expected that the energy levels of ions in the 4d transition series will lie about 5000 cm^{-1} below the energy levels in the corresponding ions in the 5d transition series[3].

If we use this and Jorgensen's previous assignment, the band centred at 21,500 cm^{-1} can be assigned to a $\Gamma_4(^1T_{1g})$ transition. The strong vibrational structure was also apparent in the $^1T_{1g}$ band in the $PtCl_6^{2-}$ spectrum. Three separate progressions can be seen in this band, all with a frequency interval of 270 cm^{-1}, which is assigned to the ν_1 totally symmetric vibrational mode. If the strongest progression is assigned to a Γ_4 transition plus a ν_4 vibration, then the progression starting at line 3 can be assigned to a ν_3 vibration. The third progression

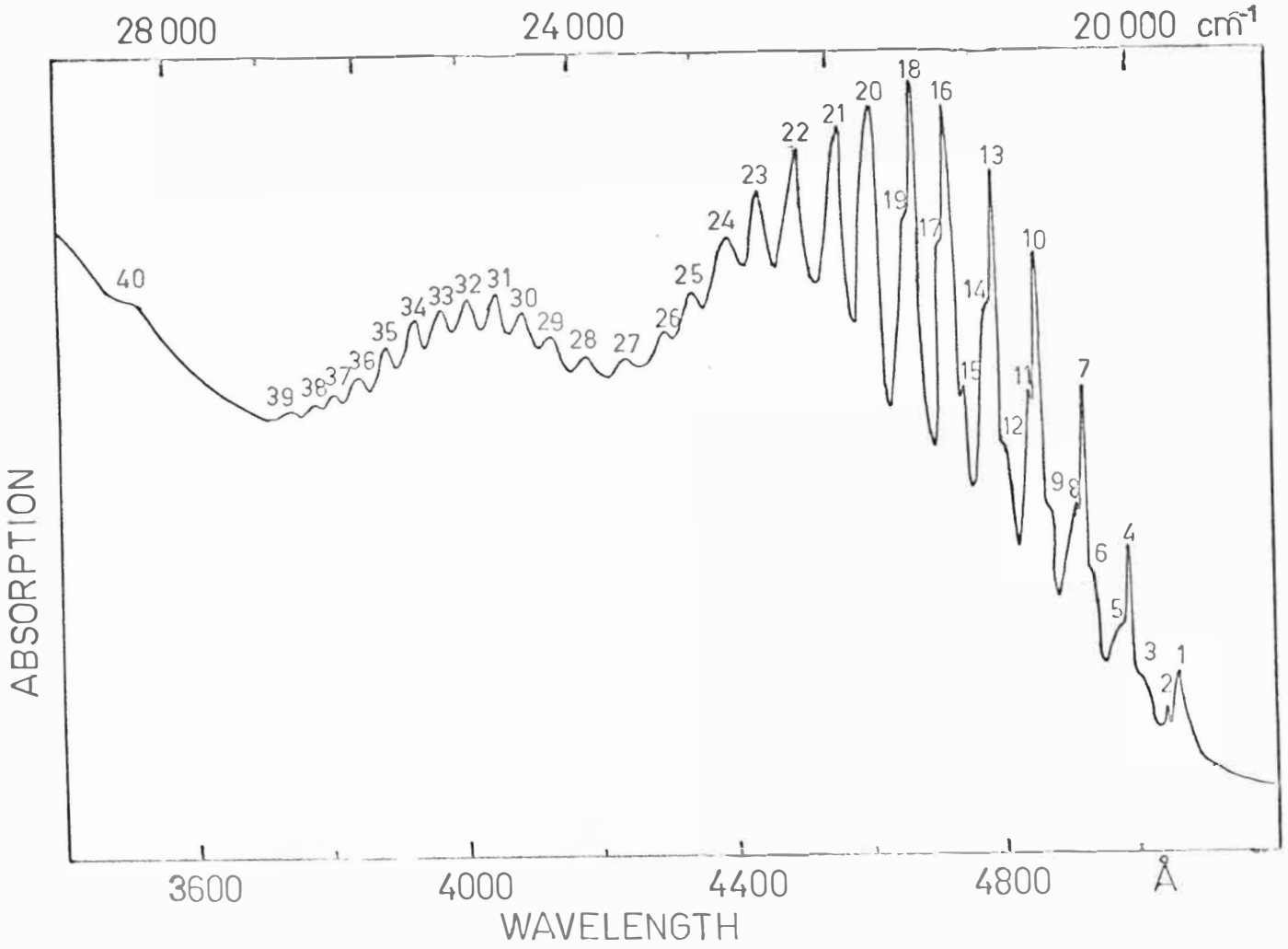

Figure 22. The low intensity and low energy spectrum of Cs_2ZrCl_6/Pd

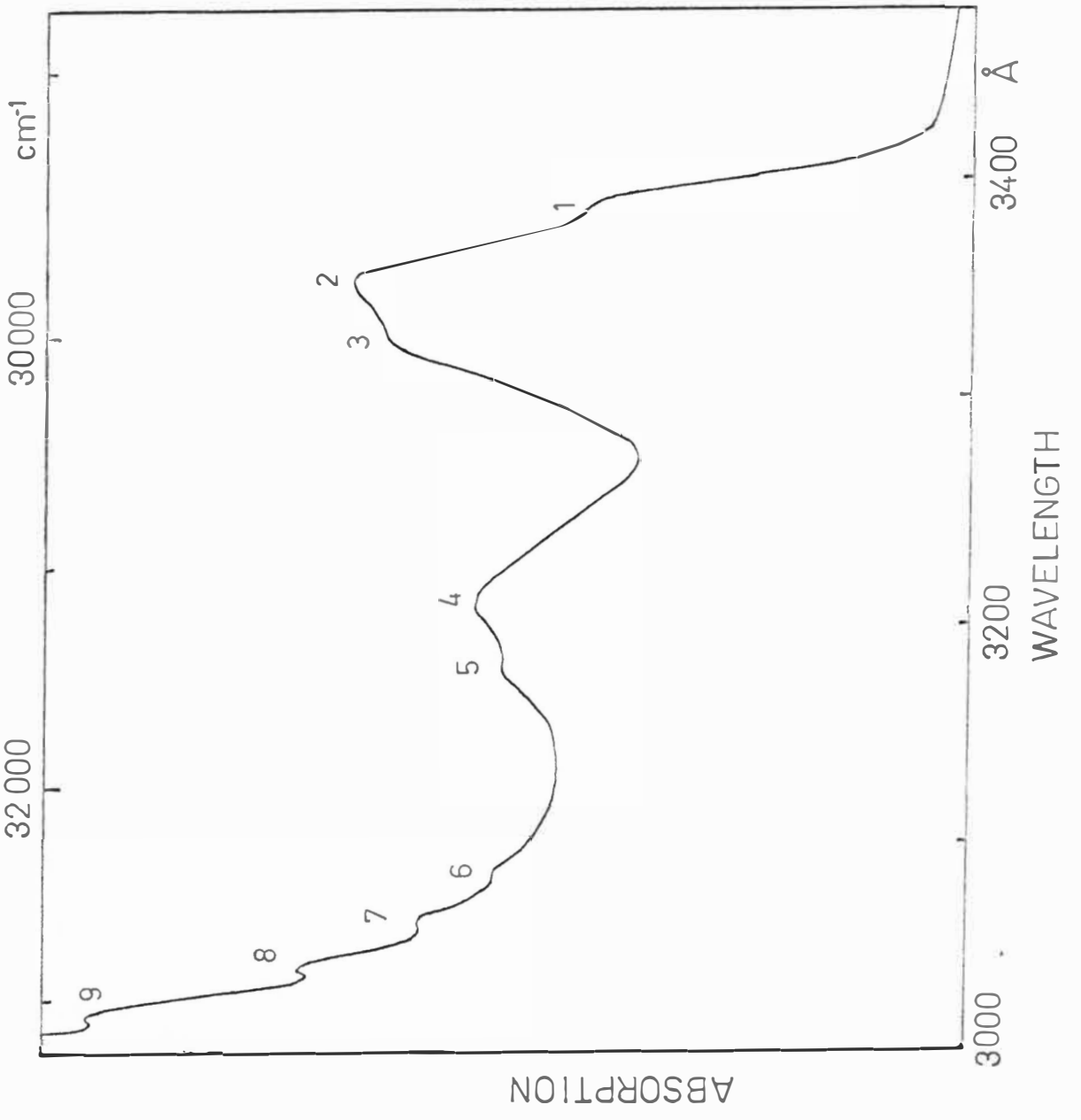

Figure 23. The high intensity and high energy spectrum of Cs_2ZrCl_6/Pd

Table XIV. The observed optical transitions of Cs_2ZrCl_6/Pd at helium temperature.

Figure - Peak	Observed energy (cm^{-1})	Assignment
22 - 1	19 828	$\Gamma_4(^1T_{1g}) + \nu_4$
2	19 887	
3	20 043	$+ \nu_3$
4	20 107	$+ \nu_1 + \nu_4$
5	20 139	
6	20 311	$+ \nu_1 + \nu_3$
7	20 382	$+ 2\nu_1 + \nu_4$
8	20 415	
9	20 558	$+ 2\nu_1 + \nu_3$
10	20 647	$+ 3\nu_1 + \nu_4$
11	20 690	
12	20 845	$+ 3\nu_1 + \nu_3$
13	20 923	$+ 4\nu_1 + \nu_4$
14	20 967	
15	21 109	$+ 4\nu_1 + \nu_3$
16	21 190	$+ 5\nu_1 + \nu_4$
17	21 235	
18	21 462	$+ 6\nu_1 + \nu_4$
19	21 504	
20	21 733	$+ 7\nu_1 + \nu_4$
21	21 996	$+ 8\nu_1 + \nu_4$

Figure - Peak	Observed energy (cm^{-1})	Assignment
22	22 265	$+ 9\nu_1 + \nu_4$
23	22 537	$+ 10\nu_1 + \nu_4$
24	22 799	$+ 11\nu_1 + \nu_4$
25	23 056	$+ 12\nu_1 + \nu_4$
26	23 325	$+ 13\nu_1 + \nu_4$
27	23 613	$\Gamma_5(^1T_{2g})$
28	23 888	$+ \nu_1$
29	24 183	$+ 2\nu_1$
30	24 467	$+ 3\nu_1$
31	24 715	$+ 4\nu_1$
32	24 980	$+ 5\nu_1$
33	25 245	$+ 6\nu_1$
34	25 502	$+ 7\nu_1$
35	25 773	$+ 8\nu_1$
36	26 021	$+ 9\nu_1$
37	26 281	$+ 10\nu_1$
38	26 574	$+ 11\nu_1$
39	26 824	$+ 12\nu_1$
40	28 385	$^5T_{2g}$

(contd)

Figure - Peak	Observed energy (cm^{-1})	Assignment	
23 - 1	29 577	Γ_4	electron
2	29 833		
3	30 085		
4	31 241	Γ_5	
5	31 547		
6	32 756		transfer
7	32 972		
8	33 202		
9	33 424		
10	33 660		

does not appear to fit any of the known vibrational frequencies. These last two progressions are both very weak.

The second, weaker band at 25,000 cm^{-1} was not observed by Jørgensen. This is assigned to the $\Gamma_5(^1T_{2g})$ transition which is expected near this energy, and is weaker than the Γ_4 transition. The only progression observed has the ν_1 frequency, 270 cm^{-1}.

The very weak, ill-defined band at 28,400 cm^{-1} is too weak to show any structure. It could be due to a spin-orbit component of the $^5T_{2g}$ level, but there is no information present to confirm this.

The triplet states, observed at lower energies in the $PtCl_6^{2-}$ spectrum, do not appear because the spin-orbit coupling, which breaks down the spin selection rule, is weaker in the 4d ions than in the 5d ions.

The remaining absorption bands at higher energies were more intense and could be observed only in the more dilute crystals. The spectrum is shown in Figure 23 and the energies are listed in Table XIV. From their intensity these transitions appear to be electron-transfer. The first two bands, which are the weaker, are assigned to transitions to the Γ_4 and Γ_5 levels which occur when an electron moves from a t_{1g} molecular orbital to the $2e_g$ orbital (Figure 1). This is a parity forbidden transition

which accounts for the lower intensity. The structure observed is probably due to the ν_1 vibrational mode. The rest of the vibrational structure appears on the side of an intense absorption band, which is either a $t_{2u} \rightarrow e_g$ electron-transfer, or the lattice absorption. The frequency of the vibration, 225 cm^{-1}, is rather low for ν_1, but it could be a progression in the ν_2 mode.

6-9 CONCLUSION

The search for an absorption band in $PtCl_6^{2-}$ at an energy lower than those previously reported, which would correspond to the bright red luminescence, was successful. The low intensity of this band, and the fact that it was observable only at helium temperature, explains why it had not been observed before. The association of this absorption and the luminescence will be discussed further in the next chapter.

Considerable vibrational structure was observed in the low temperature $PtCl_6^{2-}$ and $PdCl_6^{2-}$ spectra, most of which could be associated with known vibrational levels. However, there was not sufficient information present to use it to assign the transitions as was done with the $IrCl_6^{2-}$ spectra.

C H A P T E R 7

LUMINESCENCE IN OCTAHEDRAL PLATINUM COMPLEXES

7-1 LUMINESCENCE

Luminescence is the name given to the emission of radiation by an atom or molecule in an excited state. Originally the term was used only for emission in the visible spectrum, but it is now used to describe emissions in the ultraviolet and infrared regions of the spectrum as well.

Two important aspects of luminescence in general can be readily understood by considering the configuration coordinate diagram[73] (Figure 24). The configuration coordinate specifies the configuration of the ions around the centre. Normally the system will be in the ground state. The vibrational levels in the ground state are populated by thermal agitation according to the Boltzman distribution, so that at low temperatures only the lowest levels will be occupied and the system will be in a state A. When light is absorbed the system will be raised to the excited state B. The transition is vertical since it is assumed in the Franck-Condon principle that the electronic transition occurs in a short time compared with the time taken for the configuration

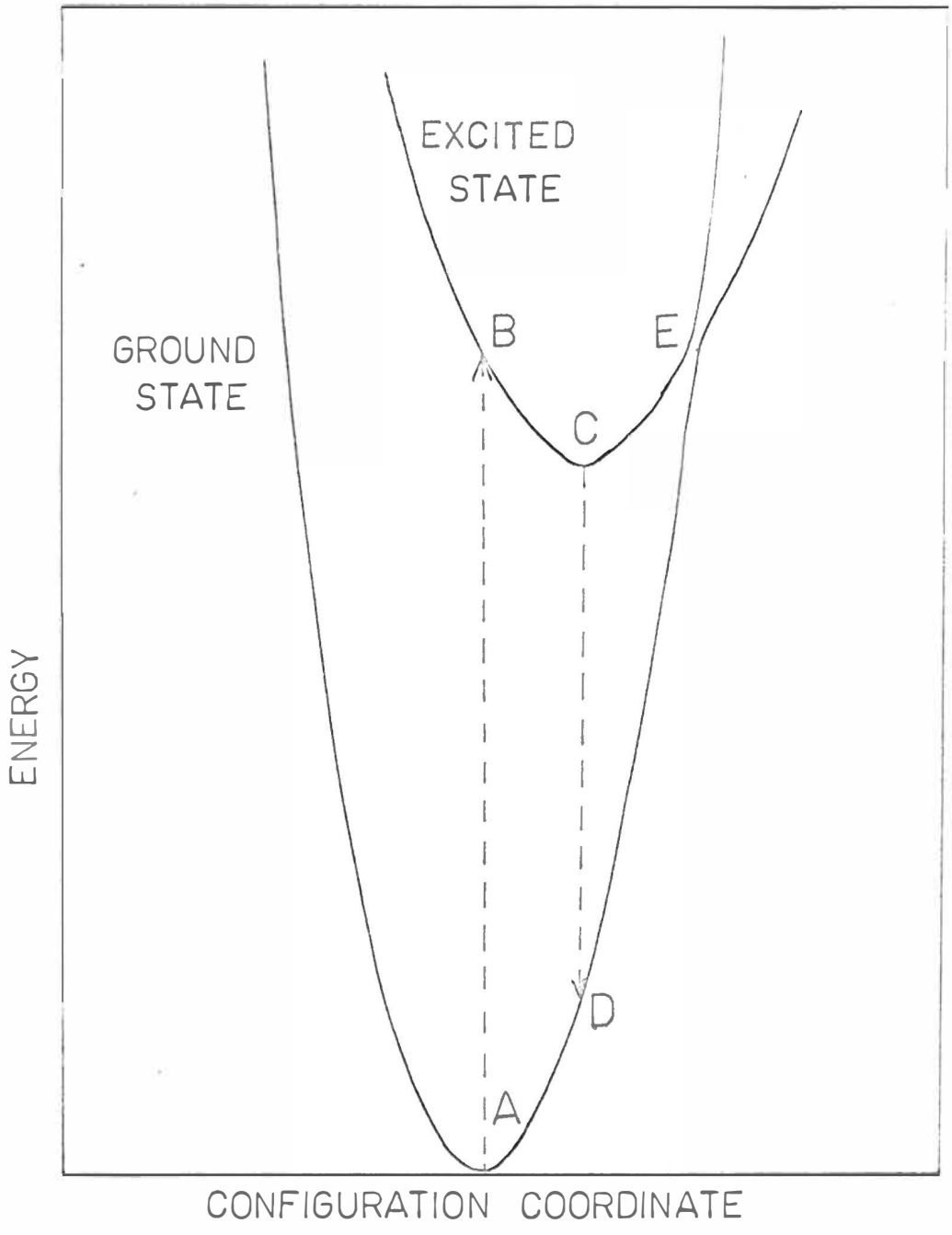

Figure 24. Schematic configuration coordinate curves

coordinate to change. The system then adjusts to the new equilibrium at C, emitting the excess energy in the form of phonons. The system may then return to the ground state D, by emitting a photon. The emission of further phonons enables the system to return to the equilibrium state A. Thus the emitted radiation is of a lower energy than the absorbed radiation. This change in energy is called the Stokes shift.

Besides explaining the Stokes shift, the configuration coordinate diagram also accounts for the decrease in luminescence at higher temperatures. If the system in the excited state gains sufficient energy from its surroundings to reach the point E, it can make a non-radiative transfer to the ground state, and no luminescence will be observed.

This model suggests that a large number of systems should luminesce, whereas in fact, there are only a limited number which do. This is because other relaxation processes, such as phonon interactions, enable the excited state to lose its energy without emitting a photon.

The classical configuration coordinate model has to be modified by quantum mechanics to describe the variation in width of the emission band at low temperatures. Dexter[74] shows that, since the quantum mechanical distribution function is Gaussian, the

emission band will also be Gaussian. The temperature dependence of the width W is given by

$$W \propto [\coth (\hbar\omega_a/2kT)]^{\frac{1}{2}}$$

where $\hbar\omega_a$ is the separation of the vibrational levels in the initial state a.

Nicholas[75] shows that a better model is obtained if a Debye spectrum is used for the density of states,

$$\rho(\omega) \propto \omega^3 \quad \text{for } \omega \leq \omega_D$$

where ω_D is the Debye cut-off frequency. The width of the band is then given by

$$W^2 = W_0^2 \left(\frac{T}{\theta_D}\right)^3 \int_0^{\theta_D/T} x^2 \coth (\tfrac{1}{2}x)\, dx$$

where $\theta_D = \frac{\hbar\omega_D}{k}$ is the Debye temperature of the lattice.

7-2 LUMINESCENCE IN OCTAHEDRAL COMPLEXES

After the initial observation of the bright red luminescence in K_2PtCl_6 at liquid nitrogen and liquid helium temperatures a survey was made of several other compounds containing the Pt^{4+} ion, in order to determine whether or not this is a general property of these ions. The compounds which luminesced and their state, crystalline or powder, are listed in Table XV with the

position of the band peak as measured from the photographic plates.

Table XV. Red luminescent bands.

Compound*	Band Peak (Å)	Vibration (cm^{-1})
K_2PtCl_6 (c,p)	6900	300
K_2PtBr_6 (c,p)	7400	190
K_2SnCl_6/Pt (c)	6900	300
Rb_2PtCl_6 (p)	7000	300
Cs_2PtCl_6 (p)	7150	300
Cs_2ZrCl_6/Pt (c)	7100	320
Cs_2HfCl_6/Pt (c)	7100	320

*c, crystal; p, powder.

The luminescence appeared as a broad band, and at low temperatures vibrational structure was observed, which, as in the absorption spectra, formed a progression in the totally symmetric mode ν_1. These vibrational frequencies are also listed in Table XV. Figure 25 is a densitometer tracing of a plate showing the vibrational structure of the Cs_2HfCl_6/Pt luminescence at 4.2°K, which is a typical example of the red luminescence observed in these compounds.

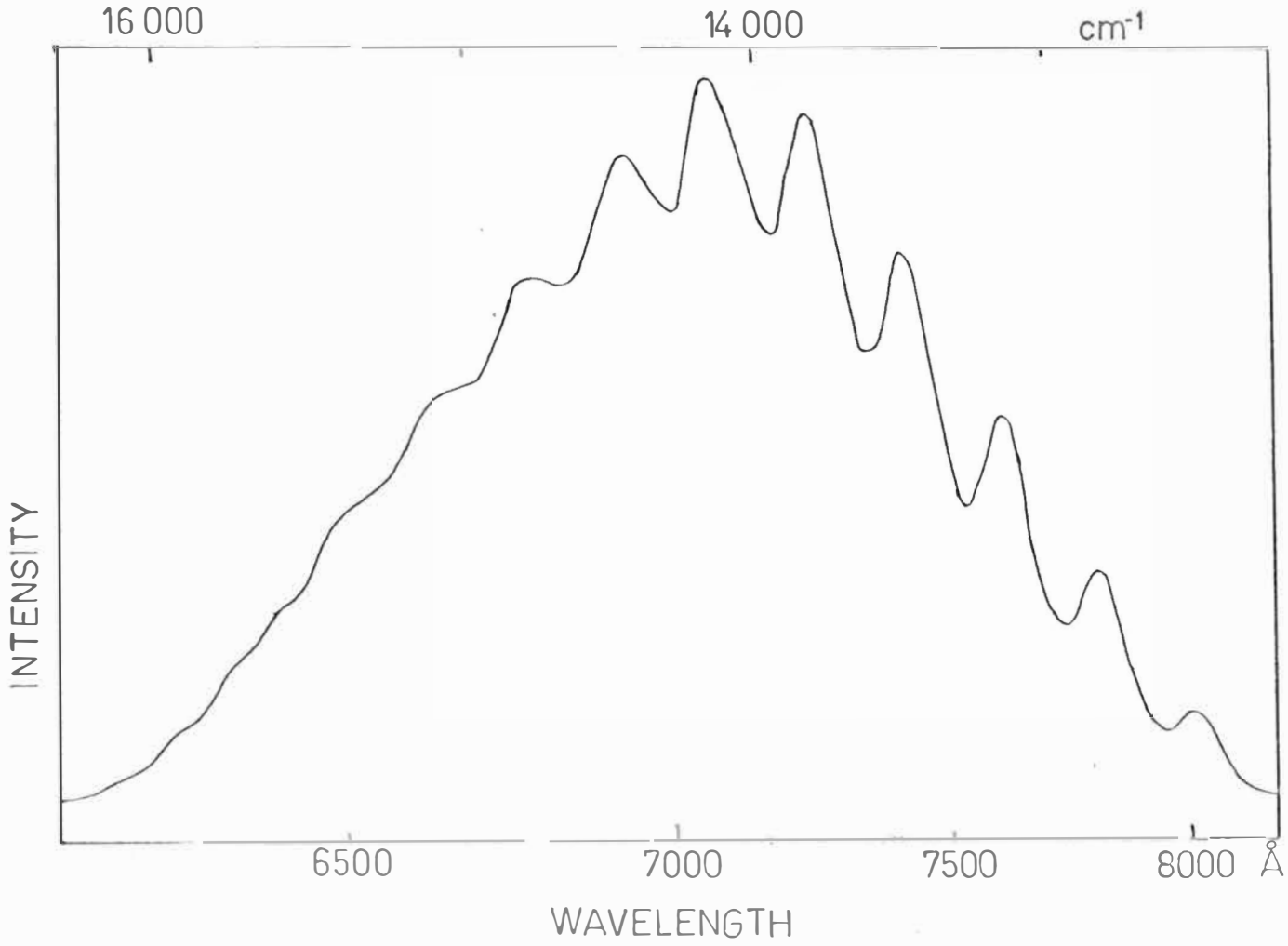

Figure 25. Red luminescent band in Cs_2HfCl_6/Pt at helium temperature

The response of the 1-N plate used to record the red luminescence is given in Figure 3. It was found, by comparing the photographic and photoelectric measurements for K_2PtCl_6 powder, that the peak observed photographically was some 300Å higher than that observed photoelectrically due to the plate response. If this correction is applied throughout the spectrum the luminescent band will be shifted to higher energies, and the vibrational frequency interval of the progression will increase. A measured frequency of 300 cm^{-1} now becomes 330 cm^{-1}, which is close to the totally symmetric ν_1 mode measured in Raman spectra[67].

Other compounds containing the Pt^{4+} ion in which no luminescence was observed were $(NH_4)_2PtCl_6$, $(NH_4)_2PtBr_6$, H_2PtCl_6, Na_2PtCl_6, K_2PtI_6, K_2PdCl_6 and PtO_2. The absence of luminescence in the compounds containing $PtCl_6^{2-}$ is unexpected, since the luminescence is due to this complex. However, the NH_4^+ has internal vibrations which can remove excess energy. H_2PtCl_6 and Na_2PtCl_6 may contain water molecules which would also absorb the excess energy.

In addition to stumbling on the red luminescence accidentally, I unintentionally overexposed a plate of the red luminescence of Cs_2ZrCl_6/Pt and found a second very weak band centred in the green at 4760Å (21,000 cm^{-1}).

1-F plates were used for a further study of this band, which was also observed in the Cs_2HfCl_6/Pt crystals, but not in any of the other samples. A densitometer tracing of this band in Cs_2HfCl_6/Pt at 4.2°K is shown in Figure 26. The observed energies of the peaks in this, and the band in Cs_2ZrCl_6/Pt, are listed in Table XVI where the numbers refer to the peaks in Figure 26. Two separate progressional series can be seen in the lines 1, 3, 5, 7, 9, 11, 13, 15, 17 and the lines 2, 4, 6, 8, 10, 12, 14, 16. The two series are separated by 145 cm^{-1}, which is the difference between the ν_3 and ν_4 vibrational frequencies. The frequency, 325 cm^{-1} in each series, belongs to the totally symmetric mode ν_1. These vibrational assignments are also listed in Table XVI. With these assignments the no-phonon transition would have an energy of 21,908 cm^{-1}. (Note, in emission the addition of phonons to the final (ground) state decreases the energy of the observed lines instead of increasing it, as in absorption.)

7-3 TEMPERATURE DEPENDENCE

The temperature dependence of the band shape of the luminescence of K_2PtCl_6 powder was investigated on the 3.4 m Jarrell-Ash using the Andonian dewar. The powder

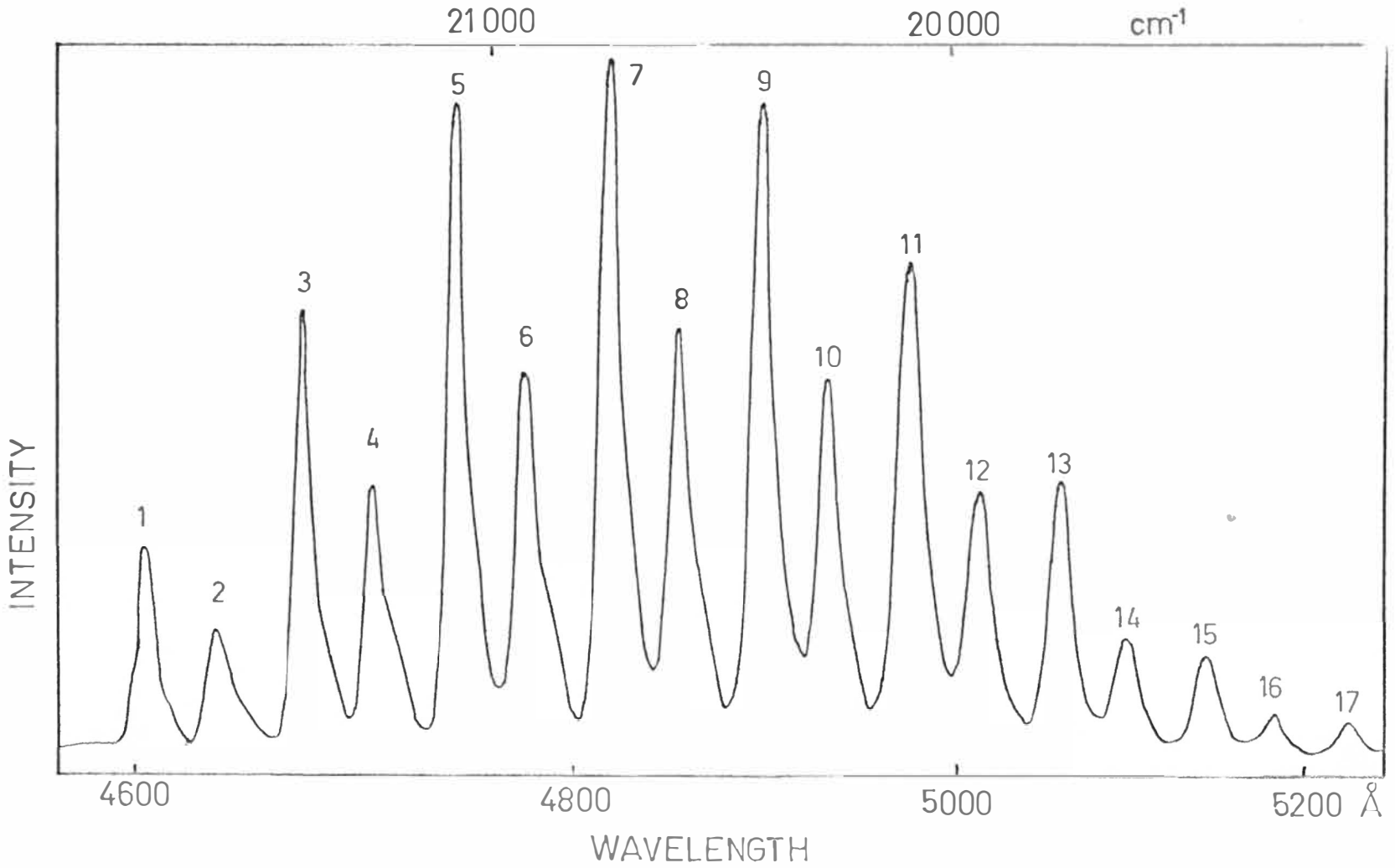

Figure 26. Green luminescent band in Cs_2HfCl_6/Pt at helium temperature

Table XVI. The energy levels observed in the green luminescent band of Cs_2ZrCl_6/Pt and Cs_2HfCl_6/Pt at helium temperature.

Peak Number	Observed energy in Cs_2ZrCl_6 (cm^{-1})	Observed energy in Cs_2HfCl_6 (cm^{-1})	Assignment
1	21 975	21 725	ν_4
2	21 835	21 580	ν_3
3	21 660	21 400	$\nu_1 + \nu_4$
4	21 515	21 260	$\nu_1 + \nu_3$
5	21 335	21 078	$2\nu_1 + \nu_4$
6	21 195	20 926	$2\nu_1 + \nu_3$
7	21 005	20 740	$3\nu_1 + \nu_4$
8	20 862	20 599	$3\nu_1 + \nu_3$
9	20 680	20 414	$4\nu_1 + \nu_4$
10	20 540	20 274	$4\nu_1 + \nu_3$
11	20 370	20 080	$5\nu_1 + \nu_4$
12	20 210	19 930	$5\nu_1 + \nu_3$
13	20 025	19 752	$6\nu_1 + \nu_4$
14	19 885	19 603	$6\nu_1 + \nu_3$
15	19 700	19 438	$7\nu_1 + \nu_4$
16	19 575	19 295	$7\nu_1 + \nu_3$
17		19 128	$8\nu_1 + \nu_4$

was the most convenient sample to use since the pure crystals were too small, and the doped crystals tended to deteriorate with time. The spectra were all corrected for the instrument response.

The position of the peak did not shift with temperature. The temperature dependence could be fitted to a coth function. Nicholas[76] found numerically that the function

$$W^2 = W_0^2 \; 1/3 \coth \left(\frac{\theta_D}{3T}\right)$$

fitted the data. Figure 27 compares this function with the experimental values for the K_2PtCl_6 luminescence.

The area under the band (the total intensity) decreased with increasing temperature, indicating that at higher temperatures more of the energy is lost through non-radiative processes.

When the band shape was corrected for instrument response, it appeared that there might be more than one band present. If two transitions are assumed, both giving a Gaussian band shape, then the observed band can be split into one transition at 14,850 cm^{-1} which is twice as intense as a second transition at 16,050 cm^{-1}. The combination of these two gives a band peaked at 15,150 cm^{-1} (6600Å), as observed. Further evidence for two transitions comes from the luminescent decay of the

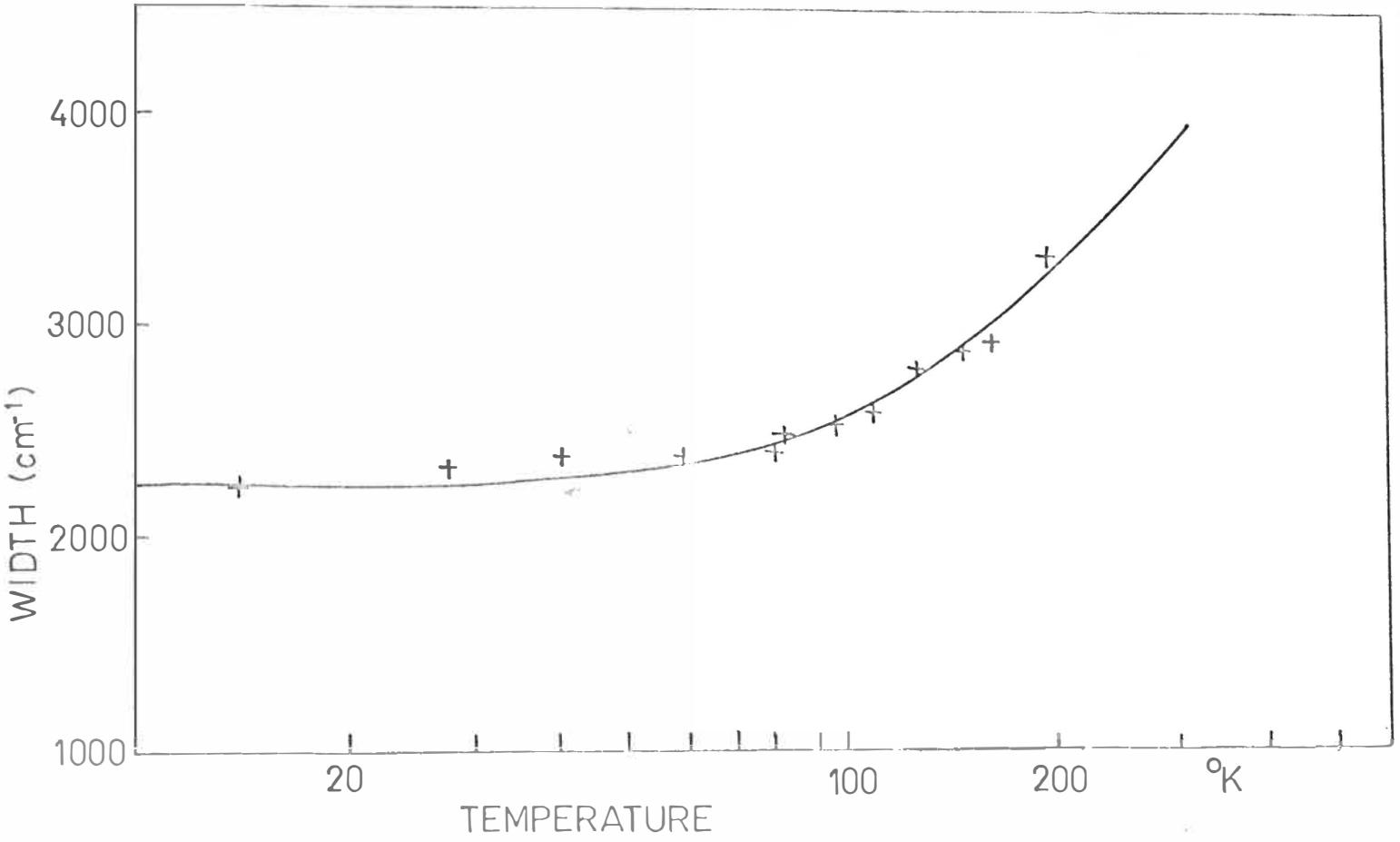

Figure 27. Temperature dependence of the half-height width of the red luminescent band in K_2PtCl_6

red band which gave two decay times of about 3×10^{-4} and 3.5×10^{-4} sec.[77]

7-4 DISCUSSION

The two lowest excited energy levels in the $PtCl_6^{2-}$ complex are $^3T_{1g}$ and $^3T_{2g}$. The two luminescent bands are assigned to transitions from these states to the ground state $^1A_{1g}$. The difference between the peaks of the $^3T_{1g}$ bands in emission and absorption, is unusually large, but no absorption could be found at lower energies. The large width of the bands means that they do overlap to a small extent. The Stokes shift in the $^3T_{2g}$ band is only 1300 cm^{-1} and there is considerable overlap.

The work on the red luminescence (except that on Cs_2ZrCl_6/Pt and Cs_2HfCl_6/Pt) was reported in the Journal of Chemical Physics[78] (see Appendix). Jorgensen[79] suggested that the luminescence might be due to an impurity, but did not say what the impurity might be. This is unlikely since most of the materials used were 99.9% pure, and the doped crystals contained only 1% of $PtCl_6^{2-}$. Also no luminescence could be found in the host crystals, nor was there any noticeable difference between the luminescence of samples obtained from different sources. Dorain[80] and Sartori[81] have also

observed the red luminescence since it was reported, but they do not mention having seen the green luminescence.

CHAPTER 8

CONCLUSION

The results from this thesis add a considerable amount of new information to that previously published on the optical spectra of the 4d and 5d transition-metal complexes. The vibrational structure of the $IrCl_6^{2-}$ and $PtCl_6^{2-}$ spectra at liquid helium temperature has been observed and interpreted for the first time, while the luminescence in $PtCl_6^{2-}$ had never been reported before.

The early luminescence results were published in a letter to the Journal of Chemical Physics[78], and a paper on the $IrCl_6^{2-}$ spectra has been accepted for publication[82] (see Appendix).

An interpretation of the vibrational structure has been made in terms of a combination of ligand field theory and molecular orbital theory. Difficulties encountered in making these interpretations show that these theories are unable to give a complete interpretation of the spectra of the 4d and 5d transition-metal ions, which are more complex than the spectra of the 3d ions. Until a new theory which will provide a satisfactory interpretation of the spectra is developed, the most profitable line of research would be the accumulation of more experimental data on the spectra of these complexes at low temperatures.

At the same time the increasing use of computers should make it possible to obtain reliable wavefunctions which could be used for molecular orbital calculations.

A more careful determination of the energies should be made using an instrument, (such as the 3.4 m Jarrell-Ash) which has better resolution than the Cary. Use of photographic plates, carefully calibrated, would enable the absolute energies to be accurately determined. The sharpest lines were measured on the Cary with a spectral slit width of 1Å (6 cm^{-1} in the visible), while the broader lines could be measured only to the nearest 5Å (30 cm^{-1}). Despite this uncertainty the vibrational frequencies could be determined with reasonable accuracy because they were repeated several times in each vibrational progression.

No measurements of intensities were made because the concentration of the dopant varied between crystals, and even within a given sample. Often some of the dopant formed a deposit at the edge of the crystal which would make any determination of the concentration valueless. Also the use of a fine gauze screen in the reference beam introduced an unknown factor into the absorption measured on the Cary. The improved technique developed to purify the host crystal (Chapter 4) should make it possible to control the concentration of the dopant and to produce single crystals of good optical quality.

The use of non-octahedral host crystals will reduce the symmetry of the system enabling polarization studies to be made, and this would give further information about the energy states. Cs_2ThCl_6 has trigonal symmetry, D^3_{3d}, with the thorium ion at the centre of a slightly distorted octahedron[83]. This would appear to be a useful host, but Axe[53] found that it cannot be grown from the melt in the same manner as Cs_2ZrCl_6, since it appears to undergo a phase change on cooling, which shatters the crystal.

Another method used to lower the symmetry of the central ion is to place it in a magnetic field. The purchase of a Zeeman magnet by the Department will enable such studies to be made.

The assignments of the vibronics would be simplified by measuring the vibrational frequencies at liquid helium temperature. Equipment now being set up or being purchased for the Department will enable the Raman and infrared spectra to be measured at low temperatures in the range from a few cm^{-1} to 400 cm^{-1}.

To determine the nature of the excited state involved in the luminescence a more difficult experiment could be tried. If the excited state could be populated sufficiently, by saturating it with ultraviolet light, it should be possible to study it using e.s.r. If it is a triplet state an e.s.r. spectrum would be observed. There

would be no interference from the ground state which is a $^1A_{1g}$ state. The main difficulty would be to keep the ions in the excited state.

The above observations indicate that, although it has been possible to assign the observed spectra, there is still a great deal of work to be done before the spectra of the 4d and 5d transition-metal ion complexes can be fully understood.

REFERENCES

1. W.A. Runciman, Rep. Prog. Phys. 21, 30 (1958).
2. D.S. McClure, *Solid State Physics*, 9, 399 (Academic Press, N.Y., 1959).
3. C.K. Jorgensen, *Absorption Spectra and Chemical Bonding in Complexes*, (Pergamon Press, Oxford, 1962).
4. C.J. Ballhausen, *Introduction to Ligand Field Theory*, (McGraw-Hill, N.Y., 1962).
5. B.N. Figgis, *Introduction to Ligand Fields*, (John Wiley and Sons, N.Y., 1966).
6. J. Ferguson, Prog. Inorg. Chem. Vol. 12 (to be published).
7. C.K. Jorgensen, Prog. Inorg. Chem. Vol. 12 (to be published).
8. K.A. Schroeder, Ph.D. thesis, University of Canterbury, 1962.
9. H.A. Bethe, Ann. Physik, 3, 133 (1929).
10. J.H. Van Vleck, J. Chem. Phys. 3, 803 (1935).
11. J.H. Van Vleck, J. Chem. Phys. 3, 807 (1935).
12. R. Finkelstein and J.H. Van Vleck, J. Chem. Phys. 8, 790 (1940).
13. Y. Tanabe and S. Sugano, J. Phys. Soc. Japan, 9, 753 (1954).
14. Y. Tanabe and S. Sugano, J. Phys. Soc. Japan, 9, 766 (1954).

15. Y. Tanabe and S. Sugano, J. Phys. Soc. Japan, 11, 864 (1956).

16. L.E. Orgel, J. Chem. Phys. 23, 1004 (1955).

17. L.E. Orgel, J. Chem. Phys. 23, 1819 (1955).

18. L.E. Orgel, J. Chem. Phys. 23, 1824 (1955).

19. R.S. Mulliken, Phys. Rev. 40, 55 (1932).

20. R.S. Mulliken, Phys. Rev. 41, 49 (1932).

21. R.S. Mulliken, Phys. Rev. 41, 751 (1932).

22. R.S. Mulliken, Phys. Rev. 43, 279 (1933).

23. J.H.E. Griffiths, J. Owen and I.M. Ward, Proc. Roy. Soc. 219A, 526 (1953).

24. J.H.E. Griffiths and J. Owen, Proc. Roy. Soc. 226A, 96 (1954).

25. J.H.E. Griffiths, J. Owen, J.G. Park and M.F. Partridge, Proc. Roy. Soc. 250A, 84 (1959).

26. A.H. Cooke, R. Lazenby, F.R. McKim, J. Owen and W.P. Wolf, Proc. Roy. Soc. 250A, 97 (1959).

27. B.R. Judd, Proc. Roy. Soc. 250A, 110 (1959).

28. E.A. Harris and J. Owen, Proc. Roy. Soc. 289A, 122 (1965).

29. J.S. Griffith, *The Theory of Transition-Metal Ions*, (Cambridge University Press, Cambridge, 1961).

30. J.C. Eisenstein, J. Chem. Phys. 34, 310 (1961).

31. J.C. Eisenstein, J. Chem. Phys. 34, 1628 (1961).

32. G. Racah, Phys. Rev. 62, 438 (1942).

33. G. Racah, Phys. Rev. 63, 367 (1943).

34. K.A. Schroeder, J. Chem. Phys. 37, 2553 (1962).

35. A.B. Robson, M.Sc. thesis, University of Canterbury, 1969.

36. J.H. Van Vleck and A. Sherman, Rev. Mod. Phys. 7, 167 (1935).

37. C.J. Ballhausen and H.B. Gray, *Molecular Orbital Theory*, (Benjamin, N.Y., 1965).

38. L.F. Phillips, *Basic Quantum Chemistry*, (John Wiley and Sons, N.Y., 1965).

39. D.S. Schonland, *Molecular Symmetry*, (Van Nostrand, London, 1965).

40. J.W. Leech and D.J. Newman, *How to Use Groups*, (Methuen, London, 1969).

41. A.D. Liehr and C.J. Ballhausen, Phys. Rev. 106, 1161 (1957).

42. S. Koide and M.H.L. Pryce, Phil. Mag. 3, 607 (1958).

43. R. Englman, Mol. Phys. 3, 48 (1960).

44. J.S. Griffith, Mol. Phys. 3, 477 (1960).

45. N.K. Hamer, Mol. Phys. 5, 455 (1962).

46. R.F. Fenske, J. Am. Chem. Soc. 89, 252 (1967).

47. P.C. Jordan, H.H. Patterson, and P.B. Dorain, J. Chem. Phys. 49, 3858 (1968).

48. R.W.G. Wyckoff, *Crystal Structures*, Vol. III, (Interscience Publishers, N.Y., 1965).

49. S.A. Pollack, J. Chem. Phys. 38, 98 (1963).

50. R.A. Satten, J. Chem. Phys. 29, 658 (1958); J. Chem. Phys. 30, 590 (1959).

51. *Handbook of Chemistry and Physics*, 47th Edition, (The Chemical Rubber Company, Cleveland, Ohio, 1966).

52. B.J. Brisdon, T.E. Lester and R.A. Walton, Spectrochim. Acta 23A, 1969 (1967).

53. J.D. Axe, Ph.D. thesis, University of California, 1960.

54. P.B. Dorain, H.H. Patterson and P.C. Jordan, J. Chem. Phys. 49, 3845 (1968).

55. P.B. Dorain and R.G. Wheeler, J. Chem. Phys. 45, 1172 (1966).

56. J.D. Axe, H.J. Stapleton and C.D. Jefferies, Phys. Rev. 121, 1630 (1961).

57. A.V. Babaeva, Bull. Acad. Sci. URSS Cl. Sci. Chim. 1943, 171.

58. Y. Inamura and Y. Kondo, J. Chem. Soc. Japan, 72, 840 (1951).

59. C.K. Jorgensen, Acta Chem. Scand. 10, 518 (1956).

60. C.K. Jorgensen, Acta Chem. Scand. 17, 1034 (1963).

61. C.K. Jorgensen, Mol. Phys. 2, 309 (1959).

62. P. Day and C.K. Jorgensen, Chem. Phys. Letters, 1, 507 (1968).

63. T.P. Sleight and C.R. Hare, J. Phys. Chem. 72, 2207 (1968).

64. G.N. Henning, A.J. McCaffery, P.N. Schatz and P.J. Stephens, J. Chem. Phys. 48, 5656 (1968).

65. A.J. McCaffery, P.N. Schatz and T.E. Lester, J. Chem. Phys. 50, 379 (1969).

66. P.J. Hendra and P.J.D. Park, Spectrochim. Acta, 23A, 1635 (1967).

67. D.M. Adams and D.M. Morris, J. Chem. Soc. (A), 1967, 1666.

68. L.A. Woodward and M.J. Ware, Spectrochim. Acta, 20, 711 (1964).

69. L.A. Woodward and J.A. Creighton, Spectrochim. Acta, 17, 594 (1961).

70. J. Hiraishi and T. Shimanouchi, Spectrochim. Acta, 22, 1483 (1966).

71. M. Debeau and M. Krauzman, Compt. Rend. 264B, 1724 (1967).

72. A.J. Cohen and N. Davidson, J. Am. Chem. Soc. 73, 1955 (1951).

73. C.C. Klick and J.H. Schulman, *Solid State Physics*, 5, 97 (Academic Press, N.Y., 1957).

74. D.L. Dexter, *Solid State Physics*, 6, 353 (Academic Press, N.Y., 1958).

75. J.V. Nicholas, Ph.D. thesis, University of Canterbury, 1966.

76. J.V. Nicholas, unpublished results.

77. R.K. Malcolm, Honours Part III Project, University of Canterbury, 1967.

78. I.N. Douglas, J.V. Nicholas and B.G. Wybourne, J. Chem. Phys. 48, 1415 (1968).

79. C.K. Jorgensen, private communication.

80. P.B. Dorain, private communication.

81. G. Sartori, private communication.

82. I.N. Douglas, J. Chem. Phys. (in press).

83. S. Siegel, Acta Cryst. 9, 827 (1956).

A P P E N D I X

PUBLISHED PAPERS

1. Luminescence of Pt^{4+} in Octahedral Complexes.

2. Optical Spectra of $IrCl_6^{2-}$ in Single Crystals of Cs_2ZrCl_6, Cs_2HfCl_6, and K_2SnCl_6 at Low Temperatures.